J/ψ production within the framework of nonrelativistic QCD

Dissertation zur Erlangung des Doktorgrades
des Departments Physik der Universität Hamburg

vorgelegt von
Mariam Saleh Khan
aus Pakistan

Hamburg
2013

Erstgutachter der Dissertation:	Prof. Dr. B. A. Kniehl
Zweitgutachter der Dissertation:	Dr. S. O. Moch
Erstgutachter der Disputation:	Prof. Dr. B. A. Kniehl
Zweitgutachter der Disputation:	Prof. Dr. G. Kramer
Datum der Disputation:	16 December 2013
Vorsitzender des Prüfungsausschusses:	Prof. Dr. G. Sigl
Vorsitzender des Promotionsausschusses:	Prof. Dr. P. Hausschild
Dekan der MIN-Fakultät:	Prof. Dr. H. Graener

Abstract

We investigate the production of J/ψ from both the color singlet and color octet states of the intermediate $c\bar{c}$ pairs, using the rigorous factorization scheme of NRQCD. We present the transverse momentum and rapidity distributions for the associated production of J/ψ with an open $c\bar{c}$ pair at DELPHI, H1, CDF and ATLAS, considering all the direct, single- and double-resolved subprocesses involved. We emphasize on the importance of considering this process as a part of the NLO studies for J/ψ production. We also calculate the NLO production of J/ψ in electron-positron annihilation, considering both the color singlet and color octet contributions.

Zusammenfassung

Wir untersuchen die Produktion von J/ψ Mesonen aus intermediaeren Farbsingulett und Farboktett Charm-Anticharm-Paaren, wobei wir das rigorose NRQCD Faktorisierungsschema verwenden. Wir berechnen Verteilungen im transversalen Impuls und in der Rapiditaet fuer die assozierte Produktion von J/ψ mit einem offenen Charm-Anticharm-Paar bei DELPHI, H1, CDF und ATLAS, wobei wir alle beteiligten direkten, einfach und zweifach aufgeloesten Unterprozesse beruecksichtigen. Wir unterstreichen die Bedeutung dieser Prozesse als ein Teil der Studien der J/ψ Produktion in der naechstfuehrenden Ordnung der Stroeungstheorie. Wir berechnen weiterhin die Produktion von J/ψ Mesonen in Elektron-Positron-Paarvernichtung in naechstfuehrender Ordnung der Stroeungstheorie, wobei wir wieder sowohl die Farbsingulett als auch die Farboktett-Beitraege beruecksichtigen.

Contents

1 Introduction **5**

2 Theoretical Framework **11**
2.1 Color Evaporation Model: 11
2.2 Color Singlet Model: 13
2.3 Non-Relativistic QCD: 14

3 Charmonium Production Formalism **18**
3.1 Covariant Projectors 20
3.2 Gluon Polarization 22
3.3 Dealing with γ_5 23
3.4 Divergences at NLO 23

4 J/ψ production with a $c\bar{c}$ pair **25**
4.1 Kinematics 25
4.2 Partonic Differential Cross Section 26
4.2.1 Phase Space Integration 28
4.3 Hadronic Differential Cross-Section 33
4.4 Numerical Analysis 38
4.4.1 LEPII-DELPHI: 40
4.4.2 HERA-H1: 43
4.4.3 TEVATRON-CDF: 45
4.4.4 LHC-ATLAS: 45
4.5 Conclusions: 46

5 J/ψ production at NLO in e^+e^- annihilation **49**
5.1 Born Cross Section: 49
5.2 Virtual Cross Section: 52
5.3 Real Cross Section: 53
5.4 Numerical Analysis: 62
5.5 Conclusions: 66

6 Summary and Outlook **69**

Appendix A: The Master Integrals **71**

Appendix B: Soft Terms **73**

1 Introduction

The discovery of a new resonance, at Stanford Linear Accelerator Center (SLAC) and Brookhaven National Laboratory (BNL), was announced simultaneously on 11 Nov, 1974. This not only confirmed the existence of already conjectured charm quark of the Standard Model, but also opened the exciting world of flavor neutral mesons. The small width of the observed resonance indicated an unexpected long life time ($0.8\text{x}10^{-20}$sec) of the particle discovered, named later J/ψ. This vector meson was interpreted as a bound state of a charm-anticharm pair with a mass much higher than the previously known light quarks (u, d and s). The importance of J/ψ observation is highlighted by the fact that the subsequent rapid experimental developments and the series of changes in theoretical high-energy physics at the time, triggered by this discovery, have become collectively known as the "November Revolution". J/ψ production generated further interest through its leptonic decays, which provided clean experimental signature. Soon after, some other charm-quark resonances, D^0 and D^+ were discovered in 1976 and then, to enrich further the elementary particle physics picture, the first bottom-antibottom bound state was observed in 1977. Ever since, bound states of a heavy quark with its antiquark, called Quarkonia ($Q\bar{Q}$), have constantly drawn a lot of attention as an active field of research both from experimental and theoretical communities.[1]

In the past years, many experiments have been dedicated to quarkonium studies. As a result, many new exotic hadronic states such as tetraquarks and meson molecules (whose interpretation is still unclear) have been discovered even recently, in addition to some predicted quarkonium states. The interest on heavy flavors, nowadays, has enhanced further by all these exciting discoveries. Therefore, with a wealth of new and accurate data coming from diverse sources [2] like:

- Quarkonium formation from BES at BEPC, the old E835 at Fermilab, KEDR (upgraded) at VEPP-4M, and CLEO-III at CESR;
- Clean samples of charmonia produced in B-decays, in photon-photon fusion and in initial state radiation, from the B-factories, BaBar at SLAC and Belle at KEK;
- Heavy quarkonia production ,measured at CDF and D$\varnothing$ experiments of Fermilab, from gluon-gluon fusion in $p\bar{p}$ annihilations at $2TeV$;
- Charmonia production study by ZEUS and H1, at DESY, in photon-gluon fusion;

[1] The top quark cannot form a bound state because of its very short lifetime, less than $\frac{1}{10^{24}}$s.

- Charmonia production and suppression, in heavy-ion collisions, studied by PHENIX and STAR, at RHIC, and NA60, at CERN;

the field of heavy quarkonia is still undergoing a rapid expansion in experiments. Even larger data samples are expected from the CLEO-c and BES-III upgraded experiments in the near future. Besides that, B-factories and the Fermilab Tevatron will continue supplying valuable data for several years. Later on, expected are many other challenges and fantastic opportunities offered by new facilities when LHC at CERN, Panda at GSI, much higher luminosity B factory at KEK, a Linear Collider, etc. will become operational. This in turn demands to improve our understanding of the crucially important theory which governs the system of these quarkonium states.

On the theoretical side, in close analogy with positronium or even with a hydrogen atom, quarkonia are treated as a simple two body system, and were expected to contain a spectrum of resonances corresponding to various excitations of the corresponding heavy quark pair. But unlike its analogs governed mainly by the electrostatic Coulomb potential, the properties of quarkonium are however determined by the $SU(3)$ gauge theory of strong interactions, called Quantum Chromodynamics (QCD). In this thesis, charmonium ($c\bar{c}$) states will be focused for further discussion. Given the large mass of charm quark, the heavy $c\bar{c}$ pair acts non-relativistically, with a small relative velocity ($v_{rel} \approx 0.5$) as compared to a similar system of lighter quarks (with $v_{rel} \approx 0.8$). The strong binding potential $V(r)$ between the heavy quark pair, considering their charge and color quantum numbers, is of the form:

$$V(r) \approx -\frac{\alpha(r)}{r} + \kappa^2 r \tag{1.1}$$

where r is the distance between the quarks, $\alpha(r)$ is the coupling constant of coulomb like first term in the potential (for strong interactions $\alpha(r) \simeq \alpha_s(1/r)$) and κ is the string tension coefficient (empirically $\kappa \simeq 450MeV$). Since κ is independent of M, it must be proportional to Λ_{QCD}.

QCD requires the phenomena of confinement and asymptotic freedom to be obeyed. The confinement presumably results from the fact that the potential energy of the two quarks increases with increasing r, as in the above equation. The quarks in the bound state can, therefore, not be separated apart until enough energy is reached to create a new quark-antiquark pair. As a result of this confinement, no free quarks are ever observed. On the other hand, this system looks similar to electrodynamic case, when the first term dominates for small r, but behaves differently from the simple Quantum Electrodynamics (QED) models. In quantum field theory, an electron can emit a virtual photon which then creates an electron-positron pair. Therefore, an electron spontaneously becomes surrounded by a cloud of virtual e^+e pairs. This cloud of charged particles gets polarized, when positrons are attracted by the charge on the original electron. Therefore, a probe far away sees the actual charge of the electron, whereas a closer probe finds a larger charge due to the polarized cloud. A similar, but opposite, effect occurs in the strong

interaction, where a probe close to the colour charge will see a lower colour charge than a probe far away. In the limit of zero separation ($r \to 0$), the charge appears to be zero. This is known as asymptotic freedom, which in short implies that at very high energies and momenta, quarks and gluons interact only weakly and act as quasifree particles. The spectrum of charmonium states, with specific radial excitation, spin and orbital angular momentum, can then be well derived by the solution of a Schrödinger equation that incorporates this asymptotic behavior of QCD [3]. The relevant quantum numbers for these states in the conventional spectroscopic notation (like for positronium) are:

$$n^{2S+1}L_J, n = 1, 2, 3, ... \tag{1.2}$$

where n is principle quantum number,S spin and L is the orbital angular momentum with total angular momentum $J = L + S_z$. Being fermions of spin 1/2, the $c\bar{c}$ pair can have either their spins anti-aligned to form the spin singlet state ($S = 0$) or aligned to form a spin triplet state ($S = 1$). These states can be further characterized by their parity $P = (-1)^{L+1}$ and charge conjugation number $C = (-1)^{L+S}$. Keeping the same analogous to hydrogen atom, the different spin states in quarkonia have different energy levels, and therefore given different names. Some members of the charmonium spectrum are listed in Table[1].

$n\,^{2S+1}L_J$	Charmonium	J^{PC}	Mass(MeV)
$1\,^1S_0$	η_c	0^{-+}	2980
$1\,^3S_1$	J/ψ	1^{--}	3097
$1\,^3P_0$	χ_{c0}	0^{++}	3415
$1\,^3P_1$	χ_{c1}	1^{++}	3511
$1\,^1P_1$	h_c	1^{+-}	3526
$1\,^3P_2$	χ_{c2}	2^{++}	3556
$2\,^1S_0$	$\eta_c{}'$	0^{-+}	3637
$2\,^3S_1$	$\psi\,'$	1^{--}	3686

As the simplest strongly bound states with rich internal structure, charmonia were hoped to provide the same testing ground for understanding hadronic dynamics or QCD, as the one provided by hydrogen atom in understanding the atomic physics. In a way, this has indeed been the case and the development of many methods in QCD is directly related to analyses of the properties of charmonium and of its heavier sibling bottomonium.

Factorization Scales

Even considering our simple analogy of positronium in QED, the description of the system of quarkonium containing two heavy quarks becomes rather challenging in QCD, due to confinement (which makes it hard to apply perturbative QCD here). But there still are some instrumental parameters/scales involved to rescue. On one hand, the large mass M of heavy quark suggests an advantageous non-relativistic treatment of heavy

quarkonium. Whereas on the other hand, the relativistic velocity v of the quarks in bound state also provides a small parameter in which the dynamical scales may be hierarchically ordered and the QCD amplitudes systematically expanded. The nonrelativistic potential models then need to include different scales to accommodate all properties of QCD. Therefore, a heavy quarkonium bound state, with radius r, is characterized by three intrinsic scales:

- mass of the heavy quark,M (**hard scale**),
- relative momentum of the heavy quark-antiquark pair in center of mass frame, $|\mathbf{p}| \sim Mv$ ($\sim \frac{1}{r}$), for $v << 1$ (**soft scale**),
- kinetic energy of the heavy quark in the bound state, $E \sim Mv^2$ (**ultrasoft scale**).

If we integrate out the hard scale from QCD, a non-relativistic effective theory is obtained. Another important energy scale in quarkonium physics is the scale of nonperturbative effects involving gluons and light quarks, Λ_{QCD} [4]. The hierarchy of the energy scales thus becomes;

$$M \gg \Lambda_{QCD} \gg Mv, Mv^2. \tag{1.3}$$

For the study of charmonium physics, the important observables are their production or decays rates. This dissertation will discuss the production side. The above hierarchy of energy scales, for this purpose, provides the ground to construct a self consistent effective field theory, factorized into two steps:

- a heavy quark pair production during the first phase of a hard collision
- formation of a charmonium bound state out of this heavy quark-antiquark pair

The first step takes place with sufficiently high momentum transfers to create such high mass of the heavy quarks, and is thereby treated perturbation. The mass M_c then sets the scale for point like production of the $c\bar{c}$ pair, at small range. Due to this high charm mass and small relative velocity of the $c\bar{c}$ pair in the bound state of charmonia, the second step is described using the non perturbative or low energy/momentum scales, Mv^2 or Mv, at long distance compared to r.
This factorization of scales remains reliable only when $v \ll 1$ to widely separate the dynamics of short distance and long distance. The long distance part, accounting for QCD confinement, then is not influenced significantly by the short distance one. Therefore, once phenomenologically extracted from one special process, the long distance matrix elements (LDMEs) should remain valid for any other process. This implies the universality of LDMEs, which in turn enhances the predictive power of the factorization approach. Charmonia, with $v^2 \approx 0.2$, are the lightest system in heavy quarkonia, to which this approach apply. Based on the separation of different energy scales involved, a few models have been developed over the years to study the production cross sections and decay rates of different quarkonium states. Most commonly applied of them are the Color Evaporation Model (CEM), Color Singlet Model (CSM) and Nonrelativistic Quantum Chromodynamics (NRQCD), which will be briefly discussed in the next chapter.

Being the most robust theoretically and the most successful phenomenologically so far, NRQCD factorization is selected for the investigation of J/ψ production in this dissertation. With the inclusion of color octet mechanism, NRQCD was able to resolve the issue of infrared divergences which appeared during the calculations of the P-wave charmonium production in CSM. It also could reconcile the discrepancies between the J/ψ hadroproduction data at Tevatron and the theoretical predictions of the CSM. Despite these undeniable successes, there still remain number of discrepancies between NRQCD predictions and the observed data at different experiments. For example, in contrast to CEM, NRQCD expected J/ψ to be transversely polarized at large p_T, but the CDF data at $\sqrt{s} = 1.96TeV$ revealed it to be unpolarized [6]. The experimental data for charmonium photoproduction at HERA [9] invites for an even deeper theoretical insight into different channels involved in the production. Also, further phenomenological investigations are required to establish the universality of experimental LDMEs. Another open challenge to NRQCD was recently posed by the experimental data at Belle [7], where $J/\psi + c\bar{c}$ associated production is much larger than the NRQCD expectations. A similar large discrepancy was seen earlier in the cross section of exclusive double charmonium production at B-factories [8]. These unexpected measurements motivates further to investigate this process at other colliders, and for photo- and hadro-productions as well, where it also plays an important contribution at the next-to-leading order (NLO) corrections. There have already been some theoretical discussion on the importance of this process at B-factories[10], at LEP [11], and at Tevatron and LHC [12] using different classical approaches. Being equally important at different collider energies and having incomplete theoretical information so far, the process in which J/ψ is produced with an open $c\bar{c}$ pair is one of the main works of this dissertation.

The large contributions of the Next to Leading Order (NLO) calculations found recently in several studies performed for the inclusive and exclusive charmonium production could reduce the conflict between the CSM predictions and the experimental results. It thus implies to study the CO mechanism more carefully in order to investigate its contribution in the charmonium production. A list of these studies in indicated in the reference [15], and the references therein. The study of charmonium production in the annihilation of electro-positron at B-factories can not only test the NRQCD but also investigate the importance of CO contributions. The recent experimental results by the Belle Collaboration [7] of the full cross-sections (rather than Born) for the processes $e^+e^- \to J/\psi + X$, $e^+e^- \to J/\psi + c\bar{c}$ and $e^+e^- \to J/\psi + X_{non-c\bar{c}}$, indicate the inconsistencies with the already existing theoretical predictions. We therefore get the motivation to perform a NLO calculation for J/ψ production at B-factories.

The thesis is organized as follows:
The second chapter gives a brief summary of classical approaches to study charmonia like Color Evaporation Model and Color Singlet Model along with the review on non relativistic QCD based on the concepts of effective field theory.
A short application formalism of NRQCD framework is described in chapter three. Some

important details used in our calculations are also discussed in this chapter. In the fourth chapter, NRQCD tools are applied to study associated production of J/ψ with a $c\bar{c}$ pair. This process will be considered as part of the next to leading order contributions to J/ψ production at DELPHI, H1, CDF and LHC. A comparison of the results with inclusive J/ψ production in [13] is presented.
Since higher-order corrections are expected to play an important role to understand the process of charmonium production, the fifth chapter for this reason deals with NLO J/ψ production at B-factories.
The last chapter summarizes the work done and presents conclusions, with an outlook.

2 Theoretical Framework

In the following decade of the discovery of first charmonium states, many new resonances were observed above and below the $D\bar{D}$-threshold, where D is the lowest mass meson containing the charm quark. The plethora of new quarkonia unleashed a flood of extensive theoretical investigations over the last three decades [16]. After two decades of almost a 'dry spell' in charmonium experiments, some new exotic charmonium like states have been observed very recently at BABAR, Belle, BES, CLEO-c etc. Due to these exciting discoveries, the modern era is often referred to as the new Renaissance in excited charmonium spectroscopy. This has offered further intriguing puzzles to the theory of charmonium physics which has regained a great renewed interest [5]. To make precise and solid theoretical predictions in different regimes, need for a rigorous and sophisticated theory for charmonium production is highly felt.

From the earlier discussion, it is known that a colour neutral charmonium bound state is formed from two charm quarks. But, in principle, these two heavy quarks are not necessarily carriers of one colour and the corresponding anti-colour. In $SU(3)$ symmetry group of QCD, there are three colour triplet e.g. R, G, and B and their corresponding descriptors $\bar{R}$, $\bar{G}$ and $\bar{B}$. Out of these, $3 \oplus 3 = 8 \oplus 1$ combinations are formed, which contain both the octet (colored) and the singlet (color-neutral) states. So the combination in the initially produced $c\bar{c}$ pair might be coloured. Thus charmonium production is needed to be studied under variety of conditions. For this purpose, different models were proposed/developed. Most extensively used of those are Color Evaporation Model, Color Singlet Model and NRQCD. As discussed in the previous chapter, the multiscale system of charmonium exhibits both perturbative and non-perturbative behavior. All theses models, therefore, are based on the factorization of QCD scales into high energy/short distance and low energy/long distance. But the roles played in the production process by the colors and spins of the initial $c\bar{c}$ pair are assumed to be very different in theses models.These three models are discussed here briefly, in their historical order.

2.1 Color Evaporation Model:

Soon after the discovery of J/ψ, the Color Evaporation Model (CEM) was proposed in 1977 to apply QCD on charmonium hadroproduction [17]. This model allows perturbative creation of a $c\bar{c}$ pair in all possible color and spin states, with an invariant mass M between twice the charm quark mass $2m_c$ (a threshold for a charmonium state) and twice the D meson mass $2m_D$ (a threshold for producing an open-flavor heavy meson). This takes into account the color octet production also. The $c\bar{c}$ pair is presumed to

neutralize any surplus color via different processes like interaction with collision-induced color field and exchange/emission of soft gluons. This $c\bar{c}$ pair with small relative momentum can then evolve nonperturbatively into a specific charmonium state, without any constraints on its color and spin [1]. It is assumed that the probability of forming this final charmonium state is almost completely independent of the color and, in some other versions, independent also of the spin of the initial states in which the $c\bar{c}$ pair is produced [18]. It can be safely said that the initial color and spin states of the $c\bar{c}$ pair 'evaporates' later, and have no effects on its hadronization into a charmonium state. Therefore, in CEM, the production cross section of a charmonium state H is given by [16]:

$$d\sigma^{CEM}(H+X) = f_H \int_{2m_c}^{2m_D} dM_{c\bar{c}} \frac{d\hat{\sigma}(c\bar{c}+X)}{dM_{c\bar{c}}} \tag{2.1}$$

where $\hat{\sigma}(c\bar{c}+X)$ is partonic cross-section for producing a $c\bar{c}$ pair with invariant mass below $D\bar{D}$ threshold, and summed over all the color and spin states of $c\bar{c}$ pair. The universal long distance factor f_H is a phenomenological parameter of inclusive $c\bar{c}$ production cross section (below the $D\bar{D}$ threshold) used to designate the constant fraction of this mass region which evolves into a particular $c\bar{c}$ state. For the model to have any predictive power, f_H must be constant.

CEM enjoyed considerable phenomenological successes initially, by predicting the constant production ratios for any two quarkonium states, independent of the process and kinematic/energy region e.g.

$$\frac{\sigma(h)}{\sigma(J/\psi)} = \frac{f_H}{f_{J/\psi}}; \tag{2.2}$$

which was consistent with hadroproduction data at Fermilab [19]. But there were some serious challenges presented to the model, when some conflicts with experimental observations were observed in these ratios (e.g. different hadroproduction and photoproduction cross-section ratios for χ_c and J/ψ). Also, no attempts were made by CEM to relate these production cross-sections to annihilation decays. As is obvious from eq.(2.1), that there is an upper limit on the mass of $c\bar{c}$ pair production cross section but there is no imposition of any constraints on color or spin of the final charmonium state. This is why CEM suffers from a crucial lack i.e. a distinction of different quarkonium states varying in their spin and orbital angular momentum structure is not allowed. This issue is solved in Color Singlet Model. The large number of processes involved in color evaporation results in a relatively large number of unknown parameters, those have to be extracted by comparison to existing experimental data. This large number of the undetermined parameters also limits the predictive power of the CEM. Furthermore, any polarization of the charmonium state would be washed out by the same soft processes those were

[1] Or some other heavy hadrons/charmed mesons are produced when either of the c or $\bar{c}$ combine with light quark q, for invariant mass between $2m_c$ and $2m_{[cq]}$

responsible for the evaporation of color from color octet states, and hence no predictions for polarization in the J/ψ production. Due to the limitations of CEM, another model entered into the study circles of charmonium physics.

2.2 Color Singlet Model:

The Color Singlet Model (CSM) is considered as the most effective classical approach to study charmonium physics, based on factorization. This model assumes that a $c\bar{c}$ pair that is produced during the short distance/high energy interactions will evolve later to form a particular charmonium state only if the initial $c\bar{c}$ pair is in the color singlet Fock state, with the spin (S) and angular momentum quantum number (L), that match exactly those of the bound state. This physical charmonium state with total angular momentum J is then denoted as $^{2S+1}L_J$, retaining the quantum numbers of the initial $c\bar{c}$ pair (which now has an almost vanishing relative momentum, compared to m_c, inside the bound state). For example, for a J/ψ formation, the $c\bar{c}$ pair must initially be produced in a color-singlet $^3S_1$ state. While this part is treated perturbatively, all the long distance effects of the transition of this $|c\bar{c}\rangle$ Fock state into the physical charmonium bound state are factorized into a non- perturbative parameter, provided by the bound state radial wave function, $R(r)$. The inclusive differential cross section for J/ψ production, in the CSM is expressed in the form [21];

$$d\sigma^{CSM}(J/\psi + X) = d\hat{\sigma}(c\bar{c}(^3S_1, \underline{\mathbf{1}}) + X)|R_{J/\psi}(0)|^2, \tag{2.3}$$

and for P-wave χ_{cJ} as;

$$d\sigma^{CSM}(\chi_{cJ} + X) = d\hat{\sigma}(c\bar{c}(^3P_J, \underline{\mathbf{1}}) + X)(2J+1)|R'_{\chi_{cJ}}(0)|^2, \tag{2.4}$$

where $|R(0)|^2$ and $|R'(0)|^2$ are the universal non-perturbative factors at origin, for S-wave and for P-wave respectively. A similar factorization applies to charmonium decay rates, where this universal factor gives the probability of the $c\bar{c}$ pair in the charmonium bound state, being close enough to annihilate. These are the only factors in this model which need to be extracted from experimental measurements. Charmonium production at relatively low energies had been successfully calculated with this model [22] .

Unlike CEM, the CSM predicts variations in the ratios of cross sections of different charmonium states from process to process, due to angular momentum selection rules. It also gives nontrivial predictions about the dependence of the cross section on the polarization of charmonium state.The model was taken seriously until around 1995, when CDF collaboration measured the cross sections for prompt charmonium production[2] from $p\bar{p}$ collision at Tevatron [23] . The experimental results showed that CSM under-predicted the cross section by about a factor of 30, for J/psi hadroproduction at large transverse momentum. As is obvious from the name, the CSM rejects all color octet

[2]Prompt means production of charmonium states via direct QCD interaction instead of weak decays of B-mesons.

states of initial $c\bar{c}$ pair and also ignores relativistic corrections which relate to the non-zero relative velocity of the $c\bar{c}$ pair, it was inferred to consider them as well in order to solve the discrepancy that appeared in Tevatron data. The color-octet $c\bar{c}$ pair was then assumed to evolve through a nonperturbative transition to an observable color-singlet state by radiating a soft gluon. While calculating these radiative corrections at next to leading order (NLO), it was found that the short-distance production cross section of the P-wave charmonia contained logarithmic infrared divergences that could not be factored into $|R'(0)|^2$. This was assimilated, to some extent, in the phenomenological applications of the CSM by introducing an infrared cutoff, identified with one of the low-energy scales present in non-relativistic bound states of charmonia i.e. the binding energy of the $c\bar{c}$ pair. However, the presence of infrared divergences in the production cross sections of the P-wave charmonia made evident the theoretical inconsistencies in the model, which thus implied the CSM to be incomplete.

2.3 Non-Relativistic QCD:

After the failure of the CSM to explain experimental data of charmonium hadroproduction, it was strongly felt that a new rigorous framework is needed to study charmonium production in QCD. The solutions to some of the problems listed above was proposed by Bodwin, Braaten and Lepage (BBL) [26] in 1995. Considering a relativistic treatment of the $c\bar{c}$ pair in QCD, they provided a new framework for the study of charmonium production, called non-relativistic QCD (NRQCD).

In their theory, the roles of the quantum numbers of the initially produced $c\bar{c}$ pair is somewhat a combination of those in the CEM and CSM. In addition to the color singlet state, the color octet states (in different angular momentum configurations) are equally important in the production of the initial $c\bar{c}$ pair. These initial color octet states then evolve into a charmonium bound state, by neutralizing its color through a mechanism provided by the long distance dynamics e.g. soft gluon emission. The hadronization of the initial $c\bar{c}$ pair into a charmonium bound state is encoded in the long distance matrix elements of NRQCD. Additionally, the angular momentum of the physical charmonium state depends on that of pre-resonant $c\bar{c}$ state.

Different energy scales involved in this production of charmonia are disentangled via factorization, as discussed already in chapter 1. Now the explicit roles played by these energy scales of eq.(1.3) are:

- m_c, sets the scale for the mass of charmonium bound state,
- $m_c v$, is the scale for size of this bound state,
- $m_c v^2$, governs the scale for splitting between radial excitations and between orbital angular momentum excitations,

- Λ_{QCD}, is the scale associated with non-perturbative effects of light quarks and gluons.

All the effects of the scale m_c are contained in the short distance coefficients, which describe the initial production of the on-shell $c\bar{c}$ pair. The existence of the scales $m_c v$ and $m_c v^2$ owe to the smallness of the relativistic velocity v of the $c\bar{c}$ pair inside the bound state, where for charmonia $v^2 \approx 0.2$. This makes the bound state dynamics insensitive to the creation details of the initial $c\bar{c}$ pair, thus fully exploiting the role of factorization. One crucial feature of this factorization phenomena is that in NRQCD, a charmonium state is not solely regarded as a single state of the $c\bar{c}$ pair, but is rather taken as a superposition of color singlet and color octet states, with different quantum numbers. The Fock state expansion of a charmonium state, e.g. J/ψ, in powers of v is then:

$$|J/\psi\rangle = |(c\bar{c}(^3S_1, \underline{\mathbf{1}})\rangle + O(v)|c\bar{c}(^3P_J, \underline{\mathbf{8}})g\rangle + O(v^2)|c\bar{c}(^1S_0, \underline{\mathbf{8}})g\rangle + O(v^2)|c\bar{c}(^3S_1, \underline{\mathbf{8}})gg\rangle + O(v^4), \tag{2.5}$$

where g represents a soft gluon, $^{2S+1}L_J$ is the angular momentum of the $c\bar{c}$ in each Fock state, and $\underline{\mathbf{1}}/\underline{\mathbf{8}}$ represents its color configuration. This shows that BBL approach not only handles soft gluons properly but also incorporates the relativistic corrections in a systematic manner (where v serves as an expansion parameter). Therefore, NRQCD is considered to be the effective field theory of heavy quarkonia, which provides a convenient recipe to separate different energy scales involved [25]. It is derived from QCD by integrating out the energy scales of order m_c or higher. The arbitrary factorization scale of this theory, $\Lambda \sim m_c$, is identified with the ultra-violet (UV) cutoff in the NRQCD effective Lagrangian, in the matrix elements at short distance. This dependence on Λ gets canceled by that in NRQCD matrix elements at long distance. Therefore, the physical results are independent of Λ. The general expression of the cross section for the production of a charmonium state H is of the form:

$$d\sigma(a + b \to H + X) = \sum_n d\hat{\sigma}(a + b \to c\bar{c}[n] + X)\mathcal{O}^H[n]\,, \tag{2.6}$$

where the short distance part comprises of the cross section $\hat{\sigma}(a+b \to c\bar{c}[n]+X)$ for the production of a $c\bar{c}$ pair in a specific Fock state of a particular color, spin and angular momentum, labeled by $[n] = {}^{2S+1}L_J^{(i)}$ with S, L, J representing the spin, orbit, and total angular momentum quantum numbers of the $c\bar{c}$ respectively and $i = 1(8)$ indicating that the $c\bar{c}$ pair is produced in a color-singlet (-octet) state. These short distance coefficients are calculable order by order as a perturbative series in which QCD coupling constant $\alpha_s(m_c)$ is treated as an expansion parameter. The other part $\mathcal{O}^H[n]$ represents the long distance matrix elements which encode the nonperturbative effects and are proportional to the probability for a point like $c\bar{c}$ pair in the state $[n]$, to eventually form a physical charmonium bound state H. These long distance matrix elements (LDMEs) are then scaled by an expansion in v, within effective Lagrangian of NRQCD. With no reliable theoretical calculations at hand, these LDMEs are extracted from experiments by fitting to the data, as phenomenological parameters.

The NRQCD factorization in the above eq. (2.6) therefore projects a double expansion i.e. in $\alpha_s(m_c)$ and v, and contains infinitely many terms, $[n]$. The velocity scaling rules of NRQCD [24] then compare the relative contributions of various terms, and allow the truncation of the series (at any desired order of accuracy) in eq. (2.6), thus enabling to project out the pre-dominant state, which for example is the color singlet S-wave state for J/ψ. NRQCD description of S-wave charmonium production at the lowest order in v, then reduces to the colour-singlet model. The velocity scaling rules for the production of J/ψ are listed in Table[2].

scaling	v^3	v^7	v^{11}
n	${}^3S_1^{[1]}$	${}^1S_0^{[8]}$, ${}^3S_1^{[8]}$, ${}^3P_J^{[8]}$	...

In case of the P-wave charmonia, color octet contributions from the S-wave states of the initial $c\bar{c}$ pair are of the same order in v, as the leading color singlet contributions from the P-wave states of the initial $c\bar{c}$ pair. Therefore, both of these contributions must be included in a consistent theoretical analysis in NRQCD. The infrared divergences appearing in the short distance cross section of the colour singlet P-wave states of the $c\bar{c}$ pair at next-to-leading order are canceled by a matching infrared singularity from the radiative corrections to the long distance matrix element of the colour-octet S-wave state [26]. This inclusion of the colour octet S-wave states of the $c\bar{c}$ pair is crucial for the removal of the infrared divergence from the production cross section, ensuring a consistent and well defined overall description of P-wave charmonia in NRQCD. A more comprehensive and detailed treatment of these infrared divergences for P-wave charmonium production can be found in references [27].

The effect of these color octet contributions can even be more important phenomenologically in case of S-wave charmonium states like J/ψ. Predicted by the power counting rules [26], the effects of these color octet matrix element for the production of S-wave charmonia are suppressed by powers of v as compared to the leading order colour-singlet contribution. But at lower order of α_s, colour-octet contributions can become significant, if the corresponding short distance coefficients (for producing a $c\bar{c}$ pair in a colour-octet state) is enhanced [28]. This approach celebrated several successful implications. The inclusion of these color octet processes, alongwith the observation that the dominant contributions to their short distance coefficients at large p_t is provided by gluon fragmentation, gave the very first phenomenological success for NRQCD; by providing a satisfactory explanation of the Tevatron data [29], for the cross section of J/ψ hadroproduction. Making use of its self consistence, NRQCD could thus resolve most of the confronting issues of CEM and CSM. Although the dependence on $[n]$ of $\mathcal{O}^H[n]$ extends the summation in eq. (2.6) to all possible configurations, requiring an infinite number of phenomenological parameters as input, but thanks to their well defined velocity scaling behavior that only few leading ones of theses LDMEs are left behind for practical applications. This preserves the predictive power of the NRQCD. But not all predictions of this theory have proved to be true. It also suffers from some discrepancies

between its predictions and the experimental data. There still exist some uncertainties in the LDMEs, one of the vital foundations for the predictive power of NRQCD. This demands further investigations into the universality of these nonperturbative parameters. The predicted dependence of the charmonium production cross-section on its polarization at large p_t has also not been verified. With all its elegance and practical applicability, NRQCD needs even more theoretical work and experimental information to be established firmly as THE THEORY for charmonium production.

3 Charmonium Production Formalism

The physical bound states of the $c\bar{c}$ pair incorporate all the energy regimes of QCD, from the hard region at high energies, where an expansion in the coupling constant is possible, to the low-energy region, where nonperturbative effects dominate. Charmonia are thus an ideal system to probe nonperturbative QCD and its interplay with perturbative QCD within a controlled manner. As discussed in the previous chapters, the formalism to study charmonium production will be based on the factorization of cross section in this dissertation. A diagramatic representation of the factorization formulas at work is provided by fig.[3.1]. This figure depicts the production process of the initial $c\bar{c}$ pair by interaction of two on shell photons which may be radiated off the incoming electron-positron (e^+e^-) pair, or by interactions of the partonic contents of these initial photons via single- and double-resolved partonic subprocesses, stemming respectively from one or both photons resolved. This pre-resonant $c\bar{c}$ pair then evolves to form a physical charmonium bound state.
The differential cross section for the photoproduction of J/ψ at e^+e^- colliders is generally expressed by the formula,

$$d\sigma(e^+e^- \to e^+e^- + J/\psi + X) = \int dx_1 f_{\gamma/e^+}(x_1) dx_2 f_{\gamma/e^-}(x_2) \times \sum_{i,j} \int dx_i f_{i/\gamma}(x_i) dx_j f_{j/\gamma}(x_j) \times d\sigma(i+j \to J/\psi + X), \tag{3.1}$$

where:

- the labels i and j denote the partonic contents of photons, such as gluons or light quarks (u, d, s) or antiquarks $(\bar{u}, \bar{d}, \bar{s})$;
- $f_{\gamma/e}(x)$: is the spectrum of the initial bremsstrahlung photon distribution, described by the Weizsacker-Williams approximation (WWA) as [30]

$$f_{\gamma/e}(x) = \frac{\alpha}{2\pi}\left(2m_e^2(\frac{1}{Q^2_{max}} - \frac{1}{Q^2_{min}})x + \frac{(1+(1-x)^2)}{x}\log(\frac{Q^2_{max}}{Q^2_{min}})\right), \tag{3.2}$$

  with $x = E_\gamma/E_e$, α is the fine structure constant and m_e is the electron mass, while Q^2_{max} and Q^2_{min} are defined as:

$$Q^2_{min} = \frac{m_e^2 x^2}{1-x}, \tag{3.3}$$

$$Q^2_{max} = (\frac{\sqrt{s}\theta}{2})^2(1-x) + Q^2_{min}, \tag{3.4}$$

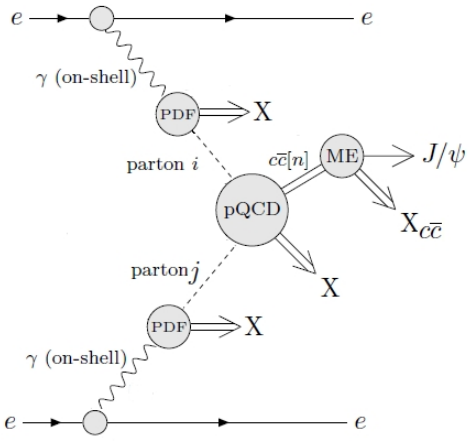

Figure 3.1: Diagramatic representations of the factorization formula 3.1.

with θ being the angle between the initial photon momentum and the direction of the electron beam. In case J/ψ is produced via direct interaction of two photons, the distribution function $f_{\gamma/\gamma}(x) = \delta(1-x)$;

- $f_{i/\gamma}(x)$: is the probability for a parton i to be found in a photon, called a Parton Distribution Function (PDF) of the photon, where x is the energy fraction of i to γ. In the case of hadro-production, these PDFs are replaced with those of the proton;

- $\sigma(i+j \to J/\psi + X)$: is the cross section for partonic subprocess $i+j \to J/\psi + X$.

Here, we can also distinguish between different classes of subprocesses involved in a particular interaction of initial state particles. In the above reaction, when both the initial photons directly couple to the charm quarks in the final state, it is called a 'direct' process. When one of the photons fluctuates to any of its partonic contents and collides with the other photon, this is a 'single-resolved' process. Similarly, production of final state particles from only partons, originating from both of the initial state photons is called a 'double-resolved' process.

As discussed in the previous chapter, the above partonic cross section is factorized into short distance (perturbative) and long distance (non-perturbative) parts, on the basis of NRQCD factorization theorem (following the notation used in [31]), as;

$$d\sigma(i+j \to J/\psi + X) = \sum_n d\hat{\sigma}(i+j \to c\bar{c}[n] + X) \frac{\langle \mathcal{O}^{J/\psi}[n] \rangle}{N_{col}(n) N_{pol}(n)}. \tag{3.5}$$

where $\hat{\sigma}(i+j \to c\bar{c}[n]+X)$ is the production cross section for the intermediate $c\bar{c}[n]$ state, for $[n] = {}^{2S+1}L_J{}^{[1,8]}$. $\langle \mathcal{O}^{J/\psi}[n] \rangle$ is proportional to the transition probability of the this perturbatively produced intermediate state into a physical J/ψ, at long distance. $N_{col}(n)N_{pol}(n)$ represent the color and polarization degrees of freedom of the intermediate $c\bar{c}[n]$ state respectively as;

$$N_{col}(n) = \begin{cases} 1, & for \quad color \quad singlet \quad state \quad n \\ 2C_A C_F, & for \quad color \quad octet \quad state \quad n \end{cases} \tag{3.6}$$

where $C_A = N_c$ and $C_F = \frac{N_c^2-1}{2N_c}$ for $N_c = 3$ within QCD calculations. The short distance partonic cross section for the production of a particular state $c\bar{c}[n]$ is then calculated by the general formula

$$d\hat{\sigma}(i+j \to c\bar{c}[n]+X) = \frac{1}{2s} dPS \frac{1}{N_{col,in}N_{pol,in}} \sum_{col,pol} |\mathcal{M}(i+j \to c\bar{c}[n]+X)|^2 \tag{3.7}$$

where the flux factor $\frac{1}{2s}$ contains the partonic center of mass energy squared $s \equiv (k_i+k_j)^2$, the matrix elements squared $|\mathcal{M}(i+j \to c\bar{c}[n]+X)|^2$ is averaged over the degrees of freedom $N_{col,in}N_{pol,in}$ of the initial state particles and summed over those of the final state particles $c\bar{c}[n]$. The Lorentz invariant differential phase space, denoted by dPS, depends on the number of final state particles. In order to calculate these matrix elements for the creation of a $c\bar{c}$ pair in a particular Fock state $[n]$, a set of certain covariant projectors is applied onto the amplitudes of perturbative QCD states. From now on, we will be strictly following the notations used in [34], with the normalization of [26] for the projectors [32] [33] discussed below.

3.1 Covariant Projectors

In this dissertation, only S- and P-wave states of charmonium will be considered. As per our earlier discussion, the $c\bar{c}$ pair binding together to form these charmonium states can either be in a color singlet or in a color octet state. So the decomposition of the color structure of production amplitude is carried out using the operators

$$\mathcal{C}_1 = \frac{1}{\sqrt{2}C_A} \qquad \text{for the singlet state} \tag{3.8}$$

$$\mathcal{C}_8^c = \sqrt{2}T^c \qquad \text{for the octet state,} \tag{3.9}$$

which project out the colour singlet or color octet content respectively of the given state. T^c here represents a color matrix, with c being an open color index. To disentangle the spin singlet and spin triplet contributions in the production amplitude, the projectors

$$\Pi_0 = \frac{1}{\sqrt{8{m_c}^3}} \left(\frac{\not{P}}{2} - \not{q} - m_c \right) \gamma_5 \left(\frac{\not{P}}{2} + \not{q} + m_c \right), \tag{3.10}$$

$$\Pi_1^\alpha = \frac{1}{\sqrt{8{m_c}^3}} \left(\frac{\not{P}}{2} - \not{q} - m_c \right) \gamma^\alpha \left(\frac{\not{P}}{2} + \not{q} + m_c \right) \tag{3.11}$$

are used, where $P/2+q$ and $P/2-q$ identify respectively the momenta for the outgoing c and $\bar{c}$ quarks, each of them having mass m_c. Therefore, total momentum of their bound state is P, with $2q$ being the relative momentum between the $c\bar{c}$ pair inside the charmonium bound state (which is J/ψ in our case). If $\mathcal{A}$ is taken to be the standard perturbative QCD amplitude for the production of open $c\bar{c}$ pair, with amputated charm quark spinors, the matrix elements for the states with orbital angular momentum $L=0$ or $L=1$ are defined as:

$$\mathcal{M}_{c\bar{c}[^1S_0^{[8]}]} = \mathrm{Tr}\left[\mathcal{C}_8^c\,\Pi_0\,\mathcal{A}_{c\bar{c}[n]}\right]|_{q=0} \tag{3.12}$$

$$\mathcal{M}_{c\bar{c}[^3S_1^{[1]}]} = \mathcal{E}_\alpha \mathrm{Tr}\left[\mathcal{C}_1\,\Pi_1^\alpha\,\mathcal{A}_{c\bar{c}[n]}\right]|_{q=0} \tag{3.13}$$

$$\mathcal{M}_{c\bar{c}[^3S_1^{[8]}]} = \mathcal{E}_\alpha \mathrm{Tr}\left[\mathcal{C}_8^c\,\Pi_1^\alpha\,\mathcal{A}_{c\bar{c}[n]}\right]|_{q=0} \tag{3.14}$$

$$\mathcal{M}_{c\bar{c}[^3P_J^{[8]}]} = \mathcal{E}^{(J)}_{\alpha\beta}\frac{d}{dq_\beta}\mathrm{Tr}\left[\mathcal{C}_8^c\,\Pi_1^\alpha\mathcal{A}_{c\bar{c}[n]}\right]|_{q=0} \qquad (J=0,1,2) \tag{3.15}$$

with the insertion of color projectors $\mathcal{C}$ and spin projectors Π into the open $c\bar{c}$ chain. In the above notation, $\mathcal{E}_\alpha$ and $\mathcal{E}^{(J)}_{\alpha\beta}$ are the polarization vectors of the $c\bar{c}$ state and the trace is to be taken over the $c\bar{c}$ chain both in the Dirac space and in the color space. Any state with orbital angular momentum L is projected out by differentiating L times its already spin-color projected amplitude with respect to q, at the point $q=0$. These expressions are then squared to be used in eq. (3.7), alongwith the summation performed on the polarization vectors of $c\bar{c}$ for the selection of total angular momentum.

In order to apply this set of projectors for next to leading order calculations where all the divergences appearing are handled through dimensional regularization, their generalized character will be considered in $D=4-2\epsilon$ dimensions of space-time. Therefore, for S- and P-wave states, the sums over the polarizations in D dimensions are:

$$\sum_{pol}\mathcal{E}_\alpha\mathcal{E}^*_{\alpha'} = \Pi_{\alpha\alpha'} \tag{3.16}$$

$$\sum_{pol}\mathcal{E}^{(0)}_{\alpha\beta}\mathcal{E}^{(0)*}_{\alpha'\beta'} = \frac{1}{D-1}\,\Pi_{\alpha\beta}\Pi_{\alpha'\beta'} \tag{3.17}$$

$$\sum_{pol}\mathcal{E}^{(1)}_{\alpha\beta}\mathcal{E}^{(1)*}_{\alpha'\beta'} = \frac{1}{2}\left[\Pi_{\alpha\alpha'}\Pi_{\beta\beta'}-\Pi_{\alpha\beta'}\Pi_{\alpha'\beta}\right] \tag{3.18}$$

$$\sum_{pol}\mathcal{E}^{(2)}_{\alpha\beta}\mathcal{E}^{(2)*}_{\alpha'\beta'} = \frac{1}{2}\left[\Pi_{\alpha\alpha'}\Pi_{\beta\beta'}+\Pi_{\alpha\beta'}\Pi_{\alpha'\beta}\right]-\frac{1}{D-1}\,\Pi_{\alpha\beta}\Pi_{\alpha'\beta'}, \tag{3.19}$$

of the nature of a vector, a scalar, an antisymmetric tensor and a symmetric traceless tensor, respectively corresponding to the states $^3S_1$ and ^3P_J for $J=0,1,2$. The symbol $\Pi_{\alpha\beta}$ used in the above equations is an abbreviation of the expression:

$$\Pi_{\alpha\beta}\equiv -g_{\alpha\beta}+\frac{P_\alpha P_\beta}{4m_c^2}. \tag{3.20}$$

The number of polarization degrees of freedom of the intermediate state $[n]$ appearing in eq. (3.5) are calculated by the total contraction of these polarization tensors. Therefore, for the ${}^3S_1$ state, it becomes

$$\begin{aligned} N_{pol}({}^3S_1) &= \textstyle\sum_{pol} \mathcal{E}_\alpha \mathcal{E}^*_\alpha \\ &= \Pi_{\alpha\alpha} \\ &= D-1, \end{aligned}$$

and for the ${}^3P_J$ states is

$$N_{pol}({}^3P_J) = \textstyle\sum_{pol} \mathcal{E}^{(J)}_{\alpha\beta} \mathcal{E}^{(J)*}_{\alpha\beta} = \begin{cases} 1, & for \quad J=0 \\ \frac{1}{2}(D-1)(D-2), & for \quad J=1 \\ \frac{1}{2}(D+1)(D-2), & for \quad J=2 \end{cases} \tag{3.21}$$

while dealing in $D = 4 - 2\epsilon$ dimensions. In case of four dimensions, we get

$$N_{pol}(n) = 2J+1, \tag{3.22}$$

with J being the total angular momentum of the intermediate state n. Another frequently used symbol in our dimensional regularization for the next to leading order calculations in $D = 4 - 2\epsilon$ dimensions, consistent with [34] is

$$C_\epsilon \equiv (\frac{4\pi\mu^2}{m_c^2} e^{-\gamma_E})^\epsilon \tag{3.23}$$

where μ represents the renormalization scale and γ_E denotes the Euler's gamma.

3.2 Gluon Polarization

In QED, summation over the external photon polarization comes as a direct consequence of Ward identity. So in the Feynman gauge, one can simply replace

$$\sum_{pol} \epsilon^\mu \epsilon^{*\nu} = -g_{\mu\nu}, \tag{3.24}$$

for any number of photons in the initial or final states. While in QCD, this is not valid for processes involving more than one gluon, due to the presence of three gluon vertices. These vertices then allow propagation of longitudinal degrees of freedom which are non-physical. Hence, the physical or transverse polarization sum is expressed as

$$\sum_{pol} \epsilon^\mu \epsilon^{*\nu} = -g_{\mu\nu} + \frac{k_\mu p_\nu + k_\nu p_\mu}{k\cdot p} - \frac{p^2 k_\mu\ k_\nu}{(k\cdot p)^2}, \tag{3.25}$$

where k is the gluon momentum and p is an arbitrary light-like four vector (or momentum of the other initial gluon appearing in the calculations) with property $k{\cdot}p \neq 0$. In order to

speed up the calculations, we want to use eq.(3.24). So the non-physical or longitudinal contributions need to be compensated. This is done by considering additional gluon ghosts/antighosts, which replace external gluons appearing in the Feynman diagrams. So having subtracted these ghost/antighost contributions from the corresponding gluon processes, one can safely make use of the eq.(3.24) even for gluons.

3.3 Dealing with γ_5

Another important point to note is the occurrence of γ_5 in our calculation, while working on D-dimensional amplitudes at next to leading order. During our evaluation of the pure QCD diagrams, a γ_5 appears while applying the projector in eq. (3.10), which then gets included into the evaluation of spin traces with other γ matrices. In order to define it in arbitrary dimensions, there have been some efforts starting from defining γ_5 in 4 dimensions. One of them, called *naive* dimensional regularization scheme, depends on the anti-commutation property,

$$\{\gamma_5, \gamma^\mu\} = 0 \tag{3.26}$$

(for $\mu = 0, 2, \cdots, D-1$) and the trace,

$$\text{Tr}\left[\gamma_5\gamma_\alpha\gamma_\beta\gamma_\gamma\gamma_\delta\right] = 4i\epsilon_{\alpha\beta\gamma\delta} \tag{3.27}$$

satisfying the identity

$$(\gamma_5)^2 = 1. \tag{3.28}$$

The equations (3.26) and (3.27) are incompatible in D dimensional regularization and give ambiguous results. Therefore, to remain consistent with the approach used in [34], a unique and well defined construction of γ_5 is considered, called the *t'Hooft-Veltman* dimensional regularization scheme, which defines

$$\gamma_{\ 5} := \frac{i}{4!}\,\epsilon_{\mu\nu\rho\sigma}\,\gamma^\mu\gamma^\nu\gamma^\rho\gamma^\sigma, \tag{3.29}$$

with γ's being D-dimensional, but ϵ being 4-dimensional Levi-Civita tensor. While calculating the square of short distance matrix elements, these ϵ tensors are left untouched, and at the end treated separately in terms of 4 dimensional metric tensors $\tilde{g}^{\mu\nu}$, satisfying contraction properties $\tilde{g}_{\mu\nu}g^{\nu\rho} = \tilde{g}_\mu{}^\rho$, $\tilde{g}_{\mu\nu}p^\nu = \tilde{p}_\mu$, $\tilde{g}^\mu_\mu = 4$, with D dimensional $g^{\nu\rho}$. This definition of γ_5 turns out to be self-consistent and in compliance with, for example, Ward identities.

3.4 Divergences at NLO

For calculating square of the short distance matrix elements perturbatively at next to leading order in QCD, alongwith born level diagrams, we need to consider one loop diagrams for virtual corrections and also the diagrams for real emissions, in D-dimensions.

The one loop diagrams for virtual corrections may contain singularities in their loop integrals, appearing in different regions of the loop momenta. One need to distinguish between the singularities coming from high momentum limit of the loop integral called ultraviolet (UV) divergences and those from zero momentum limit called infrared (IR) singularities. Absorption of the ultraviolet singularities into various parameters appearing in the Lagrangian of the theory in use is a well established fact. This is done by calculating counterterms via dimensional regularization (in $D = 4 - 2\epsilon$, as $\frac{1}{\epsilon}$ terms) and making an appropriate choice of the Z-factors to be multiplied with these parameters of the Lagrangian (renormalization of the parameters). For infrared divergences, the cancellations take place through wave function/field renormalization constants (as $\frac{1}{\epsilon}$ terms) and divergences appearing in real corrections (both as $\frac{1}{\epsilon}$ and $\frac{1}{\epsilon^2}$ terms).

In our QCD calculations, the parameters needed to be renormalized are the charm quark mass m_c, charm quark field ψ and gluon field A, and the strong coupling constant $g_s = \sqrt{4\pi\alpha_s}$ from their definitions;

$$\begin{aligned} m_c^0 &= Z_m m_c, \\ \psi^0 &= \sqrt{Z_\psi}\psi, \\ A_\mu^0 &= \sqrt{Z_A} A_\mu, \\ g_s^0 &= Z_g g_s, \end{aligned} \tag{3.30}$$

where the superscripts 0 indicate the bare quantities and $Z_i = 1 + \delta Z_i$ for $i = m, \psi, A, g$ are the renormalization constants containing counterterms δZ_i, as:

$$\begin{aligned} \delta Z_m^{\rm OS} &= -\frac{3g_s^2}{16\pi^2} C_F C_\epsilon \left[\frac{1}{\epsilon_{\rm UV}} + \frac{4}{3}\right] + \mathcal{O}(\alpha_s^2), \\ \delta Z_\psi^{\rm OS} &= -\frac{g_s^2}{16\pi^2} C_F C_\epsilon \left[\frac{1}{\epsilon_{\rm UV}} + \frac{2}{\epsilon_{\rm IR}} + 4\right] + \mathcal{O}(\alpha_s^2), \\ \delta Z_A^{\rm OS} &= \frac{g_s^2}{48\pi^2} \left(5C_A - 2n_{lf}\right) C_\epsilon \left[\frac{1}{\epsilon_{\rm UV}} - \frac{1}{\epsilon_{\rm IR}}\right] + \mathcal{O}(\alpha_s^2), \\ \delta Z_g^{\overline{\rm MS}} &= \frac{g_s^2}{16\pi^2} \left(-\frac{11}{6} C_A + \frac{1}{3} n_{lf}\right) C_\epsilon \left[\frac{1}{\epsilon_{\rm UV}} + \ln\frac{\mu^2}{m_c^2}\right] + \mathcal{O}(\alpha_s^2), \end{aligned} \tag{3.31}$$

with superscripts indicating the scheme chosen for renormalization as On-Mass-Shell (OS) or modified minimal subtraction ($\overline{\rm MS}$), number of light quark flavors included n_{lf}, the renormalization constant μ, and the symbol C_ϵ defined in eq. (3.23). The counterterms δZ_m and δZ_g are taken care of by including the charm mass counterterm diagrams and the strong vertex counter term diagrams respectively, at $\mathcal{O}(\alpha_s)$. It is important to note that we do not encounter any Coulomb singularities, as argued in [34]. Other details of our calculations will be discussed in the following chapters.

4 J/ψ production with a $c\bar{c}$ pair

The huge amount of data collection at different colliders in recent years supplies a very important opportunity to the physicists for performing a systematic study on J/ψ production, both theoretically and experimentally. Although many dedicated investigations contributed to large improvements achieved in theoretical predictions so far, the experimental data still remain to be fully understood. Alongwith some other production channels as discussed in chapter one, the study of the associated production of J/ψ with a $c\bar{c}$ pair is hoped to provide some missing links between the theory and different experiments. It is, therefore, the main topic of the contents following.
In this chapter, we will investigate all the subprocesses involved in the production of $J/\psi + c\bar{c}$ within NRQCD at DELPHI, HERA-H1, CDF and ATLAS, to present a complete picture of this process at different collider energies. We start with the partonic level calculations for short distance matrix elements with two incoming and three outgoing particles, as:

$$a(k_1) + b(k_2) \to c\bar{c}[n](P) + c(k_3) + \bar{c}(k_4), \tag{4.1}$$

where a, b represent $\gamma, g, q/\bar{q}$ (for $q = u, d, s$) or gluon-ghosts/-antighosts as interacting particles at the initial state, with k_i and P being the corresponding four-momenta of the particles involved in the process above. Based on the conservation of energy-momentum $k_1 + k_2 = P + k_3 + k_4$, we'll now introduce the useful Mandelstam invariants of the process while following closely the notations used in [34].

4.1 Kinematics

Considering the light flavored quarks/antiquarks ($q = u, \bar{u}, d, \bar{d}, s, \bar{s}$) to be massless i.e. $k_1^2 = 0 = k_2^2$, compared to much heavier mass of $c\bar{c}[n]$ state as $P^2 = 4m_c^2$, and $k_3^2 = m_c^2 = k_4^2$, we define:

$$\begin{aligned}
s &\equiv (k_1 + k_2)^2 = 2k_1 \cdot k_2 && (4.2)\\
s_4 &\equiv (P + k_4)^2 - 5m_c^2 = 2P \cdot k_4 && (4.3)\\
s_5 &\equiv (P + k_3)^2 - 5m_c^2 = 2P \cdot k_3 && (4.4)\\
s_3 &\equiv (k_3 + k_4)^2 = 2k_3 \cdot k_4 + 2m_c^2 && (4.5)\\
t1 &\equiv (P - k_1)^2 - 4m_c^2 = -2P \cdot k_1 && (4.6)\\
u1 &\equiv (P - k_2)^2 - 4m_c^2 = -2P \cdot k_2 && (4.7)\\
t_6 &\equiv (k_2 - k_3)^2 - m_c^2 = -2k_2 \cdot k_3 && (4.8)
\end{aligned}$$

$$u_6 \equiv (k_1 - k_3)^2 - m_c^2 = -2k_1 \cdot k_3 \tag{4.9}$$
$$t' \equiv (k_1 - k_4)^2 - m_c^2 = -2k_1 \cdot k_4 \tag{4.10}$$
$$u' \equiv (k_2 - k_4)^2 - m_c^2 = -2k_2 \cdot k_4, \tag{4.11}$$

with charm quark having mass m_c. Here s, t_1, and u_1 can be used to additionally define:

$$s_1 \equiv s - 4m_c^2 \tag{4.12}$$
$$t \equiv t_1 + 4m_c^2 \tag{4.13}$$
$$u \equiv u_1 + 4m_c^2, \tag{4.14}$$

for the completion of the set of Mandelstam variables. For the process (4.1) with three particles in the final state, only five of the invariants are linearly independent, out of all the invariants defined above. All the quantities appearing in our calculations will be expressed in terms of these variables. With only tree level Feynman diagrams, and only heavy (massive) particles in the final state, we do not have to deal with any singularities appearing. Therefore, in this section, we can perform our further calculations in four dimensions.

4.2 Partonic Differential Cross Section

In order to reach the formula (3.1) through (3.5), we work systematically according to the formalism described in the previous chapter. We, therefore, have to start from the calculation of the partonic cross section (3.7), which needs perturbatively calculated short distance matrix elements. For this purpose, we consider the following subprocesses:

$$\gamma + \gamma \to c\bar{c}[n] + c + \bar{c}, \tag{4.15}$$
$$\gamma + g \to c\bar{c}[n] + c + \bar{c}, \tag{4.16}$$
$$g + g \to c\bar{c}[n] + c + \bar{c}, \tag{4.17}$$
$$q + \bar{q} \to c\bar{c}[n] + c + \bar{c}, \tag{4.18}$$

with particles having momenta as per eq.(4.1) with $q = u, d, s$, $\bar{q} = \bar{u}, \bar{d}, \bar{s}$. Remember that all the incoming particles are taken to be on mass shell. These subprocesses involve 40, 48, 72 and 14 Feynman diagrams, respectively. For making use of eq.(3.24) for gluons, the process with gluon-ghost and gluon-antighost in the initial state has also to be considered, and its contribution later subtracted from (4.17). The number of Feynman diagrams is 14 for this subprocess. Figures 4.1-4.4 show typical diagrams for these subprocesses.

The two charm quarks and two anticharm quarks generated in the final state of these Feynman diagrams can utilize different permutations to bind together as $c\bar{c}[n]$ both in color-singlet and color-octet states, and the left over come out as an open charm-anticharm pair.

For the evaluation of the squared matrix elements analytically, we have used the same format of programming codes as by [34], also partly using some of the modified sections of their scripts. We first generate the Feynman diagrams for all the partonic subprocesses

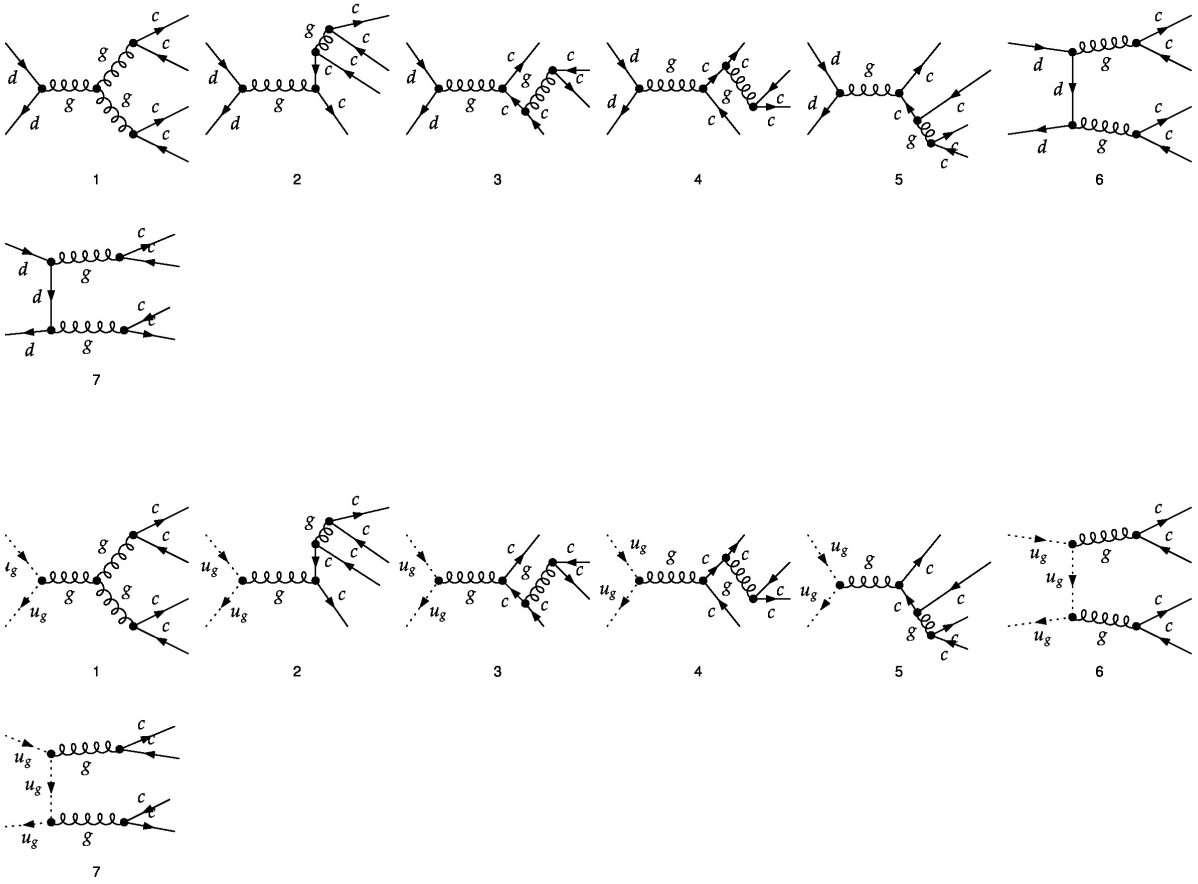

Figure 4.1: Half of the Feynman diagrams for subprocesses $q + \bar{q} \to c\bar{c}[n] + c + \bar{c}$ and $u_g + \bar{u}_g \to c\bar{c}[n] + c + \bar{c}$ where u_g represents gluon-ghost and $q/\bar{q}$ denote u, d, s quarks and the corresponding antiquarks. The other half can be obtained by reversing the fermion lines.

using FeynArts [35]. A Mathematica based script then reads the amplitude files created by FeynArts, separates out color structure for each of the diagram and then applies color and spin projectors on these separated parts of the various $c\bar{c}[n]$ states' amplitudes, as described in the covariant projectors section of the previous chapter. The FeynCalc [36] is used in this script to calculate all the color traces, categorizing different $c\bar{c}[n]$ states into color singlet and color octet ones, separating also the $S-$ and $P-$wave contributions. A FORM [37] script then calculates the amplitude squares by multiplying the separated non-color part with its complex conjugate, taking care of the polarization summation and fermion traces, and recombining the outcome for every combination of diagrams with the separately calculated corresponding color factors. Further simplification of these results is done using another Mathematica script. The results are expressed in terms of the Mandelstam variables defined above. At this stage, we could compare our

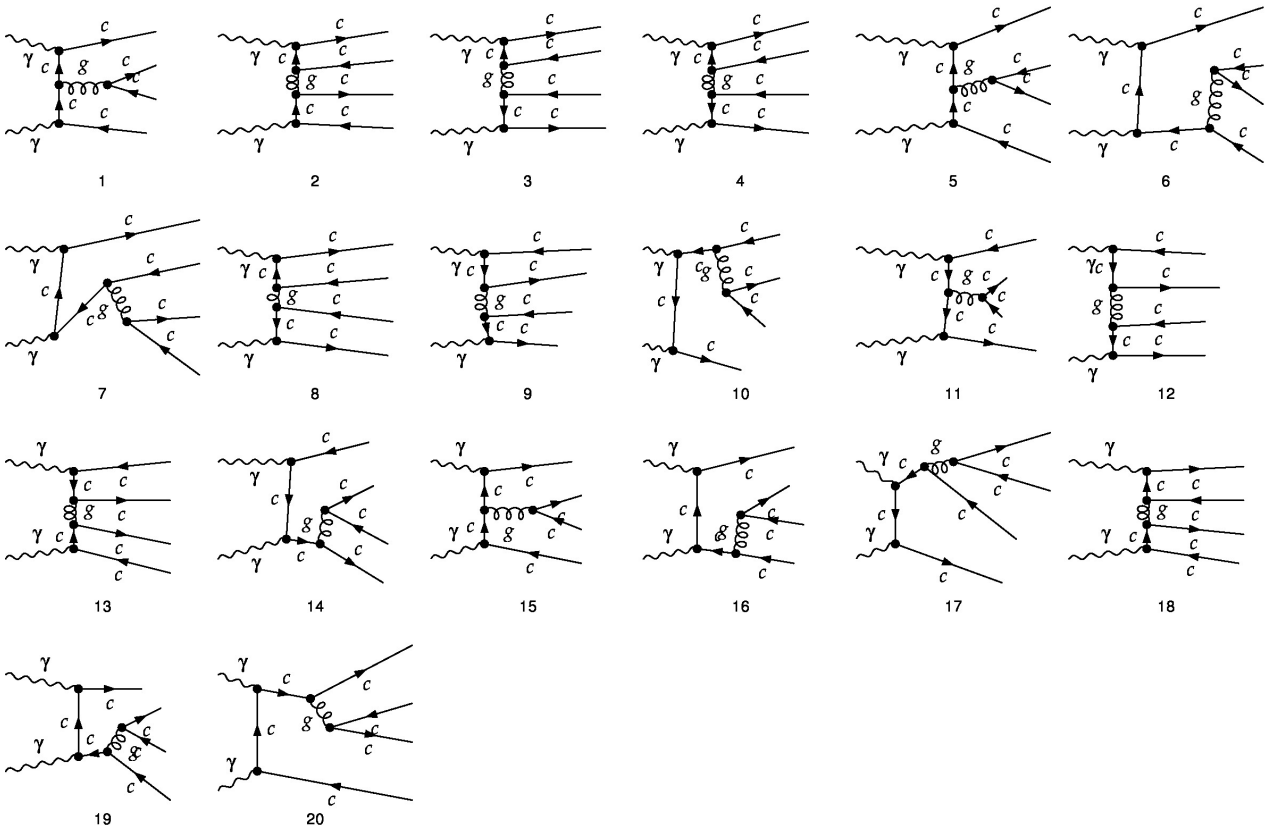

Figure 4.2: Half of the Feynman diagrams for subprocess $\gamma + \gamma \to c\bar{c}[n] + c + \bar{c}$.

analytical results with MadOnia [38] and check the validity of our codes. Mathematica is used again to finally convert these results as FORTRAN routines, to perform numerical analysis using VEGAS for phase space integrations.

4.2.1 Phase Space Integration

Another important quantity left to be calculated in (3.7) is the phase space. We have to deal with $2 \to 3$ particle phase space, for all of the final state particles being heavily massive. To start with the general formula for f final state particles [39]:

$$dPS_{i+j\to\sum f} = \prod_f \frac{d^3k_f}{(2\pi)^3}\frac{1}{2E_f}(2\pi)^4\delta^{(4)}(k_i + k_j - \sum k_f), \tag{4.19}$$

the explicit expression for our differential phase space is:

$$dPS_{2\to3} = \frac{d^3P}{(2\pi)^3 2E_{J/\psi}}\frac{d^3k_c}{(2\pi)^3 2E_c}\frac{d^3k_{\bar{c}}}{(2\pi)^3 2E_{\bar{c}}}(2\pi)^4\delta^{(4)}(k_i + k_j - P - k_c - k_{\bar{c}}). \tag{4.20}$$

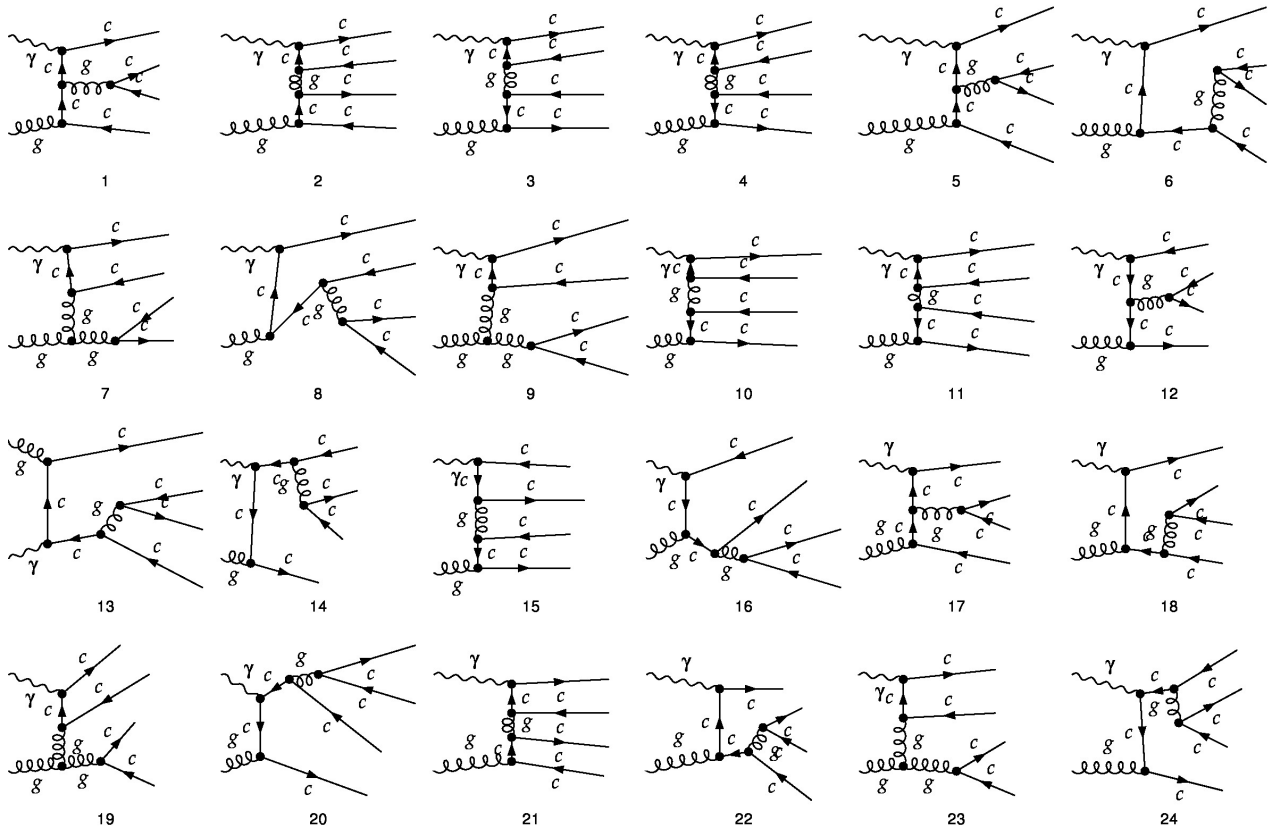

Figure 4.3: Half of the Feynman diagrams for subprocess $\gamma + g \to c\bar{c}[n] + c + \bar{c}$.

For $k_{c\bar{c}} := k_c + k_{\bar{c}}$ and $k_{c\bar{c}}^2 = s_3$, we can insert the identity [40];

$$1 = \delta(k_{c\bar{c}}^2 - s_3)ds_3 \times \delta^{(4)}(k_{c\bar{c}} - k_c - k_{\bar{c}})d^4k_{c\bar{c}} \tag{4.21}$$

into eq.(4.20) and replacing;

$$\frac{d^3k}{2E_k} \to d^4k\delta(k^2 - m_k^2) \tag{4.22}$$

eq.(4.20) can then be factorized as:

$$dPS_{2\to3} = \frac{1}{(2\pi)^5} \times dPS_{2\to2}^* \times dPS_{1\to2}^{'} \times ds_3, \tag{4.23}$$

where

$$dPS_{2\to2}^* \equiv \frac{d^3P}{2E_{J/\psi}} \frac{d^3k_{c\bar{c}}}{2E_c\bar{c}} \delta^{(4)}(k_i + k_j - P - k_{c\bar{c}}) \tag{4.24}$$

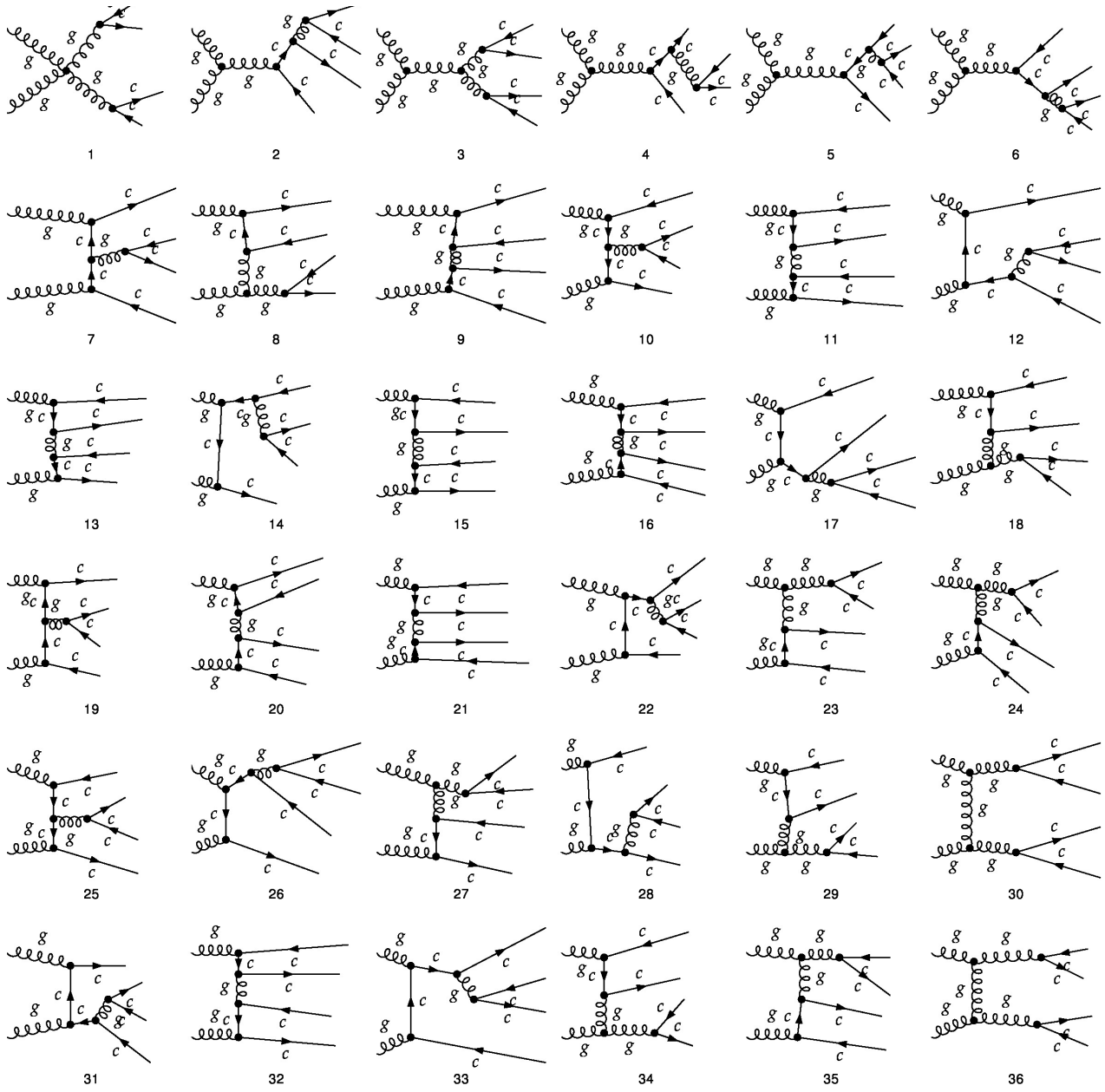

Figure 4.4: Half of the Feynman diagrams for subprocess $g + g \to c\bar{c}[n] + c + \bar{c}$.

$$dPS'_{1\to 2} \equiv \frac{d^3k_c}{2E_c}\frac{d^3k_{\bar{c}}}{2E_{\bar{c}}}\delta^{(4)}(k_{c\bar{c}} - k_c - k_{\bar{c}}). \tag{4.25}$$

So that this simpler expression for the $2 \to 3$ body phase space makes it easier for evaluation. In order to calculate $dPS^*_{2\to 2}$ in the center-of-mass system of the incoming particles, we parametrize the momenta as:

$$\begin{aligned} k_i &= \frac{\sqrt{s}}{2}(1,0,0,1)\,, \\ k_j &= \frac{\sqrt{s}}{2}(1,0,0,-1)\,, \\ P &= \left(E_{J/\psi}, 0, p_{J/\psi}\sin\theta, p_{J/\psi}\cos\theta\right) \end{aligned} \tag{4.26}$$

where in terms of the Mandelstam variables:

$$\begin{aligned} E_{J/\psi} &= \frac{t+u-8m_c^2}{-2\sqrt{s}}, \\ p_{J/\psi} &= \sqrt{E^2_{J/\psi} - 4m_c^2}, \\ \cos\theta &= \frac{t-u}{2\sqrt{s}p_{J/\psi}}. \end{aligned} \tag{4.27}$$

We then change the integration variables $(p_{J/\psi}, \cos\theta)$ also into Mandelstam variables (t,u) making use of the Jacobian, and integrate over one of the delta functions, to get:

$$\begin{aligned} dPS^*_{2\to 2} &= \frac{1}{2E_{J/\psi}}p^2_{J/\psi}dp_{J/\psi}d(\cos\theta)d\varphi\delta(s+t+u-4m_c^2-s_3) \\ &= \frac{1}{4s}dtdud\varphi\delta(s+t+u-4m_c^2-s_3) \end{aligned} \tag{4.28}$$

Since the cross section does not depend on azimuthal angle of J/ψ, we therefore integrate over $d\varphi$ in the limit $0 \to 2\pi$. Integrating also over delta function for one of the variables, we get:

$$dPS^*_{2\to 2} = \frac{\pi}{2s}dt, \tag{4.29}$$

with $s+t+u = 4m_c^2 + s_3$. Now for the calculation of $dPS'_{1\to 2}$, we parametrize the particle momenta in the rest frame of the open c and $\bar{c}$ quarks, as

$$\begin{aligned} k'_i &= E'_i(1,0,\sin\theta'_1,\cos\theta'_1) \\ k'_j &= (E'_j, 0, -E'_i\sin\theta'_1, p'_{J/\psi} - E'_i\cos\theta'_1) \\ P' &= (E'_{J/\psi}, 0, 0, p'_{J/\psi}) \\ k'_{c\bar{c}} &= (\sqrt{s_3}, 0, 0, 0) \\ k'_c &= (E'_c, |\vec{k}'_c|\sin\theta'\sin\varphi', |\vec{k}'_c|\sin\theta'\cos\varphi', |\vec{k}'_c|\cos\theta') \\ k'_{\bar{c}} &= (E'_{\bar{c}}, |\vec{k}'_{\bar{c}}|\sin\theta'\sin\varphi', |\vec{k}'_{\bar{c}}|\sin\theta'\cos\varphi', |\vec{k}'_{\bar{c}}|\cos\theta'), \end{aligned} \tag{4.30}$$

for $|\vec{k}^{'}_{c/\bar{c}}| = E^{'}_{c/\bar{c}} - m_c^2$ with $E^{'}_c = E^{'}_{\bar{c}}$, $|\vec{k}^{'}_c| = -|\vec{k}^{'}_{\bar{c}}|$ and making use of Mandelstam variables again

$$\begin{aligned} E^{'}_i &= \frac{s+t_1}{2\sqrt{s_3}} \,, \\ E^{'}_j &= \frac{s_3-t}{2\sqrt{s_3}} \,, \\ E^{'}_{J/\psi} &= \frac{s-s_3-4m_c^2}{2\sqrt{s_3}} \,, \end{aligned} \tag{4.31}$$

where the other variables also expressed in terms of the already defined Mandelstam variables as:

$$\begin{aligned} p^{'}_{J/\psi} &= \sqrt{E^{'2}_{J/\psi} - 4m_c^2} \,, \\ \cos\theta^{'}_1 &= \frac{1}{p^{'}_{J/\psi}} \left(E^{'}_{J/\psi} + \frac{t_1}{2E^{'}_i} \right) \,, \\ \cos\theta^{'} &= \frac{1}{p^{'}_{J/\psi}} \left(\frac{s_4 - \sqrt{s_3} E^{'}_{J/\psi}}{\sqrt{s_3 - 4m_c^2}} \right) \,, \\ \cos\varphi^{'} &= \frac{1}{\sin\theta^{'}_1 \sin\theta^{'}} \left(\frac{u_6}{E^{'}_i} + \sqrt{s_3} - \sqrt{s_3 - 4m_c^2} \cos\theta^{'}_1 \cos\theta^{'} \right) . \end{aligned} \tag{4.32}$$

Now using the relation $\int \frac{d^4k}{2E_k} \to \int d^3k \delta(k^2 - m_k^2)\theta(k_0)$ in eq.(4.25) and integrating over $\delta^4(k_{c\bar{c}} - k_c - k_{\bar{c}})$ for $k_{\bar{c}} = k_{c\bar{c}} - k_c$, we get;

$$\begin{aligned} dPS^{'}_{1\to 2} &= \frac{d^3k^{'}_c}{2E_c^{'}} \delta\left((k^{'}_{c\bar{c}} - k^{'}_c)^2 - m_c^2 \right) \\ &= \frac{1}{2} |\vec{k}^{'}_c| \delta(s_3 - 2\sqrt{s_3} E^{'}_c) dE^{'}_c d(\cos\theta^{'}) d\varphi^{'} \\ &= \frac{1}{4\sqrt{s_3}} \sqrt{E^{'2}_c - m_c^2}\, \delta(E^{'}_c - \frac{\sqrt{s_3}}{2}) dE^{'}_c d(\cos\theta^{'}) d\varphi^{'} \\ &= \frac{\sqrt{s_3 - 4m_c^2}}{8\sqrt{s_3}} d(\cos\theta^{'}) d\varphi^{'} , \end{aligned} \tag{4.33}$$

with $E^{'}_c = \frac{\sqrt{s_3}}{2} = E^{'}_{\bar{c}}$.

The $2 \to 3$ particles phase space in eq.(4.23) then becomes,

$$dPS_{2\to 3} = \frac{1}{(2\pi)^5} \times \frac{\pi}{2s} dt \times \frac{\sqrt{s_3 - 4m_c^2}}{8\sqrt{s_3}} d(\cos\theta^{'}) d\varphi^{'} \times ds_3 \tag{4.34}$$

that we can use in eq.(3.7) alongwith the calculated matrix elements squares as prescribed above to calculate the partonic cross section, as:

$$d\hat{\sigma}(i+j \to c\bar{c}[n] + c + \bar{c}) = \frac{1}{2s} dPS_{2\to 3} \frac{1}{N_{col,in} N_{pol,in}} \sum_{col,pol} |\mathcal{M}(i+j \to c\bar{c}[n] + c + \bar{c})|^2 \,,$$

$$d\hat{\sigma}(i+j \to c\bar{c}[n]+c+\bar{c}) = \frac{\pi\sqrt{1-4m_c^2/s_3}}{(2\pi)^5 32 s^2} dt ds_3 d(\cos\theta^{'}) d\varphi^{'} \times \frac{1}{N_{col,in}N_{pol,in}} \sum_{col,pol} |\mathcal{M}(i+j \to c\bar{c}[n]+c+\bar{c})|^2. \quad (4.35)$$

The integration limits over the variables involved in the phase space formula are [40]:

$$2m_c < \sqrt{s_3} < \sqrt{s} - 2m_c, \quad -1 < \cos\theta^{'} < 1, \quad 0 < \varphi^{'} < 2\pi. \quad (4.36)$$

Now we have all our expressions in terms of Mandelstam invariants, and can implement these for the calculation of hadronic cross section for each of the subprocesses involved, dependent on the integration variables.

4.3 Hadronic Differential Cross-Section

In order to compare our results with the experimentally available quantities, we calculate the hadronic cross section with respect to different variables, using eq.(3.1). To investigate a general kinematical situation in the center of mass of the incoming particles, we consider the interaction process depicted in the figure 4.5. The incoming particles radiate two bremsstrahlung photons, one off e^+ and the other off e^-, with momenta $k_1 = x_{g_1}k_{e^+}$ and $k_2 = x_{g_2}k_{e^-}$. Each of these photons then emits a parton of momentum $k_a = x_a k_1$ and $k_b = x_b k_2$ respectively, which interact on the partonic level to produce J/ψ with an associated $c\bar{c}$ pair. This picture actually represents the so called 'double-resolved' subprocess, which we have discussed previously. The momenta of the particles involved in the reaction are parametrized as:

$$\begin{aligned}
k_{e^+} &= \frac{\sqrt{S_H}}{2}(1,0,0,1) \\
k_{e^-} &= \frac{\sqrt{S_H}}{2}(1,0,0,-1) \\
k_1 &= x_{g_1}\frac{\sqrt{S_H}}{2}(1,0,0,1) \\
k_2 &= x_{g_2}\frac{\sqrt{S_H}}{2}(1,0,0,-1) \\
k_a &= x_a x_{g_1}\frac{\sqrt{S_H}}{2}(1,0,0,1) \\
k_b &= x_b x_{g_1}\frac{\sqrt{S_H}}{2}(1,0,0,-1) \\
P &= (m_t \mathrm{cosh}y,\ p_t \mathrm{cos}\phi,\ p_t \mathrm{sin}\phi\ , m_t \mathrm{sinh}y)
\end{aligned} \quad (4.37)$$

where S_H is the hadronic center of mass energy, p_t and $m_t \equiv \sqrt{p_t^2 + 4m_c^2}$ the transverse momentum and transverse mass of the J/ψ, and y being its rapidity. Since we have expressed all our calculations in terms of the Mandelstam variables, so here we need to

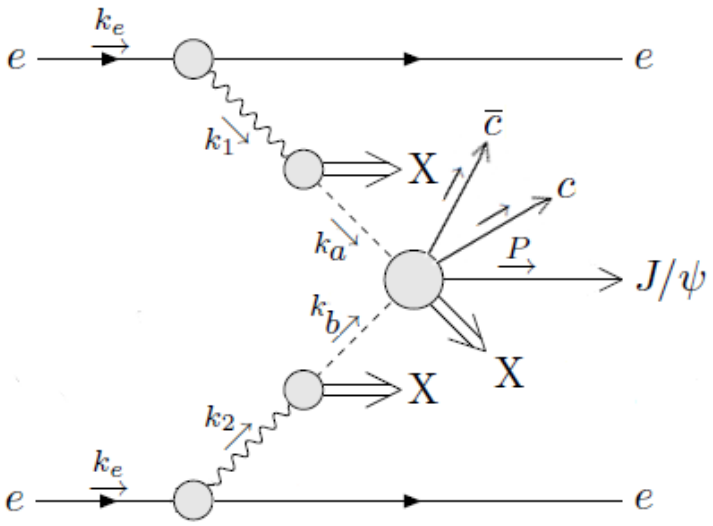

Figure 4.5: Diagramatic representation of the kinematics involved in hadronic cross section

define them as:

$$s = (k_a + k_b)^2 = x_a x_b x_{g_1} x_{g_2} S_H \tag{4.38}$$

$$t = (P - k_a)^2 = 4m_c^2 - x_a x_{g_1} \sqrt{S_H} m_t e^{-y} \tag{4.39}$$

$$u = (P - k_b)^2 = 4m_c^2 - x_b x_{g_2} \sqrt{S_H} m_t e^{+y}. \tag{4.40}$$

Using the relation $s + t + u = 4m_c^2 + s_3$ for $2 \to 3$ processes, as derived during phase space calculations, we can rearrange the equations describing t and u as:

$$x_{g_1} x_a = \frac{x_b x_{g_2} m_t \sqrt{S_H} e^{+y} - 4m_c^2 + s_3}{x_b x_{g_2} S_H - m_t \sqrt{S_H} e^{-y}}, \tag{4.41}$$

and analogously:

$$x_{g_2} x_b = \frac{x_a x_{g_1} m_t \sqrt{S_H} e^{-y} - 4m_c^2 + s_3}{x_a x_{g_1} S_H - m_t \sqrt{S_H} e^{+y}}. \tag{4.42}$$

These equations are used to change the integration variables and set the corresponding integration limits, as per the conditions governing the interaction process. The general form of hadronic cross sections is then as presented in eq.(3.1), for a double-resolved subprocess at e^+e^- colliders. We'll now discuss different subprocesses at various detectors to for associated J/ψ production with a $c\bar{c}$ pair, and will present the kinematical relations and the limits on them calculated analytically, for the experiments to be considered later in this chapter.

Photoproduction at $e^+e^-/\gamma\gamma$ Colliders:

Three classes of subprocesses are involved there in $\gamma+\gamma \to J/\psi+c+\bar{c}+X$ for example at DELPHI. These are direct, single- and double-resolved processes. For a thorough investigation of the process considered, the subprocesses needed to be included in are:

$$\gamma+\gamma \to J/\psi+c+\bar{c}, \tag{4.43}$$
$$\gamma+g \to J/\psi+c+\bar{c}, \tag{4.44}$$
$$g+g \to J/\psi+c+\bar{c}, \tag{4.45}$$
$$q+\bar{q} \to J/\psi+c+\bar{c}, \tag{4.46}$$

with gluon-ghost contributions to be subtracted from the $g+g$ interaction. So the general expression for the differential cross section (via double-resolved process), after change of variables from (t, x_{g_2}) to (y, p_t^2) is given by:

$$\frac{d\sigma}{dp_t^2 dy} = \int_{x_{a,min}}^{1} dx_a \int_{x_{b,min}}^{1} dx_b \int_{x_{g_1,min}}^{1} dx_{g_1} \frac{d\sigma}{dp_t^2 dy dx_a dx_b dx_{g_1}} \tag{4.47}$$

with integration limits as:

$$x_{b,min} = \frac{x_a x_{g_1} m_t e^{-y}}{x_a x_{g_1}\sqrt{S_H} - m_t e^{+y}} \tag{4.48}$$
$$x_{a,min} = \frac{m_t e^{+y}}{x_{g_1}(\sqrt{S_H} - m_t e^{-y})} \tag{4.49}$$
$$x_{g_1,min} = \frac{m_t e^{+y}}{\sqrt{S_H} - m_t e^{-y}}. \tag{4.50}$$

Integrating further over one of the variables y or p_t^2 can give a differential cross-section as a function of only one variable. For $\frac{d\sigma}{dp_t^2}$ we integrate over y under the limits:

$$-\cosh^{-1}\left(\frac{\sqrt{S_H}}{2m_t}\right) \leq y \leq +\cosh^{-1}\left(\frac{\sqrt{S_H}}{2m_t}\right) \tag{4.51}$$
$$p_t \leq \sqrt{\frac{S_H}{4} - 4m_c^2} \tag{4.52}$$

or for $\frac{d\sigma}{dy}$, the integration limits become:

$$p_t \leq \sqrt{\frac{S_H}{4\cosh^2 y} - 4m_c^2} \tag{4.53}$$
$$-\cosh^{-1}\left(\frac{\sqrt{S_H}}{4m_c}\right) \leq y \leq +\cosh^{-1}\left(\frac{\sqrt{S_H}}{4m_c}\right). \tag{4.54}$$

The additional three integrations over s_3, $\cos\theta'$ and φ' are contained through the integration ranges:

$$4m_c^2 \leq s_3 \leq 4m_c^2 + x_b(x_a x_{g_1} S_H - \sqrt{S_H} m_t e^{+y}) - x_a x_{g_1}\sqrt{S_H} m_t e^{-y}, \tag{4.55}$$
$$-1 < \cos\theta' < 1, \quad 0 < \varphi' < 2\pi. \tag{4.56}$$

For the other subprocesses involved, we can use the same expressions with little modifications. In case of a single-resolved process, we have either $x_a = 1$ or $x_b = 1$. So we have one less integration in the eq.(4.47), and the limits change accordingly. For direct photoproduction, both $x_a = 1 = x_b$, reducing two integrals in the eq.(4.47) with appropriate bounds. The role played by these integration limits is to encompass the parameter space which is kinematically accessible. While performing the actual integrations numerically, additional cuts are applied from the experimental measurements to compare both the results.

Photoproduction at ep Colliders:
The classes of direct and resolved subprocesses at partonic level considered for these situations are:

$$\gamma + g \to J/\psi + c + \bar{c}, \tag{4.57}$$
$$g + g \to J/\psi + c + \bar{c}, \tag{4.58}$$
$$q + \bar{q} \to J/\psi + c + \bar{c}, \tag{4.59}$$

where the gluon in $\gamma + g$ interaction stems from proton, thus indicating a proton PDF also involved in the process, alongwith the photon PDF for resolved process. Subtraction of gluon-ghost contributions from the $g + g$ interaction is mandatory in our approach. In this case, we define two additional parameters,i.e. the photon-proton invariant mass, and the fraction of the photon energy transferred further to the J/ψ particle in the proton rest frame, respectively as:

$$W^2 \equiv (k_1 + k_{proton})^2 = x_{g_1} S_H, \tag{4.60}$$
$$z \equiv \frac{P \cdot k_{proton}}{k_1 \cdot k_{proton}} = \frac{m_t e^y}{x_{g_1} S_H}. \tag{4.61}$$

Making a shift of integration variables from (x_{g_1}, x_{g_2}, t) to (W, z, p_t^2), the formula (3.1) for resolved process then gets the form in terms of these new variables as:

$$\frac{d\sigma}{dW\,dz\,dp_T^2} = \int_{x_{a,min}}^{1} dx_a \int_{x_{b,min}}^{1} dx_b \frac{d\sigma}{dW\,dz\,dp_T^2\,dx_a\,dx_b} \tag{4.62}$$

, where we can further integrate over any two of the variables and get the differential cross-section with respect to one of the variables W, z or p_t left. The limits of integration involved are then listed as:

$$x_{b,min} = \frac{x_{g_1} x_a \sqrt{S_H} m_t e^{-y} - 4m_c^2 + s_3}{x_{g_1} x_a S_H - m_t \sqrt{S_H} e^{+y}}$$
$$x_{a,min} = \frac{m_t e^{+y}}{x_{g_1}(\sqrt{S_H} - m_t e^{-y})}$$
$$W_{min} = \sqrt{\frac{m_t^2}{z(1-z)}}$$
$$z_{min} = \frac{1}{2S_H}(S_H - \sqrt{S_H^2 - 4S_H m_t^2})$$

$$
\begin{aligned}
z_{max} &= \frac{1}{2S_H}(S_H + \sqrt{S_H^2 - 4S_H m_t^2}) \\
z'_{min} &= \frac{1}{2W^2}(W^2 - \sqrt{W^4 - 4W^2 m_t^2}) \\
z'_{max} &= \frac{1}{2W^2}(W^2 + \sqrt{W^4 - 4W^2 m_t^2}) \\
p_{t,max}^2 &= z(1-z)S_H - 4m_c^2 \\
p_{t,max}^{2'} &= \frac{W^2 - 16m_c^2}{4}.
\end{aligned} \tag{4.63}
$$

As per our earlier discussion, we also need to utilize the range of some other variables during our calculations like,

$$
\begin{aligned}
\frac{m_t^2}{S_H z(1-z)} &\leq x_{g_1} \leq 1 \,, \\
4m_c^2 &\leq s_3 \leq x_{g_1} S_H (x_a - z) - \frac{x_a m_t^2}{z} + 4m_c^2.
\end{aligned} \tag{4.64}
$$

Again the argument stands for use of all the above relations and integration limits in case of direct photoproduction (when the photon originating from electron itself interacts with the parton stemming from the proton). It is achieved by putting $x_a = 1$, and leaving out integration over it. Additional experimental limits are implemented during numerical evaluation of these expressions.

Hadroproduction at $pp/p\bar{p}$ Colliders:
In case of the hadroproduction of charmonium, the most dominant process is the gluon-gluon interaction. But for the sake of completeness, all the possible initial state particles will be considered. The subprocesses studied, therefore, are:

$$g + g \rightarrow J/\psi + c + \bar{c}, \tag{4.65}$$
$$q + \bar{q} \rightarrow J/\psi + c + \bar{c}, \tag{4.66}$$

and obviously the gluon- ghost-antighost contribution to be subtracted. Here the initial partons in both of these processes are emitted from the each of the proton/antiproton. So that the set of PDF used is that of proton. We are mainly interested in the calculation of differential cross section with respect to the transverse momentum of J/ψ. The analytical expressions involved can be obtained from the double-resolved process of the photoproduction section at the $e^+e^-/\gamma\gamma$ colliders (eq.4.49-4.58). The main difference is that we have to take $x_a = 1 = xb$, while x_{g_1}/x_{g_2} in this case represent the fraction of the parton momenta to that of the proton. The number of integrals involved also reduces accordingly, and so do the integration limits on the variables considered.
In the following section, we shall discuss the input parameters taken including the long distance matrix elements and shall present the numerical results of the integrations performed.

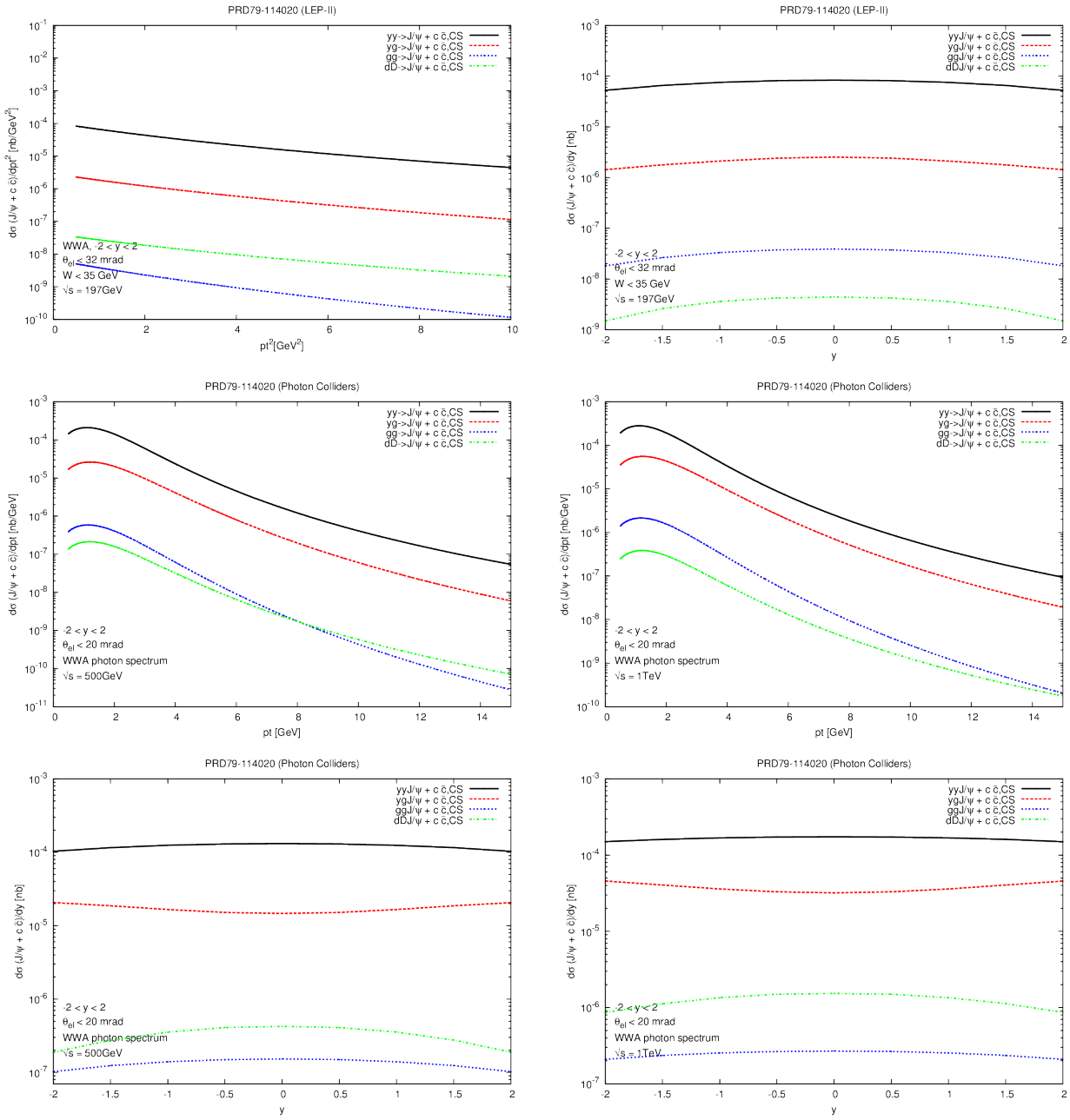

Figure 4.6: Verification of existing literature-1.

4.4 Numerical Analysis

We use a FORTRAN code to perform the phase space integrations numerically. This is done by implementing the integration routine VEGAS[41], based on importance sampling, into our FORTRAN code. During the computation process, the most time consuming of the subprocesses were those with more number of gluons involved. Here we start with the specification of the input parameters used generally in our analysis.

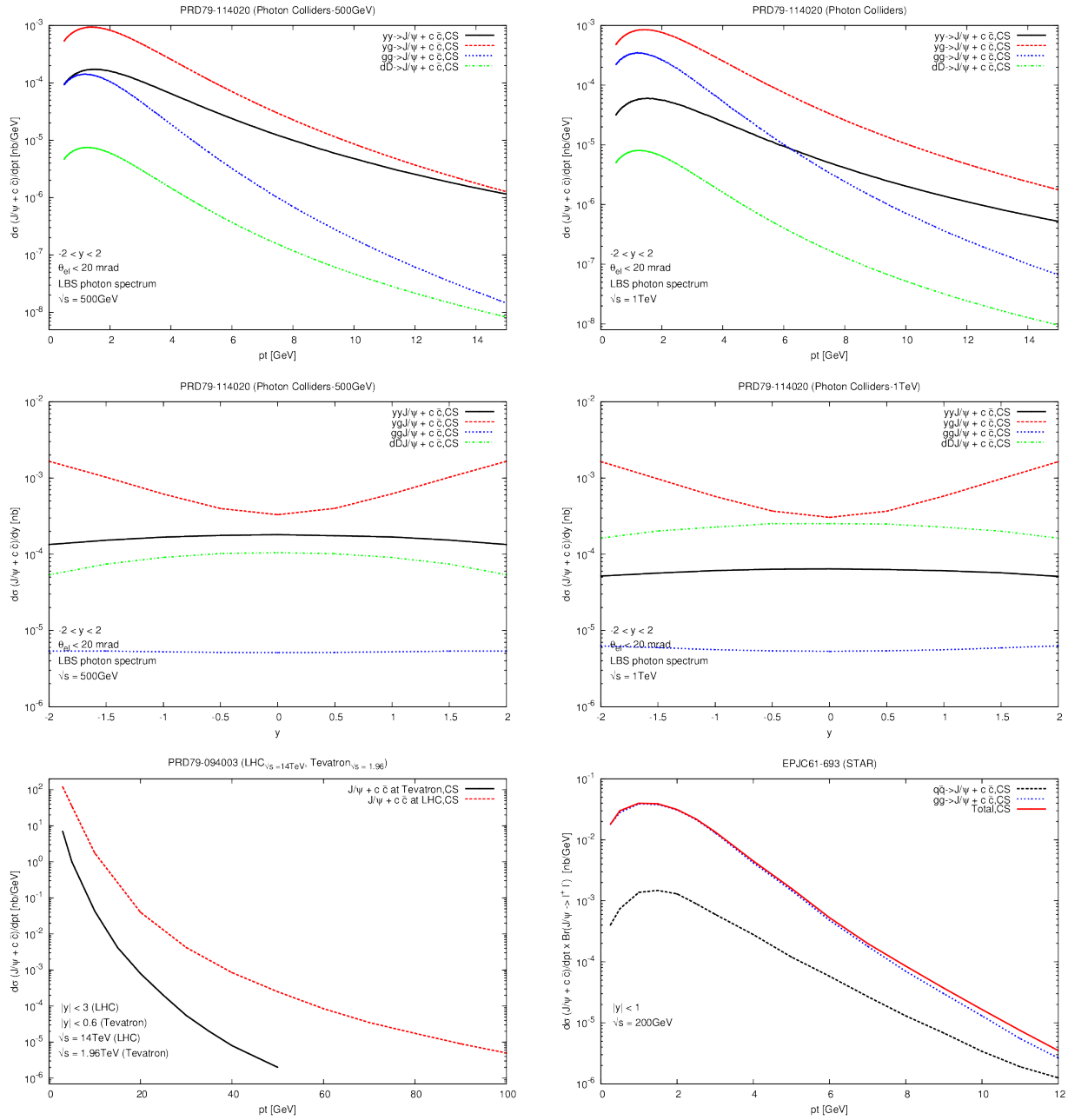

Figure 4.7: Verification of existing literature-2.

General Parameters: We want to compare our results with the inclusive J/ψ production cross section without considering the $J/\psi + c + \bar{c}$ contribution, presented in MB [13]. Therefore, we shall be using mainly the same values for input parameters as in that paper. From the particle data group [1], values for the following parameters are extracted:

The electromagnetic fine structure constant with elementary charge e,

$$\alpha = \frac{e^2}{4\pi} = \frac{1}{137.036}; \tag{4.67}$$

mass of the electron,

$$m_e = 0.51100\text{keV}; \tag{4.68}$$

mass of the charm quark defined as $m_c \equiv \frac{M_{J/\psi}}{2}$, having value

$$m_c = \frac{3.0969}{2}\text{GeV}. \tag{4.69}$$

For the set of photon PDFs, we use AFG04[42] while for proton PDFs, CTEQ6M[43] is used for proton PDFs. Since the cross section is already of $\mathcal{O}(\alpha_s)$, the running coupling constant $\alpha_s(\mu_r^2)$ is taken to be with two loop formula, as:

$$\alpha_s(\mu_r^2) = \frac{4\pi}{\beta_0}\left[\frac{1}{\log(\frac{\mu_r^2}{\Lambda^2})} - \frac{\beta_1}{\beta_0^2}\frac{\log\log(\frac{\mu_r^2}{\Lambda^2})}{(\frac{\log(\mu_r^2)}{\Lambda^2})^2}\right], \tag{4.70}$$

for QCD beta $\beta_0 = 11 - \frac{2}{3}n_f$ and the two-loop coefficient of the QCD beta function as $\beta_1 = 51 - \frac{19}{3}n_f$ for $n_f = 4$, $\Lambda^{(4)}_{QCD} = 0.326\text{GeV}$.

Long Distance Matrix Elements: For the LDMEs, we shall again be using the values given by the global fit in [13] for color octet contributions, with feed down contributions from the higher charmonium states. The table below shows the list of operators used with their corresponding values.

CO LDME	with feed − downs
$\langle\mathcal{O}^{J/\psi}[^1S_0^{[8]}]\rangle$	4.97 $\times 10^{-2}$ GeV^3
$\langle\mathcal{O}^{J/\psi}[^3S_1^{[8]}]\rangle$	2.24 $\times 10^{-3}$ GeV^3
$\langle\mathcal{O}^{J/\psi}[^3P_0^{[8]}]\rangle$	-1.61 $\times 10^{-3}$ GeV^5

These values alongwith the value for CS LDME i.e. $\langle\mathcal{O}^{J/\psi}[^3S_1^{[1]}]\rangle = 1.32\text{GeV}^3$, will be used in all of our calculations. The other parameters used for different experiments are mentioned in their respective sections below.

4.4.1 LEPII-DELPHI:

For comparison with DELPHI data, we first chose the input parameters according to the second paper in ref. [11] i.e. $\langle\mathcal{O}^{J/\psi}[^3S_1^{[1]}]\rangle = 1.4\text{GeV}^3$, $\alpha = \frac{1}{137}$, $m_c = 1.5\text{GeV}$, $m_e = 0.511\text{GeV}$, with similar photon PDFs from GRS99 and α_s running evaluated

using the LO formula of GRV98. $m_t = \sqrt{p_t^2 + 4m_c^2}$ taken to fix the renormalization and factorization scales, and the results multiplied with a factor of 1.278 to include the feed-down contributions from ψ'. Our color singlet (CS) contributions match their

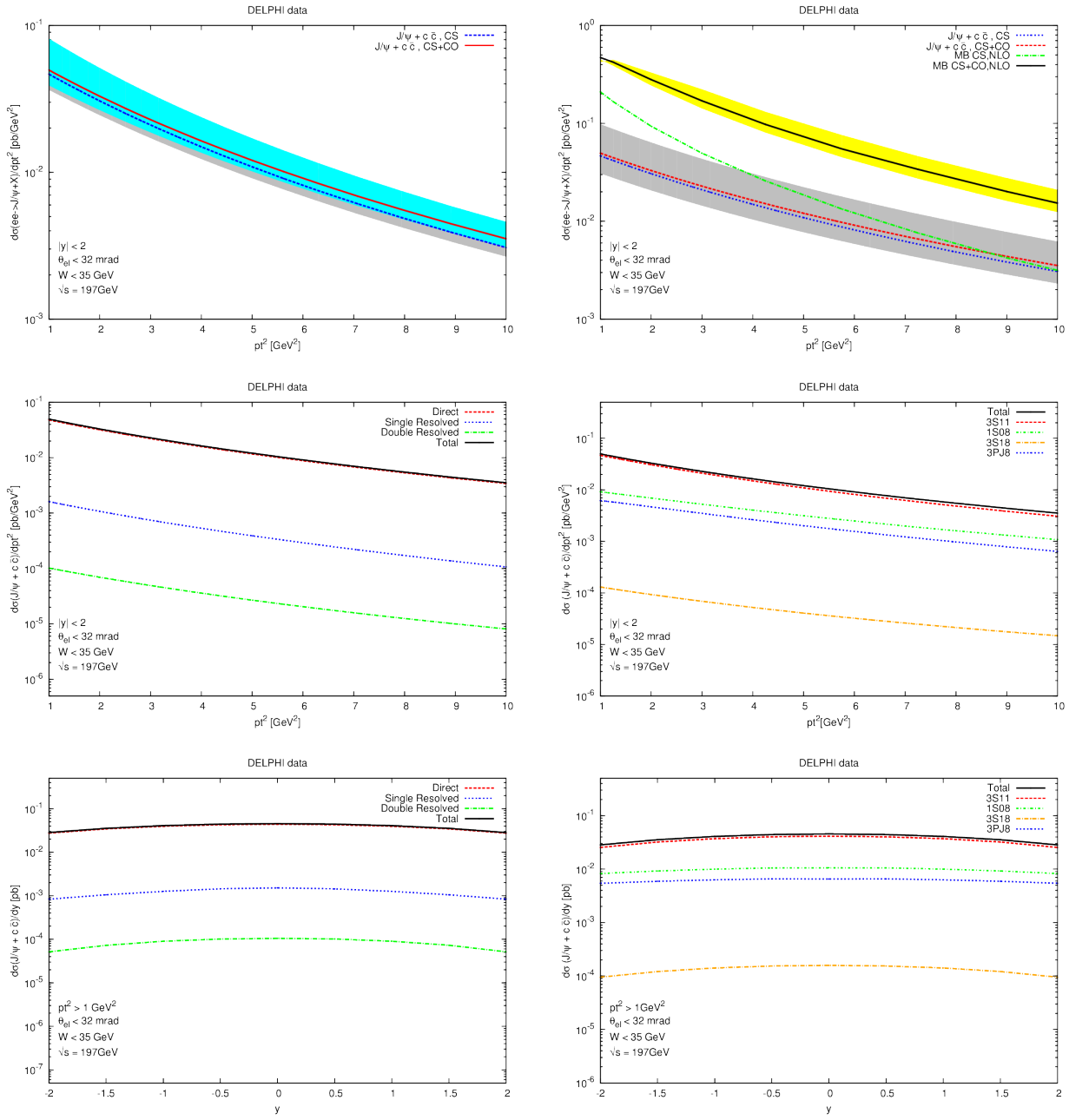

Figure 4.8: The differential cross section of $J/\psi + c + \bar{c}$ production at DELPHI, against J/ψ transverse momentum p_t^2 and rapidity y, compared with the inclusive J/ψ production cross section without $J/\psi + c + \bar{c}$ contribution, in figure 1(q) of MB [13].

results for each of the subprocess considered. Using our code, we reproduce here figures 4-6 of their paper at pages 5 and 6. As suggested by R. Li and K. T. Chao in that paper, we also consider the color octet (CO) contributions taking part in all of these interactions. For this, we take the input parameters from MB [13] used for the global fits of color octet LDMEs. With some general parameters as defined in the previous section, we take experimental conditions related to LEPII for our theoretical predictions. We choose $\sqrt{SH} = 197\text{GeV}$, $\theta_{max} < 32\text{mrad}$ for WWA photons, the rapidity cut $|y| < 2$ and the constraint on center-of-mass energy of the two photons as $W < 35\text{GeV}$. We plot our results for p_t^2 distribution of the cross sections against fig. 1q of MB, and present it also with some other plots in fig. 4.8. The shaded bands on top left are constructed by variation in charm quark mass from 1.4GeV to 1.55GeV and include CS and CO contributions, and those on top right are constructed by variation of the renormalization and factorization scales $\mu_{r/f}$ from $0.5\mu_0$ to $2\mu_0$.
The middle plots in the same figure show the decomposition of the top curves into

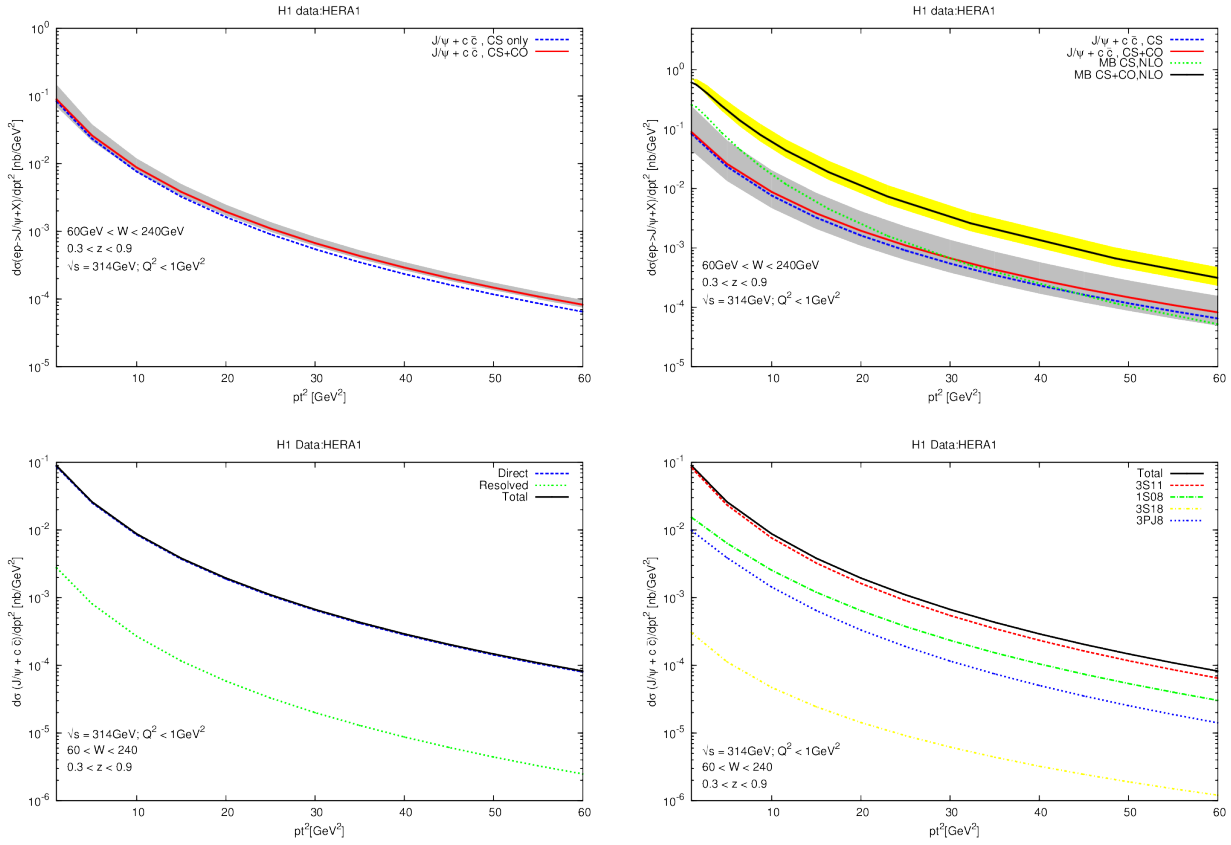

Figure 4.9: $J/\psi + c + \bar{c}$ differential cross section at HERA-H1, against J/ψ transverse momentum p_t^2, with the bands representing varied mass (top left) and varied renormalization and factorization scales (top right) to compare with figure 1(u) of MB [13] for the inclusive J/ψ production without $J/\psi + c + \bar{c}$ contribution.

the direct, single- and double-resolved photon contributions (left) and the contributions from each of the intermediate $c\bar{c}$ states (right), which can be compared respectively with figures 3a and 2b of MB [13]. Similarly, the bottom plots show the cross section against J/ψ rapidity distribution. The middle and the bottom plots are the short distance cross sections already multiplied with the corresponding LDMEs. It is important to note that the blue line in the middle right represents the negative values, since the positive contribution of the ${}^3P_J^{[8]}$ intermediate state to differential cross section is multiplied with the negative value of the LDME for the same state. Therefore, the CO contributions are much smaller than the CS contributions due to the cancellation between the ${}^1S_0^{[8]}$ and ${}^3P_J^{[8]}$ states. Furthermore, it can be seen that the $J/\psi + c + \bar{c}$ contributions only amount to about 10% of the other contributions to $J/\psi + X$ production cross section, as can be seen in the upper right figure. Additionally, the mass uncertainties seem to be of the similar order of magnitude as the scale uncertainties, as can be seen from comparing the two upper graphs of fig.4.8. Also, we observe that the direct contributions dominate, while the resolved processes are only contributing about 1%.

4.4.2 HERA-H1:

Our results for HERA-H1 experiment are compared with figure 1(u,v,w) of MB [13], for cross sections against transverse momentum p_t^2, photon-proton invariant mass W and the inelasticity parameter z distributions as described in the previous section, and shown in figures 4.9,4.10 and 4.11. The values chosen for the parameters accordingly are: $\sqrt{SH} = 314\text{GeV}$, $0.3 < z < 0.9$ and the limits on center-of-mass energy of the two photons as $60\text{GeV} < W < 240\text{GeV}$. The negative sign must be taken into consideration for the blue lines in the decomposition graph of the intermediate $c\bar{c}$ states.

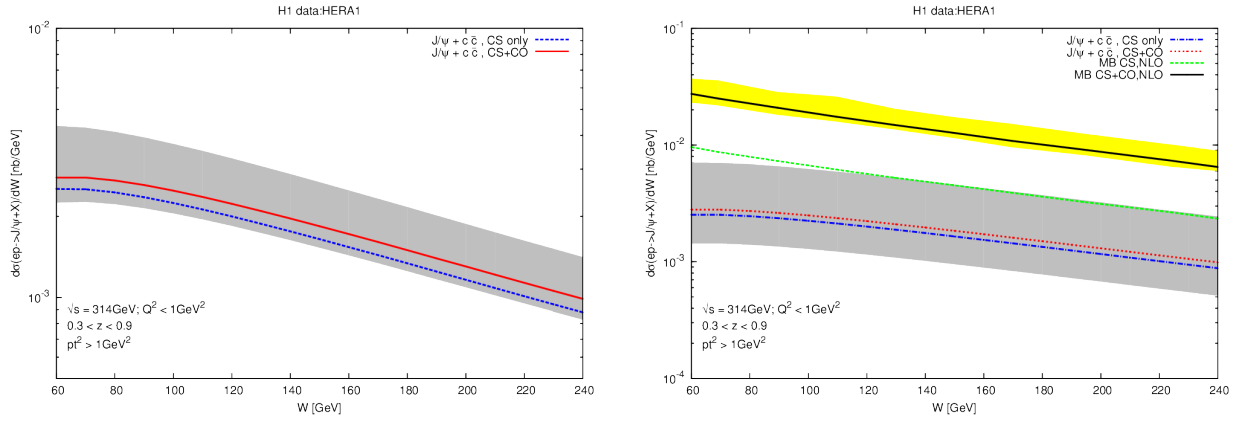

Figure 4.10: Similar to top two plots of figure 4.9, the differential cross-section of $J/\psi + c + \bar{c}$ production at HERA plotted against photon-proton invariant mass W, figure 1(v) of MB [13].

Like in the case of DELPHI above, here we also plotted the graph where the cross section

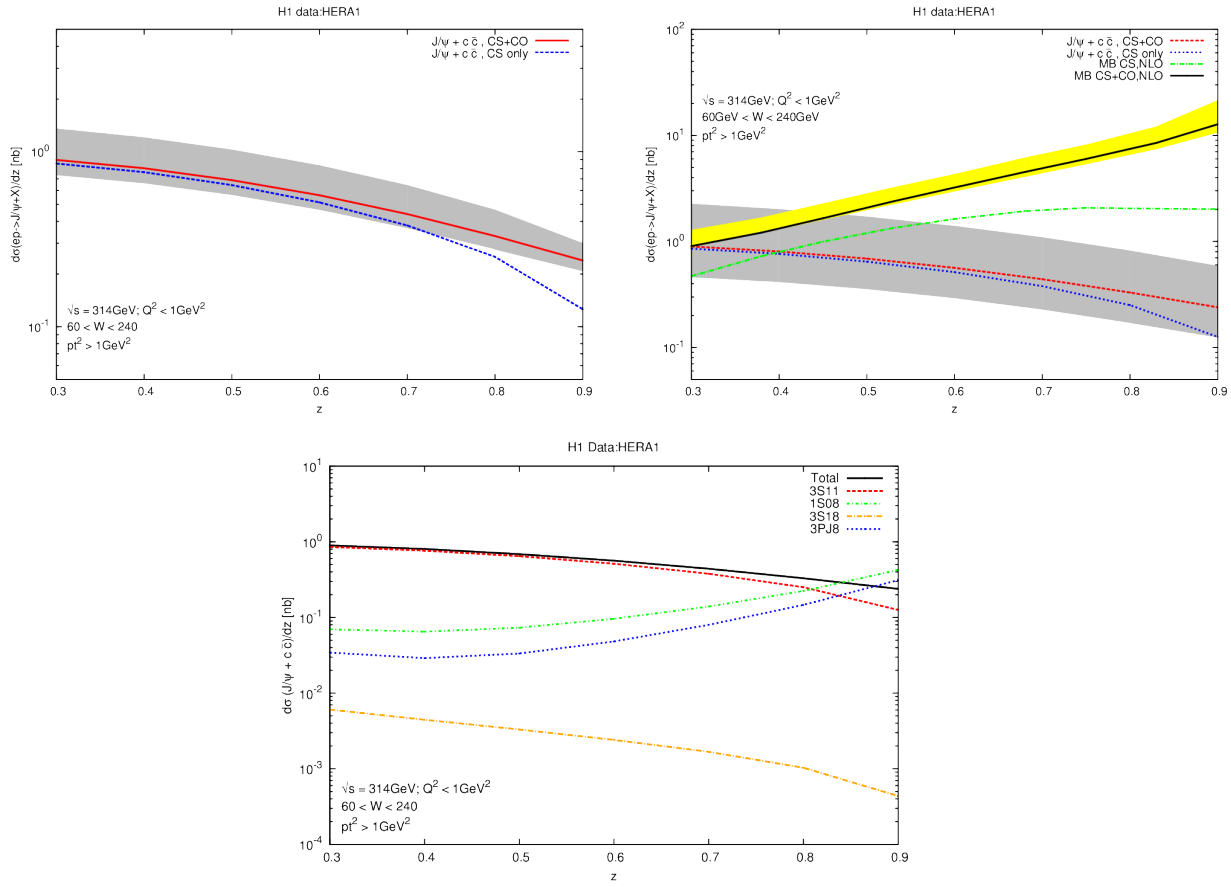

Figure 4.11: $J/\psi + c + \bar{c}$ production cross section at HERA against the inelasticity parameter z, similar to figure 4.9 and 4.10, and compared with figure 1(w) of MB [13]. In case of photoproduction, z is the fraction of the photon energy taken over by J/ψ, in the proton rest frame.

is decomposed into different subprocesses. For the sake of consistency, we take the same values for other input parameters like LDMEs, PDFs for photon/proton, charm quark mass, the strong coupling constant etc, as discussed in the previous section. All these plots provide us with a complete picture of $J/\psi + c + \bar{c}$ production process at HERA. As we can see here, the mass dependence is much lesser than the scale dependence. Unlike $J/\psi + X$,the $J/\psi + c + \bar{c}$ process does not show a rise with increasing z value, but enhances it at lower z. This is due to the fact that can be seen in the lower plot fig. 4.11, which shows that like in the $J/\psi + X$ case only the CO contributions show this rise, and not the CS ones. But since CS contributions dominate over the CO, so the overall z dependence is flat.

4.4.3 TEVATRON-CDF:

In case of Tevatron, we consider CDF Run2 experiment, to compare our results with MB [13]. We take the same experimental parameters for input, as in figure 1(c) of MB [13]. The values for $\sqrt{SH}$ is taken to be 1.96TeV and for the rapidity of the J/ψ is $|y| < 0.6$. One can easily note well separated charm-mass variation bands (top left) for CS and CS+CO states at larger p_t values, contrary to the same plots for DELPHI and HERA where one could not see them separated even at higher values of p_t. Here only direct hadronic subprocesses with gg and quark-antiquark in the initial state take place, in Fig.4.12 we therefore have not plotted the corresponding graph with decomposed differential cross section into subprocesses involved. We plot instead another interesting graph to check the dependence of the differential cross section on the renormalization and factorization scales (bottom left of figure 4.12, fixing the J/ψ transverse momentum p_t at three different values. We could also still plot the contributions of individual intermediate $c\bar{c}$ states (bottom right) with negative value of the blue line, as discussed in case of DELPHI and HERA above. At large p_t values, the separation between the CS and CS+CO states is obvious again in the graph on bottom right of figure 4.12. As we can see that the ${}^3S_1^{[8]}$ channel has a significantly flatter slope compared to all the other contributions, therefore it would dominate the cross sections at high p_t values. This stems from the Feynman diagrams where the J/ψ bound state is formed by the $c\bar{c}$ pair which is produced by a direct splitting of a gluon into this $c\bar{c}$ (called the gluon fragmentation process). Due to these contributions, the $J/\psi + c + \bar{c}$ contribution will eventually dominate the color-singlet contribution of $J/\psi+X$ production cross section at high p_t values, as can bee seen very clearly in top right plot of the figure 4.12. Therefore, $J/\psi + c + \bar{c}$ can not be neglected for large momentum values.

4.4.4 LHC-ATLAS:

With the announcement of very exciting new discoveries from CERN recently, it is impossible not to include LHC experiment in our analysis of this very important process. We therefore consider the experimental parameters for ATLAS, so that we could also compare our results with figure 4 of MB [13]. The initial values are taken to be $\sqrt{SH} =$ 7TeV and $|y| < 0.75$, with the same values for other general parameters and LDMEs as discussed in the previous section. Similar to the case of Tevatron, even widely separated charm-mass and renormalization/factorization scale bands can be noticed (top left/right) in figure 4.13. Interestingly, despite the (almost) cancellation of the states ${}^1S_0^{[8]}$ and ${}^3P_0^{[8]}$ (negative blue line), the contribution of CO states looks promising at high p_t values for ATLAS, as can be seen in the bottom plot of figure 4.13. This indicates the importance of CO contributions which can be tested further on higher energy scales when LHC will be able to reach its expected energy range of 14TeV.

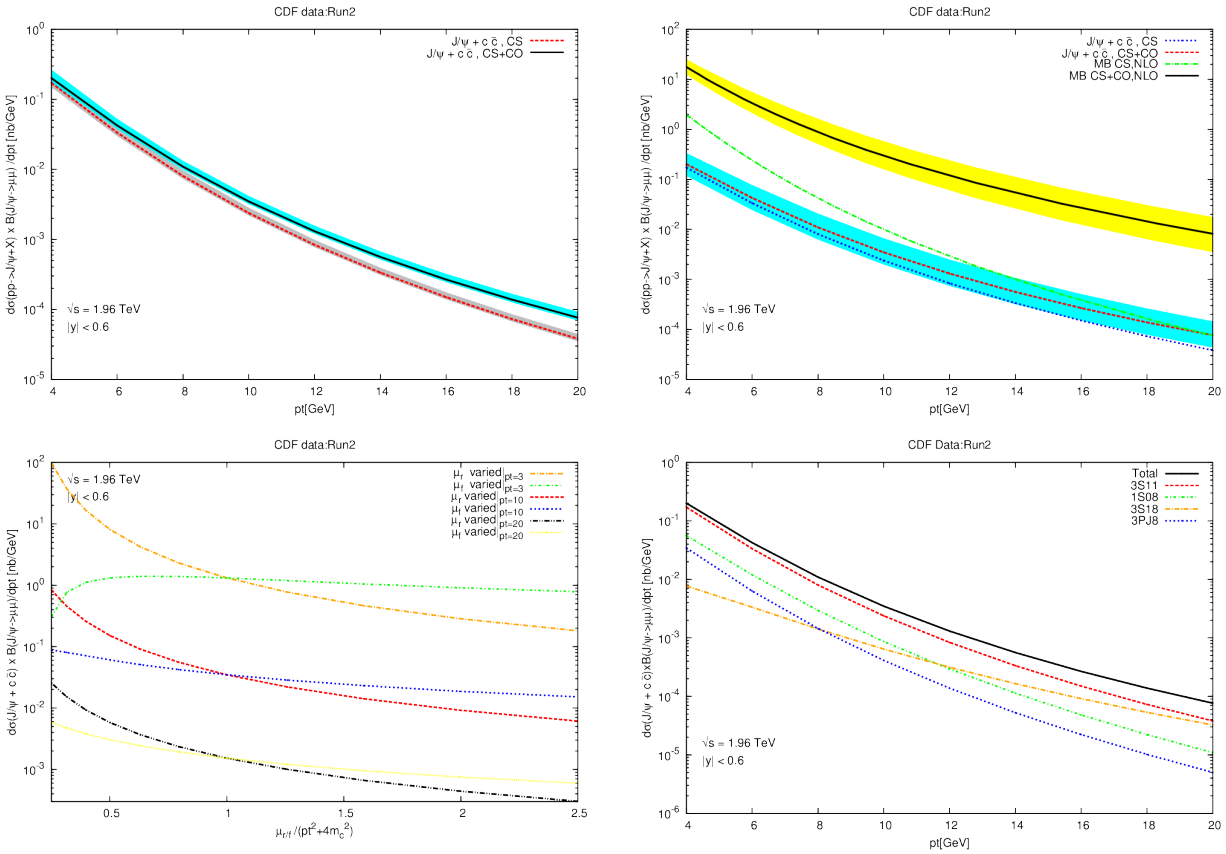

Figure 4.12: Differential cross section for J/ψ+c+$\bar{c}$ at Tevatron-CDF, against J/ψ transverse momentum p_t, with the bands again representing varied mass (top left) and varied renormalization/factorization scales (top right) to compare with the inclusive J/ψ production without $J/\psi + c + \bar{c}$ contribution, figure 1(c) of MB [13].

4.5 Conclusions:

The very first conclusion of the above analysis at various colliders with different energy ranges is that the $J/\psi + c + \bar{c}$ process is not of any less importance for the study of J/ψ production at NLO and also for the production of J/ψ with at least one meson containing a charm quark with a light quark. For all of the colliders, this process is either of the same order of magnitude, or only an order (or two) of magnitude less than the NLO production of J/ψ, when compared with the results presented in MB [13]. Our analytical results agreed to the numerical results by MadOnia [38], separately for each of the subprocesses considered. This provided a check on the working of our codes. We could also successfully reproduce the results of the second paper in ref. [11] for the CS contributions to J/ψ+c+$\bar{c}$ production at LEPII, with WWA photons. We note that this process contributes only to about 10% of the other contributions to the inclusive $J/psi + X$ production, due to the dominance of the direct subprocess while the resolved ones contribute about 1%.

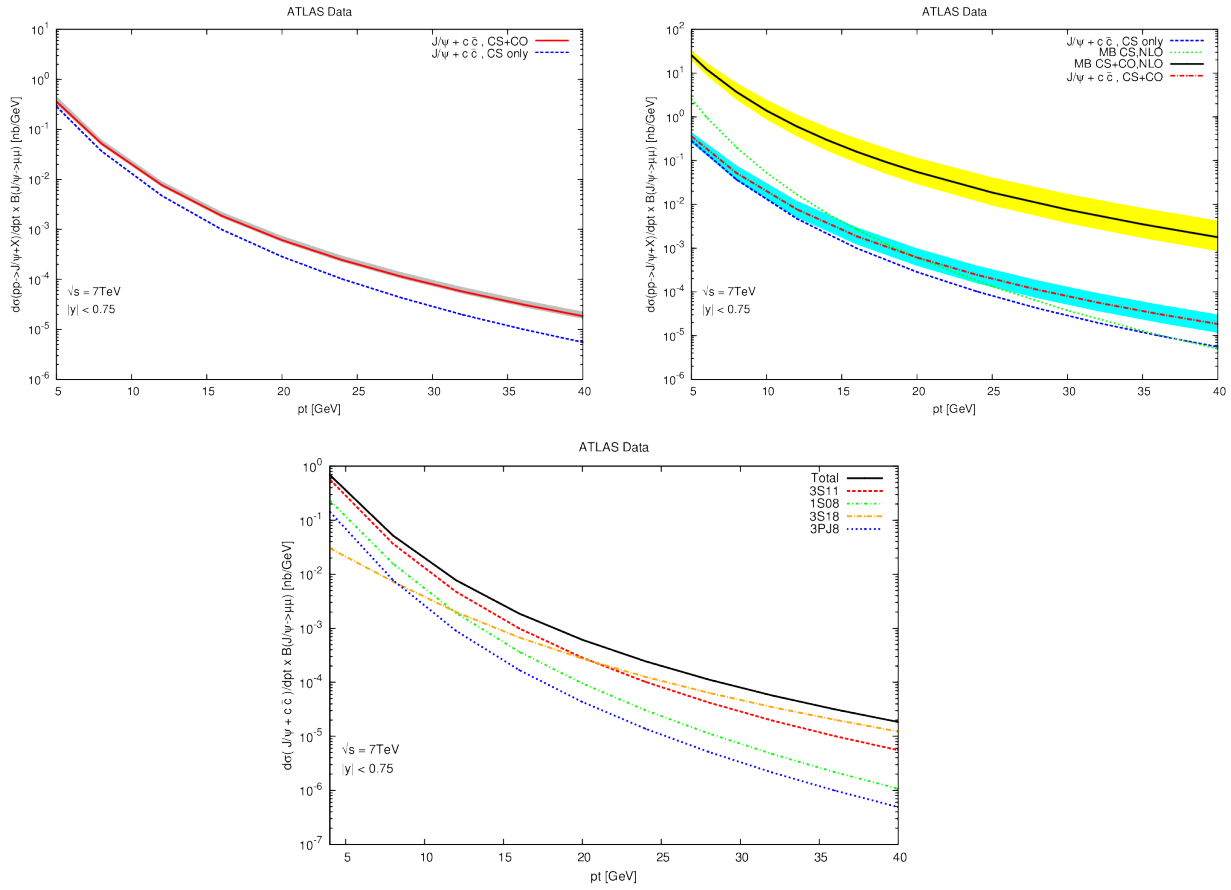

Figure 4.13: Differential cross section with respect J/ψ transverse momentum p_t for the production of $J/\psi + c + \bar{c}$ at LHC-ATLAS, similar to the previous figures 4.8, 4.9 and 4.12. This is compared to figure 4 of MB [13] for the inclusive J/ψ production (without $J/\psi + c + \bar{c}$ contribution).

We reproduced all the results presented in ref. [11], even for future photon colliders at 500GeV and 1TeV, both with WWA and LBS photon distributions. We also could generate results presented in references 5 (considering their QCD contributions) and 6 of [12], which in turn also verify results presented in the references 1-4, considering the change of variables. With the consideration of negative value for LDMEs of ${}^3P_0^{[8]}$ intermediate states, the contribution is almost canceled by the contribution from ${}^1S_0^{[8]}$ intermediate state. Also, the value of ${}^3S_1^{[8]}$ intermediate state is lower as compared to the the CS and other two CO intermediate states. Therefore, the contributions of both the sum of CS+CO states and that of the CS ${}^3S_1^{[1]}$ intermediate state, lie within the uncertainty bands of charm-mass and of renormalization/factorization scale at low energy scales of p_t distribution at DELPHI and $p_t/W/z$ distributions at HERA-H1. But for high p_t values at CDF and ATLAS, this behavior changes to well separated bands despite the cancellation of states ${}^1S_0^{[8]}$ and ${}^3P_0^{[8]}$ intermediate states. This fact indicates the importance of ${}^3S_1^{[8]}$ intermediate state for hadroproduction of $J/\psi + c + \bar{c}$ at these

high energy colliders, arising from the gluon-fragmentation diagrams. The contribution of ${}^3S_1^{[8]}$ intermediate state for $z-$distribution at HERA must also be not neglected, where the CS+CO contribution starts to get larger than that of the only CS intermediate states, at higher values of z. So that the overall z dependence gets dominated by the behavior of the CS states. At DELPHI, the direct photon-photon subprocess contributes the largest part and is more than a factor of magnitude larger than that of the single resolved one, and more than three orders in magnitude larger than the sum of double resolved subprocesses gg and quark-antiquark, for both the p_t and y distributions. Similar is the case at HERA where the direct photoproduction process is more than two orders of magnitude higher than the resolved one, at the largest value of p_t.

5 J/ψ production at NLO in e^+e^- annihilation

As discussed in chapter 1, the NLO studies calculations indicate a reduction in the difference between the theoretical predictions and the experimental measurements. Additionally, NRQCD expects the CO states to contribute an effective part in charmonium production. It is thus very important to consider the NLO contributions of both the CS and CO states of the intermediate $c\bar{c}$ pair, for the study of heavy charmonia. In this chapter, we therefore investigate the QCD corrections to J/ψ production at B-factories.

The inclusive production of J/ψ in the direct interaction of electron-positron $e^+e^- \to J/\psi + X$ involves both $2 \to 2$ and $2 \to 3$ subprocesses for NLO calculations. At the partonic level, we consider the subprocesses:

$$e^+(k_1) + e^-(k_2) \to c\bar{c}[n](P) + g(k_3) \tag{5.1}$$
$$e^+(k_1) + e^-(k_2) \to c\bar{c}[n](P) + g(k_3) + g(k_4) \tag{5.2}$$
$$e^+(k_1) + e^-(k_2) \to c\bar{c}[n](P) + q(k_3) + \bar{q}(k_4), \tag{5.3}$$

where $c\bar{c}[n]$ represents the intermediate charm-anticharm pair in the state $[n] = {}^{2S+1}L_J{}^{[1,8]}$ which evolves to form a physical J/ψ bound state and $q = u, d, s$ denotes light quarks and $\bar{q}$ represents the partner light antiquarks. The subprocess in the eq. 5.1 represents the leading order (LO) contribution. At the next to leading order, we need to consider not only the virtual corrections to this subprocess, arising from the loop diagrams, but also include the real corrections due to radiation of a real gluon (eq.5.2) or a gluon splitting into a light quark-antiquark pair (eq.5.3). One must not forget the subtraction of gluon-ghost/-antighost subprocess from eq.(5.2) for considering only the physical polarizations of the gluon.The NLO differential cross section at $\mathcal{O}(\alpha_s)$ can then be written as:

$$d\sigma^{NLO} = d\sigma^{Born} + d\sigma^{Virtual} + d\sigma^{Real}, \tag{5.4}$$

where the superscripts indicate the part of the partonic cross section involved. Now we discuss these parts one by one.

5.1 Born Cross Section:

For the process

$$e^+(k_1) + e^-(k_2) \to c\bar{c}[n](P) + g(k_3), \tag{5.5}$$

Figure 5.1: The $2 \to 2$ tree level diagrams for the process $e^+e^- \to c\bar{c}[n] + g$.

at tree level, the typical Feynman diagrams (shown in the fig.5.1) and the corresponding matrix elements for these diagrams are generated using FeynArts[35]. The further calculations of color and spin projected matrix elements square involved the same set of steps, using FeynCalc[36] and FORM[37] as discussed in chapter 3 and chapter 4, in $D = 4 - 2\epsilon$. The partonic cross section in accordance with eq.(3.7) can then be written as:

$$\begin{aligned} d\hat{\sigma}^{Born}(e^+e^- \to c\bar{c}[n] + g) &= \frac{1}{4}\frac{1}{2s} dPS_{2\to 2} \sum_{col,pol} |\mathcal{M}_{Tree}(e^+e^- \to c\bar{c}[n] + g)|^2 \,, \\ &= \frac{1}{4}\frac{1}{16\pi s^2} \sum_{col,pol} |\mathcal{M}_{Tree}(e^+e^- \to c\bar{c}[n] + g)|^2 dt \,, \end{aligned} \quad (5.6)$$

where $\frac{1}{2s}$ is the flux factor, the factor $\frac{1}{4}$ denotes the average over the spins of initial state particles, $\mathcal{M}_{Tree}$ is the tree level matrix elements, and we take the value for phase space integration (in the center-of-mass frame of the incoming particles),

$$dPS_{2\to 2} = \frac{1}{(2\pi)^2}\frac{\pi}{2s} dt, \quad (5.7)$$

from eq.(4.29). The kinematically allowed region for this phase space is contained in the limits: $4m_c^2 < s$ and $-s_1 < t < 0$. Here the Mandelstam variables for this process are defined using $k_1^2 = 0 = k_2^2 = k_3^2$ and conservation of energy-momentum $k_1 + k_2 = P + k_3$, compared to eqs. (4.2, 4.6, 4.7, 4.13, 4.14, 4.15) as:

$$\begin{aligned} s &\equiv (k_1 + k_2)^2 = 2k_1 \cdot k_2 && (5.8)\\ t &\equiv (P - k_1)^2 = -2k_2 \cdot k_3 && (5.9)\\ u &\equiv (P - k_2)^2 = -2k_1 \cdot k_3 && (5.10)\\ s_1 &\equiv s - 4m_c^2 = 2P \cdot k_3 && (5.11)\\ t_1 &\equiv t - 4m_c^2 = -2P \cdot k_1 && (5.12)\\ u_1 &\equiv u - 4m_c^2 = -2P \cdot k_2. && (5.13) \end{aligned}$$

Analogous to eq.(3.5), the born part of partonic cross section for J/ψ production can be obtained from 5.6, as:

$$d\sigma^{Born}(e^+e^- \to J/\psi + g) = \sum_n d\hat{\sigma}^{Born}(e^+e^- \to c\bar{c}[n] + g)\frac{\langle \mathcal{O}^{J/\psi}[n]\rangle}{N_{col}(n)N_{pol}(n)}, \quad (5.14)$$

where the the definitions for the long distance matrix elements $\langle \mathcal{O}^{J/\psi}[n]\rangle$ and $N_{col}(n)N_{pol}(n)$ remain the same as in chapter 3 and 4.

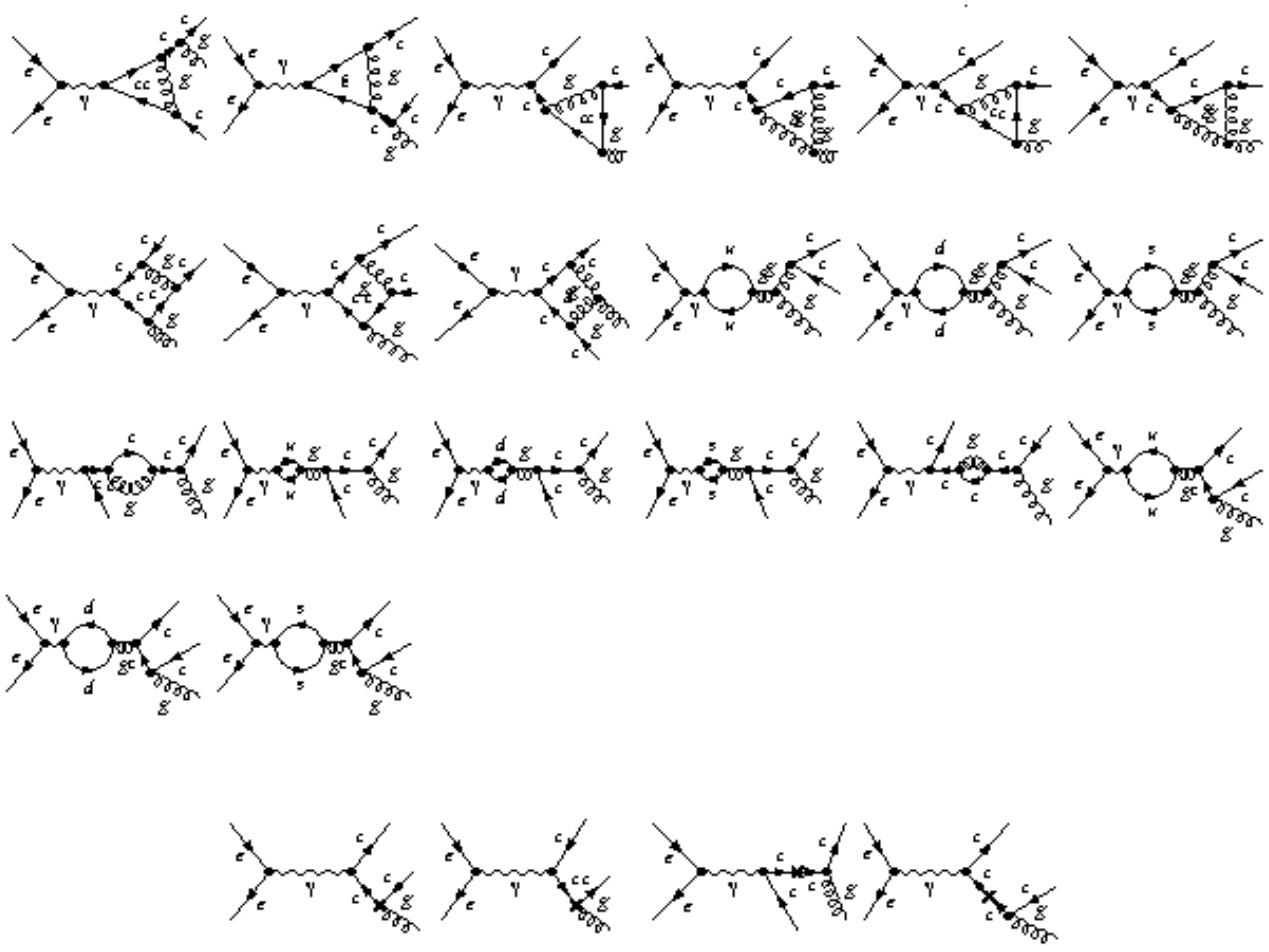

Figure 5.2: Feynman diagrams for the virtual corrections to the process $e^+e^- \to c\bar{c}[n]+g$, where the cross on the charm quark line is an insertion of the charm mass counter-term, and a cross on quark-gluon vertex represents the insertion of corresponding vertex correction counter-term.

5.2 Virtual Cross Section:

At NLO in α_s, we need to consider the loop diagrams as shown in fig.5.2. There appear ultraviolet (UV) and infrared (IR) singularities during the calculations of loop integrals, in the regions of high and low loop momenta, respectively. These two types of singularities are isolated with the help of Dimensional Regularization as discussed already in chapter 3. The UV divergences arising from the self-energy and triangle diagrams get canceled by the introduction of the renormalization. We adopt here the renormalization scheme followed by [44]. The counter-term diagrams considered to take care of the renormalization of the theory are shown in fig.5.2, and the renormalized quantities are defined in the set of equations (3.31). We then perturbatively expand the matrix elements in α_s, for the subprocess (5.1) as:

$$\mathcal{M} = \mathcal{M}_{Tree} + \mathcal{M}_{virtual} \ , \tag{5.15}$$

and the square as:

$$\begin{aligned} |\mathcal{M}|^2 &= \mathcal{M}^*\mathcal{M} \\ &= |\mathcal{M}_{Tree}|^2 + 2\mathrm{Re}(\mathcal{M}^*_{Tree}\mathcal{M}_{virtual}) + \mathcal{O}(\alpha_s^2) \ , \end{aligned} \tag{5.16}$$

where $\mathcal{M}_{virtual}$ denotes the virtual corrections at $\mathcal{O}(\alpha_s)$. For the next to leading order process $e^+e^- \to c\bar{c}[n] + g$, the $\mathcal{M}_{virtual}$ accounts for the external leg insertions defined by LSZ-reduction [39], as:

$$\mathcal{M}_{virtual}(e^+e^- \to c\bar{c}[n]+g) = \mathcal{M}_{loop}(e^+e^- \to c\bar{c}[n]+g) + (\delta Z_\psi + \frac{1}{2}\delta Z_A)\mathcal{M}_{Tree} \ , \tag{5.17}$$

where $\mathcal{M}_{loop}$ denotes the loop diagram amplitudes and the counter terms δZ_ψ and δZ_A are again referred to the set of equations (3.31). Therefore, the squared matrix elements for the process $e^+e^- \to c\bar{c}[n] + g$ at $\mathcal{O}(\alpha_s)$:

$$\begin{aligned} \sum_{col,pol} |\mathcal{M}(e^+e^- \to c\bar{c}[n]+g)|^2 &= \sum_{col,pol^*} |\mathcal{M}_{Tree}(e^+e^- \to c\bar{c}[n]+g)|^2 \\ +2\mathrm{Re} \sum_{col,pol^*} &(\mathcal{M}^*_{Tree}(e^+e^- \to c\bar{c}[n]+g)\mathcal{M}_{loop}(e^+e^- \to c\bar{c}[n]+g)) \\ &+2 \sum_{col,pol^*} (\delta Z_\psi + \frac{1}{2}\delta Z_A)|\mathcal{M}_{Tree}(e^+e^- \to c\bar{c}[n]+g)|^2, \end{aligned} \tag{5.18}$$

are UV finite but still contain IR singularities. For the calculation of loop integrals in $D = 4 - 2\epsilon$, we apply the procedures outlined in [34], to reduce the appearing loop integrals into a set of five master integrals, listed in Appendix A. We could explicitly show the cancellation of UV divergences appearing in the calculations. Therefore, in analogy with the equations (5.6) and (5.14), using the same set of kinematical variables for $2 \to 2$ process, we have the virtual cross section expressed as:

$$\begin{aligned} d\sigma^{Virtual}(e^+e^- \to J/\psi + g) = \frac{1}{4}\frac{1}{16\pi s^2} \sum_n \sum_{col,pol} |\mathcal{M}(e^+e^- \to c\bar{c}[n]+g)|^2 dt \\ \times \frac{\langle \mathcal{O}^{J/\psi}[n] \rangle}{N_{col}(n) N_{pol}(n)}, \end{aligned} \tag{5.19}$$

with $|\mathcal{M}(e^+e^- \to c\bar{c}[n] + g)|^2$ defined above in equation (5.18). For the infrared singularities still left there, we move on to the real correction processes in the next section.

5.3 Real Cross Section:

The processes in equations (5.2) and eq.(5.3) are involved in the real corrections, of the process $e^+e^- \to c\bar{c}[n] + g$. The Feynman diagrams for these two processes are shown in fig.5.3. The square of the matrix elements for these processes is conveniently calculated using the scheme already presented in the last chapter. When we integrate over the phase space of these $2 \to 3$ processes, IR singularities are generated in the regions when a soft gluon is emitted (called soft singularities, like in the process 5.2) or when two

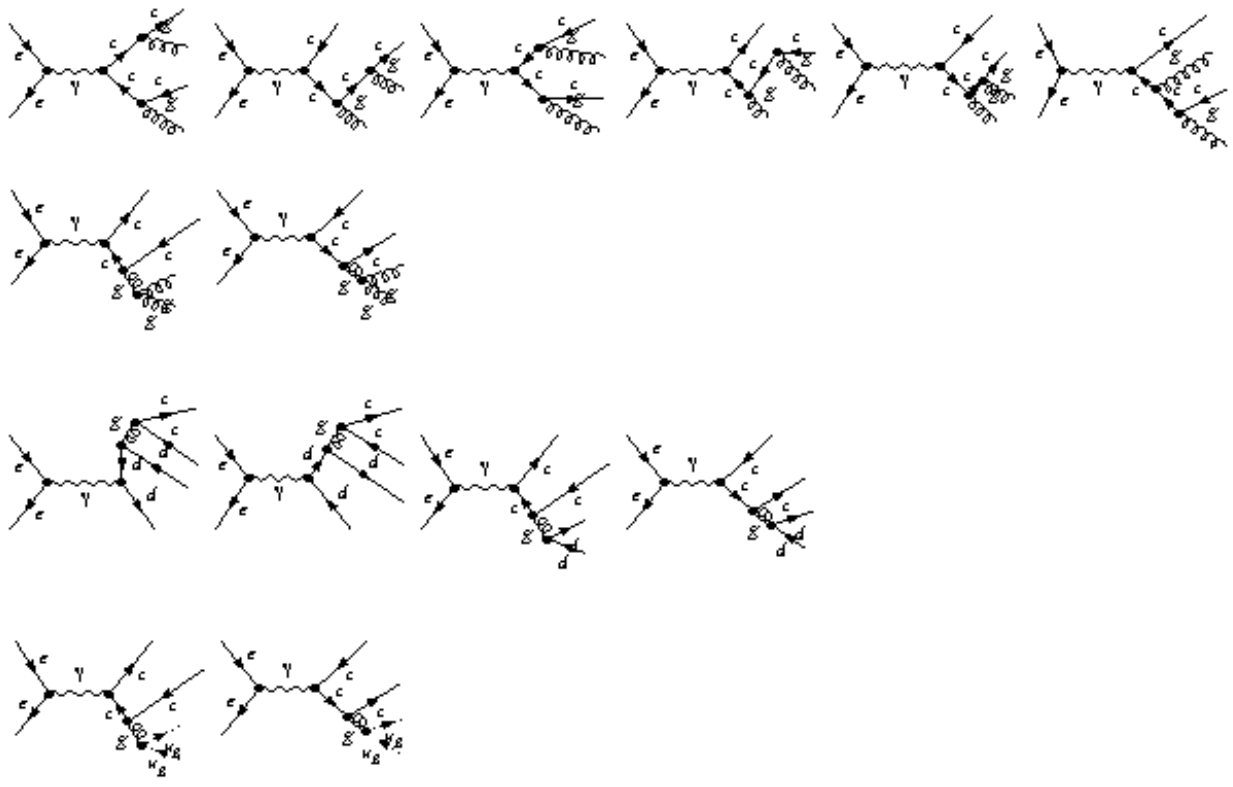

Figure 5.3: Tree level $2 \to 3$ Feynman diagrams for the processes $e^+e^- \to c\bar{c}[n] + g + g$,$e^+e^- \to c\bar{c}[n] + q + \bar{q}$ and $e^+e^- \to c\bar{c}[n] + u_g + \bar{u}_g$, where u_g represent the gluon-ghost, and other final state light quark contributions can be obtained by replacing d with u and s.

external light partons become collinear to each other (called collinear singularities, like in the process 5.3). In order to extract the IR poles, the analytical integration over phase space is performed in $D = 4 - 2\epsilon$ dimensions and the soft/collinear singularities are isolated by dividing the phase space into different regions. We here follow the two-cut-off phase space slicing method [45] in order to decompose the phase space into three parts, by introducing two small slicing parameters, δ_s and δ_c. The real differential cross section is then:

$$d\sigma^{Real} = d\sigma^{soft} + d\sigma^{hard-collinear} + d\sigma^{hard-noncollinear} \tag{5.20}$$

where the superscripts indicate the region of the phase space integration. Though the integration results for these three regions depend on the unphysical slicing parameters, δ_s and δ_c, but their sum must be independent of the specific choice of these slicing parameters. The general kinematical Mandelstam variables for $2 \to 3$ real processes, in analogy with the set of equations (4.2-4.14) and $k_3^2 = 0 = k_4^2$, are defined as:

$$\begin{aligned}
s &\equiv (k_1 + k_2)^2 = 2k_1 \cdot k_2 && (5.21)\\
s_4 &\equiv (P + k_4)^2 - 4m_c^2 = 2P \cdot k_4 && (5.22)\\
s_5 &\equiv (P + k_3)^2 - 4m_c^2 = 2P \cdot k_3 && (5.23)\\
s_3 &\equiv (k_3 + k_4)^2 = 2k_3 \cdot k_4 && (5.24)\\
t1 &\equiv (P - k_1)^2 - 4m_c^2 = -2P \cdot k_1 && (5.25)\\
u1 &\equiv (P - k_2)^2 - 4m_c^2 = -2P \cdot k_2 && (5.26)
\end{aligned}$$

$$\begin{aligned}
t_6 &\equiv (k_2 - k_3)^2 = -2k_2 \cdot k_3 && (5.27)\\
u_6 &\equiv (k_1 - k_3)^2 = -2k_1 \cdot k_3 && (5.28)\\
t' &\equiv (k_1 - k_4)^2 = -2k_1 \cdot k_4 && (5.29)\\
u' &\equiv (k_2 - k_4)^2 = -2k_2 \cdot k_4 && (5.30)\\
s_1 &\equiv s - 4m_c^2 && (5.31)\\
t &\equiv t_1 + 4m_c^2 && (5.32)\\
u &\equiv u_1 + 4m_c^2. && (5.33)
\end{aligned}$$

We shall now discuss the three parts of $d\sigma^{Real}$ below.

Soft Region:

This is the region where one of the outgoing gluons is soft. Here, the contributing Feynman diagrams are the ones where the soft gluon is attached to another external gluon or a quark line. In our case, 5.2 is thus the only real correction process containing soft singularities. Extending the techniques discussed in [46] to QCD, the amplitude of the diagram with soft gluon factorizes into the Born amplitude without that soft gluon and an eikonal factor, as displayed in the diagram below 5.4, where we follow the notations used in [34], dotted lines representing an external parton line i of momentum

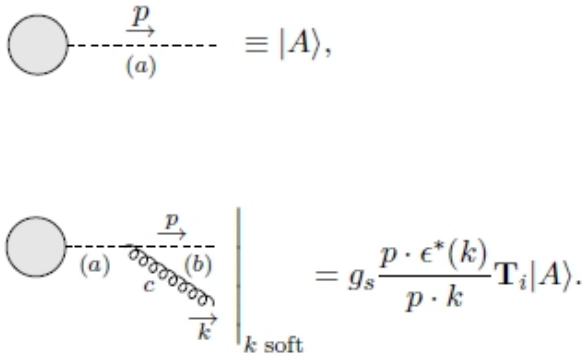

Figure 5.4: Diagramatic representations of the soft gluon emission from a parton.

p, and the color operator $\mathbf{T}_i$, defined by acting on the Born amplitude $|A\rangle$, takes the value T_c $(-T_c)$ if the emitting parton i is an outgoing quark (antiquark) or if_{bca} for the emitting parton i being a gluon, inserted into the corresponding place of the amplitude A. Additionally, another short notation for the amplitudes is defined as:

$$\langle A|\mathbf{T}_x\mathbf{T}_y|B\rangle \equiv (\mathbf{T}_x|A\rangle)^*(\mathbf{T}_y|B\rangle), \tag{5.34}$$

not to be confused with bras and kets notations of the quantum mechanical states.
Now, for the case when gluon with momentum k_4 is soft, we define here the kinematics for the phase space integration in the region $k_4 \to 0$. In the center of mass of the incoming particles (which is here same as that of J/ψ and the parton with momentum k_3), the particle momenta are parametrized as:

$$\begin{aligned} k_1 &= E_2(1, 0, -\sin\theta, \cos\theta) \\ k_2 &= E_2(1, 0, \sin\theta, \cos\theta) \\ k_3 &= E_3(1, 0, 0, 1) \\ k_4 &= E_4(1, \sin\theta_1\sin\theta_2, \sin\theta_1\cos\theta_2, \cos\theta_1) \\ P &= (E_{J/\psi}, 0, 0, -E_3), \end{aligned} \tag{5.35}$$

with the Mandelstam variables defined in the set of equations 5.8-5.13, for $2 \to 2$ process, and the soft region of the phase space is defined as,$0 \leq E_4 \leq \delta_s \frac{\sqrt{s}}{2}$ for the values;

$$E_2 = \frac{\sqrt{s}}{2}, \quad E_3 = \frac{s_1}{2\sqrt{s}}, \quad E_{J/\psi} = \frac{s + 4m_c^2}{2\sqrt{s}}, \quad \cos\theta = \frac{t - u}{s_1}. \tag{5.36}$$

Since we are considering the soft gluon with momentum k_4 attached to an outgoing parton (gluon or a charm quark line), the amplitude $|k_4 \text{ soft}\rangle$ in terms of of the color connected born amplitude $|\text{Born}\rangle$ as shown in fig.5.5, using the above relation is evaluated as:

$$|k_4 \text{ soft}\rangle = g_s \left(\frac{(\frac{P}{2} + q).\epsilon^*(k_4)}{(\frac{P}{2} + q) \cdot k_4}\mathbf{T}_c + \frac{(\frac{P}{2} - q) \cdot \epsilon^*(k_4)}{(\frac{P}{2} - q) \cdot k_4}\mathbf{T}_{\bar{c}} + \frac{k_3 \cdot \epsilon^*(k_4)}{k_3 \cdot k_4}\mathbf{T}_3 \right) |\text{Born}\rangle. \tag{5.37}$$

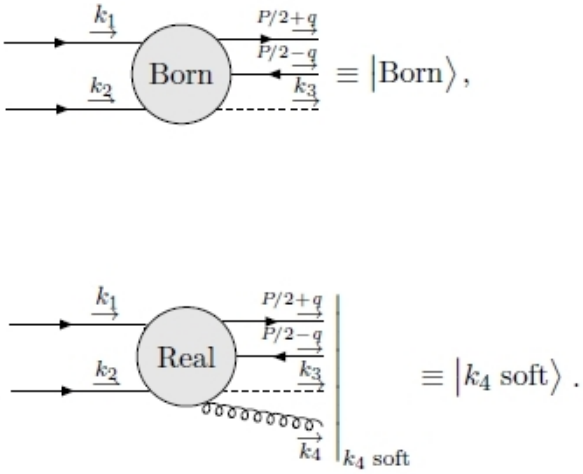

Figure 5.5: Diagramatic representation of the case when gluon with momentum k_4 is soft.

In the soft region of real corrections, we use eq.(3.25) for the summation over the soft gluon polarization in the axial gauge, so that $P \cdot \epsilon^*(k_4) = 0$. The projectors defined in section 3.1 are then applied using:

$$|k_4 \text{ soft}\rangle|_{q=0} \;=\; g_s \frac{k_3 \cdot \epsilon^*(k_4)}{k_3 \cdot k_4} \mathbf{T}_i |\text{Born}\rangle|_{q=o} \tag{5.38}$$

and the derivative with respect to the momentum transfer q,

$$\begin{aligned} \frac{\partial}{\partial q_\beta}|k_4 \text{ soft}\rangle|_{q=0} \;=\; & g_s \frac{2\epsilon^{*\beta}(k_4)}{P \cdot k_4}(\mathbf{T}_c - \mathbf{T}_{\bar{c}})|\text{Born}\rangle|_{q=0} \\ & + g_s \frac{k_3 \cdot \epsilon^*(k_4)}{k_3 \cdot k_4} \mathbf{T}_i \frac{\partial}{\partial q_\beta}|\text{Born}\rangle|_{q=o}, \end{aligned} \tag{5.39}$$

to give the squared matrix elements of the real corrections, in the region where gluon with momentum k_4 is soft, as:

$$|\mathcal{M}_{k_4 \text{ soft}}(n)|^2 = S^{(1)}_{k_4 \text{ soft}}(n) + S^{(2)}_{k_4 \text{ soft}}(n) + S^{(3)}_{k_4 \text{ soft}}(n), \tag{5.40}$$

where the terms $S^{(1)/(2)/(3)}_{k_4 \text{ soft}}(n)$ for the intermediate $c\bar{c}$ pair in the state $[n]$, are defined as:

$$S^{(1)}_{k_4 \text{ soft}}(n) = g_s \frac{k_3 \cdot \epsilon(k_4) k_3 \cdot \epsilon^*(k_4)}{(k_3 \cdot k_4)^2} \langle n, \text{Born}|\mathbf{T}_i \mathbf{T}_j|n, \text{Born}\rangle \tag{5.41}$$

$$\begin{aligned} S^{(2)}_{k_4 \text{ soft}}({}^3P_J^{[8]}) = 4g_s^2 & \frac{k_3 \cdot \epsilon(k_4)\epsilon^*(k_4)}{k_3 \cdot k_4 P \cdot k_4} \varepsilon^{(J)}_{\alpha\beta} \\ & \times \langle {}^3P_J^{[8]}, \text{Born}\,|\mathbf{T}_i(\mathbf{T}_c - \mathbf{T}_{\bar{c}})\text{Tr}[\mathcal{C}_8 \Pi_1^\alpha |\text{Born}\rangle]|_{q=0}\,, \end{aligned} \tag{5.42}$$

$$S^{(3)}_{k_4\,\mathrm{soft}}({}^3P_J^{[8]}) = 4g_s \frac{\epsilon^{\beta'}(k_4)\epsilon^{*\beta}(k_4)\varepsilon^{(J)*}_{\alpha'\beta'}\varepsilon^{(J)}_{\alpha\beta}}{(P.k_4)^2}$$
$$\times \mathrm{Tr}[\langle \mathrm{Born}|\Pi_1^{*\alpha'}\mathcal{C}_8]|_{q=0}(\mathbf{T}_c - \mathbf{T}_{\bar{c}})(\mathbf{T}_c - \mathbf{T}_{\bar{c}})\mathrm{Tr}[\mathcal{C}_8\Pi_1^{\alpha}|\mathrm{Born}\rangle]|_{q=0}, \quad (5.43)$$

while $S^{(2)/(3)}_{k_4\,\mathrm{soft}}(n) = 0$ for $n = {}^1S_0^{[8]}, {}^3S_1^{[1/8]}$. The detailed calculation of these soft terms is presented in Appendix B.

The differential cross section for the soft contributions in the real corrections, using the matrix elements square (5.40) is then

$$d\sigma^{soft} = \frac{1}{4}\frac{1}{16\pi s^2}\int^{soft-region} dPS_{k_4\,\mathrm{soft}} \sum_n \sum_{col,pol} |\mathcal{M}_{k_4\,\mathrm{soft}}(n)|^2 dt \times \frac{\langle \mathcal{O}^{J/\psi}[n]\rangle}{N_{col}(n)N_{pol}(n)} \quad (5.44)$$

where the factor $\int^{soft-region} dPS_{k_4\,\mathrm{soft}}$ is defined in $D = 4 - 2\epsilon$ as:

$$\begin{aligned}\int^{soft-region} dPS_{k_4\,\mathrm{soft}} &\equiv \int_{soft} \frac{\mu^{4-D}d^{D-1}k_4}{2(2\pi)^{D-1}E_4} \\ &= \frac{(\pi\mu^2)^\epsilon\Gamma(1-\epsilon)}{(2\pi^3)\Gamma(1-2\epsilon)}\int_0^{\frac{\delta_s\sqrt{s}}{2}} E_4^{1-2\epsilon}dE_4\int_0^\pi \sin^{1-2\epsilon}\theta_1 d\theta_1\int_0^\pi \sin^{-2\epsilon}\theta_2 d\theta_2.\end{aligned} \quad (5.45)$$

In our case when the gluon with momentum k_4 is soft, we will need the results for the integrals $\int^{soft-region}\frac{dPS_{k_4\,\mathrm{soft}}}{(P\cdot k_4)^2}$ and $\int^{soft-region}\frac{dPS_{k_4\,\mathrm{soft}}}{k_3\cdot k_4 P\cdot k_4}$, which are again listed in Appendix B. For our case, $S^{(2)}_{k_4\,\mathrm{soft}}({}^3P_J^{[8]})$ explicitly vanishes, and since the soft term $S^{(3)}_{k_4\,\mathrm{soft}}({}^3P_J^{[8]})$ is expressed in terms of the squared matrix elements of the states ${}^1S_0^{[8]}$ and ${}^3S_1^{[1]}$, which are actually zero, so that the soft term $S^{(3)}_{k_4\,\mathrm{soft}}({}^3P_J^{[8]})$ also does not contribute. Therefore, our final partonic result of the process $e^+e^- \to c\bar{c}[n] + g + g$ for this part of the real cross-section becomes:

$$\begin{aligned}d\hat{\sigma}^{soft} &= \frac{1}{4}\frac{1}{16\pi s^2}\int^{soft-region} dPS_{k_4\,\mathrm{soft}}\sum_n\sum_{col,pol} S^{(1)}_{k_4\,\mathrm{soft}}(n)dt \\ &= \frac{g_s^2 C_A}{8\pi^2}C_\epsilon d\hat{\sigma}^{Born}(e^+e^- \to c\bar{c}[n] + g)[\frac{1}{\epsilon^2} + \frac{1}{\epsilon}\left(1 - \ln(\frac{\delta_s^2 s^2}{4m_c^4})\right) - \ln(\frac{\delta_s^2 s}{m_c^2}) \\ &\quad + \frac{1}{2}\ln^2(\frac{\delta_s^2 s^2}{4m_c^4}) + \frac{s + 4m_c^2}{s_1}\ln(\frac{s}{4m_c^2}) + 2\mathrm{Li}_2(-\frac{s_1}{4m_c^2} - \frac{\pi^2}{4})]\end{aligned} \quad (5.46)$$

where $C_A = 3$, and $d\hat{\sigma}^{Born}(e^+e^- \to c\bar{c}[n] + g)$ is defined in the eq.(5.6), so that the differential cross-section for the soft part becomes:

$$d\sigma^{soft} = d\hat{\sigma}^{soft}(e^+e^- \to c\bar{c}[n] + g + g) \times \frac{\langle \mathcal{O}^{J/\psi}[n]\rangle}{N_{col}(n)N_{pol}(n)}. \quad (5.47)$$

We now move on to calculate the remaining two parts of the real corrections.

Hard Collinear Region:

When all the outgoing gluons are hard, but any two of the external light particles become collinear to each other, the phase space encounters collinear singularities in this region. These singularities appear in the Feynman diagrams where one massless gluon/light-quark line splits into two external massless gluon/light-quark lines. Following the procedures of [45], the hard-collinear region of the phase space is limited by the condition when any of the invariants s_3, t_6, u_6, t', u' becomes smaller in magnitude than $\delta_c s$, for the slicing parameter δ_c. Since in our case, we have partons only in the final state, the collinear divergences appear in the phase space region where light particle with momentum k_3 becomes collinear to the other final state light particle with momentum k_4, as shown in fig.5.6, where parton say $3'$ splits into the two outgoing partons 3 and 4. The momenta of the final state partons, with the relation $k_{3'} = k_3 + k_4$, are parametrized as:

$$k_3 = (zP + \frac{p_\perp^2}{2zP}, 0, p_\perp, zP), \tag{5.48}$$

$$k_4 = ((1-z)P + \frac{p_\perp^2}{2(1-z)P}, 0, -p_\perp, (1-z)P), \tag{5.49}$$

where z is the splitting parameter, defining the fraction of the parton 3 momentum taken away by the final state parton $3'$, the small transverse momentum $p_\perp$ is still allowed to the partons 3 and 4 despite their collinearity. This region of phase space is defined by the limits $0 \leq s_3 \leq \delta_c s$, where at the leading order in $p_\perp$,

$$s_3 = 2k_3.k_4 = \frac{p_\perp^2}{z(1-z)} \tag{5.50}$$

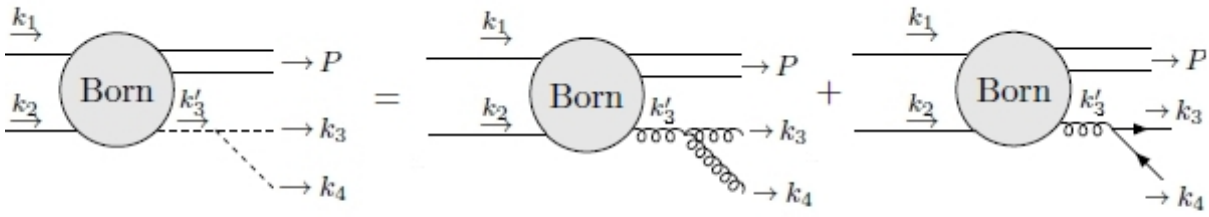

Figure 5.6: The final state parton with momentum k_3 collinear to another final state parton with momentum k_4. For our real processes $e^+e^- \to c\bar{c}[n] + g + g$ and $e^+e^- \to c\bar{c}[n] + q + \bar{q}$, we only have a gluon splitting into two gluons or a light quark-antiquark pair.

In $D = 4 - 2\epsilon$, the phase space factorizes as

$$\begin{aligned}\mathrm{dPS}_{2\to3} &= \frac{\mu^{2\epsilon}d^{D-1}P}{2(2\pi)^{D-1}E_{J/\psi}}\frac{\mu^{2\epsilon}d^{D-1}k_3}{2(2\pi)^{D-1}E_3}\frac{\mu^{2\epsilon}d^{D-1}k_4}{2(2\pi)^{D-1}E_4}\times(2\pi)^D\delta^{(D)}(k_1+k_2-P-k_3-k_4)\\ &= \mathrm{dPS}^{h.c.}_{2\to2}\times\mathrm{dPS}^{h.c.}_{k_4}\end{aligned}$$

where the factors with superscript $(h.c)$, representing the hard-collinear region of phase space, are defined as:

$$\begin{aligned}\mathrm{dPS}^{h.c.}_{2\to2} &\equiv \frac{\mu^{2\epsilon}d^{D-1}P}{2(2\pi)^{D-1}E_{J/\psi}}\frac{\mu^{2\epsilon}d^{D-1}k_{3'}}{2(2\pi)^{D-1}k_{3',0}}(2\pi)^D\delta^{(D)}(k_1+k_2-P-k_{3'})\\ \mathrm{dPS}^{h.c.}_{k_4} &\equiv \frac{\mu^{2\epsilon}d^{D-1}}{2(2\pi)^{D-1}}\frac{k_4}{E_4}\frac{k_{3',0}}{E_3}.\end{aligned}\tag{5.51}$$

With the change of variables from $k_{3'}\to k_3+k_4$, the term $\mathrm{dPS}^{h.c.}_{k_4}$ in the collinear limit $k_3\parallel k_4$, making use of the equations (5.48-5.50), is evaluated to be

$$\mathrm{dPS}^{h.c.}_{k_4} = \frac{(4\pi\mu^2)^\epsilon}{16\pi^2\Gamma(1-\epsilon)}(z(1-z)s_3)^{-\epsilon}dzds_3,\tag{5.52}$$

The squared matrix elements for the process $e^+e^-\to c\bar{c}[n]+3+4$ factorize according to the relation:

$$\begin{aligned}\sum_{col,pol}\left|\mathcal{M}_{3'\to34}(e^+e^-\to c\bar{c}[n]+3+4)\right|^2 &= \frac{2g_s^2}{s_3}(P'_{33'}(z)+\epsilon P_{33'}(z))\\ &\times\sum_{col,pol}\left|\mathcal{M}_{Born}(e^+e^-\to c\bar{c}[n]+3')\right|^2,\end{aligned}\tag{5.53}$$

where the squared matrix elements for the Born level process $e^+e^-\to c\bar{c}[n]+3$ also depends on z. The functions $P_{33'}(z)$ and $P'_{33'}(z)$ are the Altarelli-Parisi splitting functions [47] in D-dimensions, and the set of those required for our process are:

$$P_{gg'}(z) = 2C_A\left(\frac{z}{1-z}+\frac{1-z}{z}+z(1-z)\right)\tag{5.54}$$

$$P'_{gg'}(z) = 0\tag{5.55}$$

$$P_{qg'}(z) = \frac{1}{2}\left(z^2+(1-z)^2\right)\tag{5.56}$$

$$P'_{qg'}(z) = -z(1-z),\tag{5.57}$$

where g' stands for the intermediate gluon which splits into two quarks or two gluons, g is the final state gluon and q the light quark. The general partonic hard collinear

cross-section can then be written as:

$$d\hat{\sigma}^{h.c.}(e^+e^- \to c\bar{c}[n]+3+4) = \frac{1}{4}\frac{1}{2s}\int^{h.c.} \mathrm{dPS}^{h.c.}_{2\to 2}\mathrm{dPS}^{h.c.}_{k_4} \times \sum_n \sum_{col,pol} \left|\mathcal{M}_{3'\to 34}(e^+e^- \to c\bar{c}[n]+3+4)\right|^2 dt$$
$$= (1-\frac{\delta_{3,4}}{2}) d\hat{\sigma}^{Born}(e^+e^- \to c\bar{c}[n]+3') \frac{g_s^2}{8\pi^2}\frac{(4\pi\mu^2)^\epsilon)}{\Gamma(1-\epsilon)}\int_0^{\delta_c s} ds_3 s_3^{-1-\epsilon} \times \int_{z_{min}}^{z_{max}} dz (z(1-z))^{-\epsilon}(P_{33'}(z)+\epsilon P'_{33'}(z))$$

where the factor $(1-\frac{\delta_{3,4}}{2})$ comes in to take care of the additional factor $\frac{1}{2}$, which is there for the case of two external gluons in the final state. In the case of two external gluons, we are have to consider exclusion of the soft region from the hard collinear integration. The integration limits on z thus also depend on the nature of the final state partons 3 and 4. Therefore,

$$d\hat{\sigma}^{h.c.}(e^+e^- \to c\bar{c}[n]+3+4) = (1-\frac{\delta_{3,4}}{2}) d\hat{\sigma}^{Born}(e^+e^- \to c\bar{c}[n]+3') \frac{g_s^2}{8\pi^2}(\frac{4\pi\mu^2}{\delta_c s})^{(\epsilon)} \times \frac{1}{\Gamma(1-\epsilon)}(-\frac{1}{\epsilon})\int_{z_{min}}^{z_{max}} dz (z(1-z))^{-\epsilon}(P_{33'}(z)+\epsilon P'_{33'}(z)) \quad (5.58)$$

where $0 \leq z \leq 1$ for partons 3 and 4 being quarks/antiquarks and $\frac{\delta_s s}{s_1} \leq z \leq 1-\frac{\delta_s s}{s_1}$ for partons 3 and 4 being gluons.
The final partonic cross-section in the hard collinear region for the two cases when both the final state partons 3 and 4 are gluons or a light quark-antiquark pair, are obtained by integrating over z in the above equation. So that, when a gluon splits into two gluons, then

$$d\hat{\sigma}^{hard-collinear}(e^+e^- \to c\bar{c}[n]+g+g) = \frac{g_s^2 C_A}{8\pi^2} C_\epsilon d\hat{\sigma}^{Born}(e^+e^- \to c\bar{c}[n]+g)[\frac{1}{\epsilon}(2\ln(\frac{\delta_s s}{s_1}) + \frac{11}{6}) - (2\ln(\frac{\delta_s s}{s_1})+\frac{11}{6})\ln(\frac{\delta_c s}{m_c^2}) - \ln^2(\frac{\delta_s s}{s_1}) + \frac{67}{18} - \frac{\pi^2}{3}] \quad (5.59)$$

or when the gluon $3'$ splits into a light quark-antiquark pair:

$$d\hat{\sigma}^{hard-collinear}(e^+e^- \to c\bar{c}[n]+q+\bar{q}) = \frac{g_s^2}{8\pi^2}\frac{n_f}{3} C_\epsilon d\hat{\sigma}^{Born}(e^+e^- \to c\bar{c}[n]+g) \times \left[-\frac{1}{\epsilon}+\ln(\frac{\delta_c s}{m_c^2})-\frac{5}{3}\right] \quad (5.60)$$

where $C_A = 3$, n_f is the number of light quark flavors considered, $d\hat{\sigma}^{Born}(e^+e^- \to c\bar{c}[n]+g)$ defined in eq.(5.6). So analogous to the previous parts, the differential cross-section for the hard collinear part is:

$$d\sigma^{hard-collinear} = d\hat{\sigma}^{hard-collinear}(e^+e^- \to c\bar{c}[n]+gg/q\bar{q}) \times \frac{\langle \mathcal{O}^{J/\psi}[n]\rangle}{N_{col}(n)N_{pol}(n)}. \quad (5.61)$$

After the calculation of these soft and hard-collinear singularities, we could explicitly show the cancellation of the left over IR singularities from the virtual corrections. So now, the remaining matrix elements are finite.

Hard Non-Collinear Region:

The $2 \to 3$ processes contributing to this part are 5.2 and 5.3. This is the IR finite region of phase space, so that the it can be computed numerically in four dimensions using standard techniques for Monte-Carlo integration. This part is very much similar to the calculations presented in sections 4.2.1 for $2 \to 3$ process $\gamma + \gamma \to c\bar{c}[n] + c + \bar{c}$, while replacing the heavy open $c\bar{c}$ pair with a massless pair of light final state partons $gg/q\bar{q}$, with no initially interacting particles being resolved to a photon or a parton. So that eq.(4.29) remains the same with $s+t+u = 4m_c^2$ but the factor $\frac{\sqrt{s_3-4m_c^2}}{2\sqrt{s_3}}$ disappears in eq.(4.33), with only the expressions for $\cos\theta^{'}$ and $\cos\varphi^{'}$ changed to:

$$\begin{aligned} \cos\theta^{'} &= \frac{1}{p^{'}_{J/\psi}}\left(\frac{s_4}{\sqrt{s_3}} - E^{'}_{J/\psi}\right) , \\ \cos\varphi^{'} &= \frac{1}{\sin\theta^{'}_1 \sin\theta^{'}}\left(1 + \frac{u_6}{\sqrt{s_3}E^{'}_1} - \cos\theta^{'}_1 \cos\theta^{'}\right). \end{aligned} \tag{5.62}$$

by the change in parametrization of the two final state momenta of massless particles:

$$\begin{aligned} k^{'}_3 &= \frac{\sqrt{s_3}}{2}(1, \sin\theta^{'}\sin\varphi^{'}, \sin\theta^{'}\cos\varphi^{'}, \cos\theta^{'}) \\ k^{'}_4 &= \frac{\sqrt{s_3}}{2}(1, -\sin\theta^{'}\sin\varphi^{'}, -\sin\theta^{'}\cos\varphi^{'}, -\cos\theta^{'}), \end{aligned} \tag{5.63}$$

so that the partonic cross-section becomes:

$$\begin{aligned} d\hat{\sigma}^{hard-noncollinear}(e^+e^- \to c\bar{c}[n] + gg/q\bar{q}) = \frac{1}{4}\frac{1}{2s} \times \frac{\pi}{8s(2\pi)^5} dt ds_3 d(\cos\theta^{'}) d\varphi^{'} \times \left(1 - \frac{\delta_{3,4}}{2}\right) \\ \times \sum_n \sum_{col,pol} |\mathcal{M}(e^+e^- \to c\bar{c}[n] + gg/q\bar{q})|^2. \end{aligned}$$

where the tree level matrix elements for the $2 \to 3$ process involved are calculated applying the projectors as in chapter 3 and then expressed in terms of the Mandelstam invariants. The factor $\left(1 - \frac{\delta_{3,4}}{2}\right)$ takes care of two identical particles (gluons in our case) in the final state. For the case of two final state gluons, we also have to subtract the corresponding ghost contributions in order to use eq.(3.24) for the sum of gluon polarizations. The integration limits over the variables also vary as:

$$0 < \sqrt{s_3} < \sqrt{s} - 2m_c, \quad -1 < \cos\theta^{'} < 1, \quad 0 < \varphi^{'} < 2\pi. \tag{5.64}$$

Then the differential cross-section analogous to the other parts for this regions is:

$$d\sigma^{hard-noncollinear} = d\hat{\sigma}^{hard-noncollinear}(e^+e^- \to c\bar{c}[n] + gg/q\bar{q}) \times \frac{\langle \mathcal{O}^{J/\psi}[n] \rangle}{N_{col}(n) N_{pol}(n)}. \quad (5.65)$$

With all the parts of eq.(5.4) calculated analytically now and having $\frac{d\sigma^{NLO}}{dt}$ at hand, we can move on further to the calculations of the numerical results and compare them with the experimental observables.

5.4 Numerical Analysis:

In order to define the general Mandelstam invariants in the set of equations (5.8-5.13), we parametrize the momenta as:

$$\begin{aligned} k_{e^+} &= \frac{\sqrt{S_H}}{2}(1,0,0,1) \\ k_{e^-} &= \frac{\sqrt{S_H}}{2}(1,0,0,-1) \\ P &= (E_{J/\psi}, 0, P_{J/\psi}\sin\theta\ , P_{J/\psi}\cos\theta) \end{aligned} \quad (5.66)$$

for the center of mass energy S_H, the J/ψ 3-momentum $P_{J/\psi}$ and the J/ψ production angle θ. Therefore,

$$s = (k_{e^+} + k_{e^-})^2 = S_H \quad (5.67)$$

$$t = (P - k_{e^+})^2 = 4m_c^2 - \sqrt{S_H}(E_{J/\psi} - P_{J/\psi}\cos\theta) \quad (5.68)$$

$$u = (P - k_{e^-})^2 = 4m_c^2 - \sqrt{S_H}(E_{J/\psi} + P_{J/\psi}\cos\theta). \quad (5.69)$$

Since all the contributions to the cross section are $2 \to 2$ processes except for the hard-noncollinear region which is a $2 \to 3$, the expressions for $E_{J/\psi}$ and $\cos\theta$ vary according to the relation $s + t + u = 4m_c^2 + s_3$, as:

$$\begin{aligned} E_{J/\psi} &= \frac{s + 4m_c^2 - s_3}{2\sqrt{S_H}}, \\ P_{J/\psi} &= \sqrt{E_{J/\psi}^2 - 4m_c^2}, \\ \cos\theta &= \frac{s + 2t - 4m_c^2 - s_3}{2\sqrt{S_H} P_{J/\psi}}, \end{aligned} \quad (5.70)$$

where $s_3 = 0$ for $2 \to 2$ processes. The general form of the differential cross section then is given by:

$$\begin{aligned} d\sigma^{NLO} &= d\sigma_{2\to2} + d\sigma_{2\to3}, \\ &\propto dt + dt\ ds_3\ d(\cos\theta')d\varphi', \end{aligned} \quad (5.71)$$

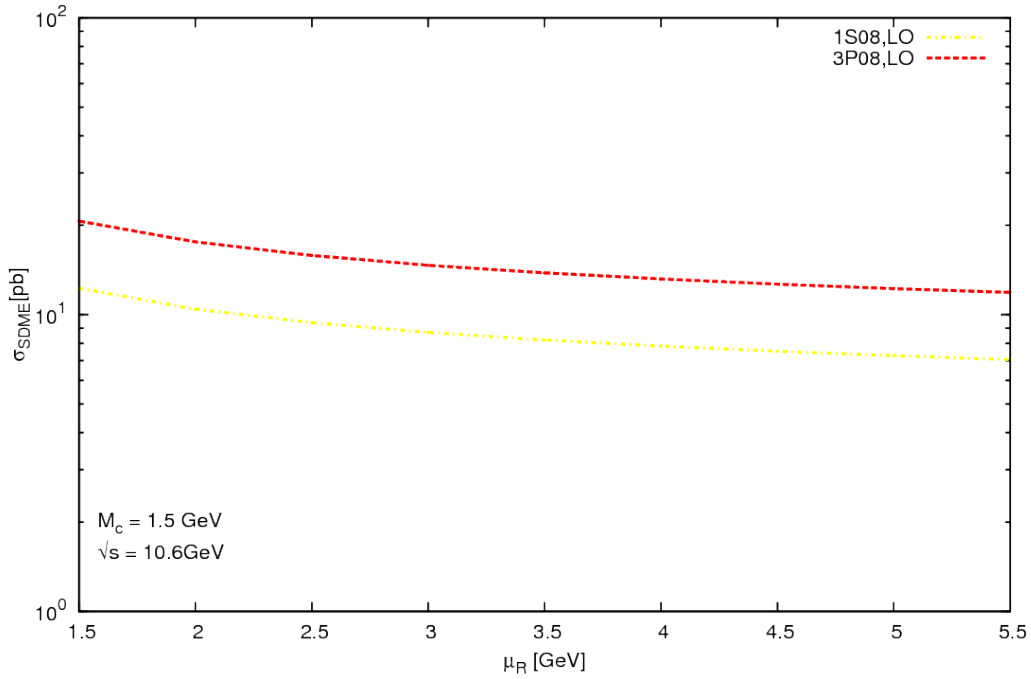

Figure 5.7: Renormalization Scale dependence of the LO short distance cross section.

which after the change of variables from t(or (t, s_3)) to $P_{J/(\psi}$ (or $(P_{J/\psi}, \cos\theta)$) for $2 \to 2$(or $2 \to 3$) processes, becomes:

$$d\sigma^{NLO} \quad \propto \quad \sqrt{s} P_{J/\psi}\, d(\cos\theta) + 2s \frac{P_{J/\psi}^2}{E_{J/\psi}}\, dP_{J/\psi}\, d(\cos\theta)\, d(\cos\theta')d\varphi'. \tag{5.72}$$

From here we can calculate $\frac{d\sigma^{NLO}}{d(\cos\theta)}$ or $\frac{d\sigma^{NLO}}{dP_{J/\psi}}$. It is important to note that for the $2 \to 2$ processes, $P_{J/\psi}$ has a constant value, namely $P_{J/\psi} \approx 4.88GeV$ for $\sqrt{s} = 10.6GeV$ and $M_c = 1.5GeV$. Thus these do not contribute to $\frac{d\sigma^{NLO}}{dP_{J/\psi}}$ distribution at other $P_{J/\psi}$ values.

The numerical analysis is performed following the same steps as discussed in section 4.4, using VEGAS[39]. We could reproduce the results of [48] for the renormalization constant and J/ψ momentum distribution, respectively, in the case of color singlet states (that is for the LO process of the reference [48]). Also, the results of [49] by the same authors were verified, for the differential cross section with respect to the production angle of J/ψ, using the input parameters as described in the respective references. The results for the renormalization scale dependence for the short distance cross section (without multiplying with the LDMEs) are presented in fig 5.7 and 5.8. The leading order results are in good agreement with those presented in [15], while we get larger corrections at NLO for this process. These NLO results for the short distance cross section distribution against renormalization constant are even larger than those in [15]. Such large corrections are very much possible since at LO, almost everything drops out. The reason for the disagreement with [15] can be the extra diagrams considered in our NLO calculations.

For the plots of our calculations presented here, the same values for the input parameters are taken as discussed earlier in section 4.4, whereas the renormalization constant $\mu_r = m_t$ for $m_t = \sqrt{\frac{(s+t-s_3)\times(4m_c^2-t)}{s}}$. We could verify the independence of the NLO cross section on the unphysical slicing parameters, as shown in 5.9. We also show the distribution of the differential cross section with respect to the production angle of J/ψ and also the 3 momentum of J/ψ, in figure 5.10 and 5.12. The results for the color singlet states are in agreement with those presented in [48]. As can be seen from figure 5.12, the momentum distribution for the states ${}^1S_0^8$ and ${}^3P_0^8$ at NLO are not reliable. The reason is obvious from fig.5.4 and eq.(5.72). The terms containing soft singularities are expressed in terms of the Born level matrix elements multiplied with an eikonal factor, as discussed earlier. Since the contribution of Born level matrix elements for the states ${}^1S_0^8$ and ${}^3P_0^8$ is non-zero, unlike the states ${}^3S_1^1$ and ${}^3S_1^8$, their eikonal factor contains a soft singularity in the form of a factor $\sim \frac{1}{k_3^2} \sim \frac{1}{(P_{J/\psi}-P_{J/\psi,max})^2}$, whereas the point $P_{J/\psi} \to P_{J/\psi,max} \simeq 4.88\text{GeV}$ is exactly the limit where the external gluon in the process $e^+e^- \to J/\psi + g$ gets soft. Therefore, cross section will be proportional to $\frac{1}{k^2}$, where k is the momentum of the external gluon. As can be seen from eq.(5.72), $\frac{d\sigma^{NLO}}{dP_{J/\psi}}$ distribution does not include the $2 \to 2$ processes, so we integrate over the whole phase space for our $2 \to 3$ process instead of making use of phase space slicing method. Therefore, the states ${}^1S_0^8$ and ${}^3P_0^8$ actually contain the singular behaviors of the external gluon in $\frac{d\sigma^{NLO}}{dP_{J/\psi}}$, which was supposed to be canceled by the corresponding $2 \to 2$ soft contribution. This uncanceled singularity then emerges as the exploding behavior for ${}^1S_0^8$ and ${}^3P_0^8$ states at

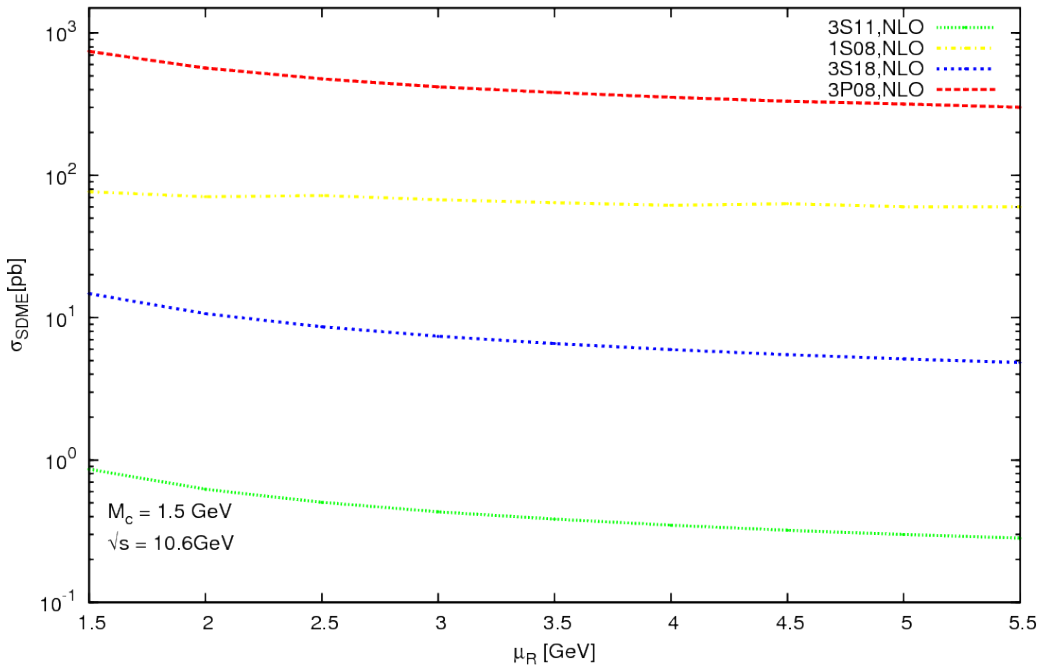

Figure 5.8: Renormalization Scale dependence of the NLO short distance cross section.

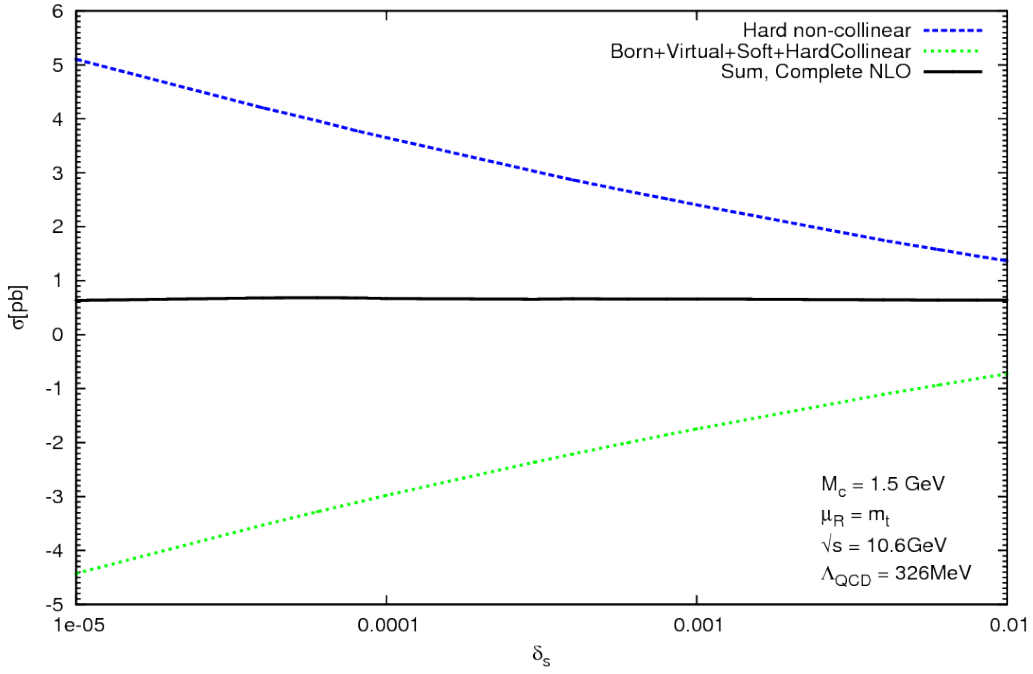

Figure 5.9: Verification of the independence on phase space slicing parameter, where $\delta_c = \delta_s/100$.

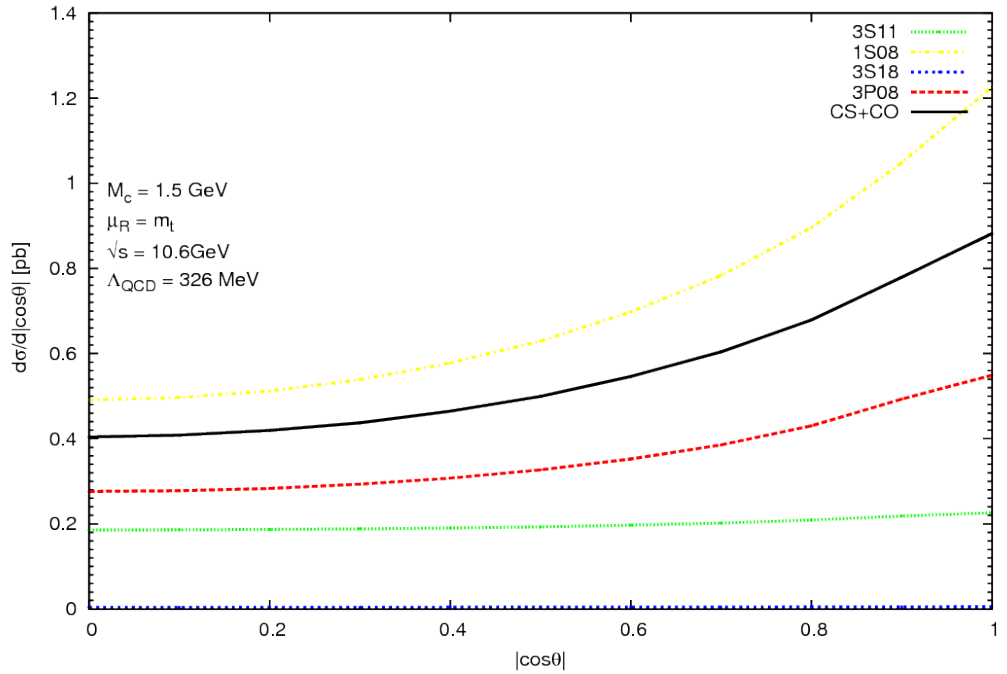

Figure 5.10: Differential cross section distribution at NLO with respect to production angle of J/ψ, where the line representing ${}^3P_0^8$ intermediate state is negative.

high momentum values. The theoretical calculations of the momentum distribution for these states are therefore not reliable. This is why, we expressed our actual results for ${}^3S_1^1$ and ${}^3S_1^8$ states in fig.5.14. If we would integrate in $D-$dimensions over the whole range of momentum, and add the $2 \to 2$ kinematics contribution at $P_{J/\psi} \simeq 4.88 GeV$, we would arrive at a finite total cross section. The results varying the renormalization constant are presented in fig.5.13, where the known fact that the momentum distribution can well be reproduced by the color singlet model alone is recovered. It can also be seen that the CS+CO contributions give a good description up to about 3.5GeV.

5.5 Conclusions:

We present our next to leading order results for $\frac{d\sigma}{d(\cos\theta)}$ and $\frac{d\sigma}{dP_{J/\psi}}$ for the J/ψ production at B-factories, considering both the color singlet and color octet intermediate states. We could reproduce some of the results available in the literature for color singlet contributions and found our results (using different input parameters) in close agreement with them too. We can see that the inclusion of color octet states contributes well to the behavior of $\frac{d\sigma}{d(\cos\theta)}$, which for the color singlet state only, was unable to describe the experimental data presented in a recent paper by the Belle collaboration [7]. But for the momentum distribution, we are unable to draw some concrete results about the contribution of these color octet states, due to the exploding behavior of ${}^1S_0^8$ and ${}^3P_0^8$ states at high momentum values, which arises as we integrate over the whole phase space for the

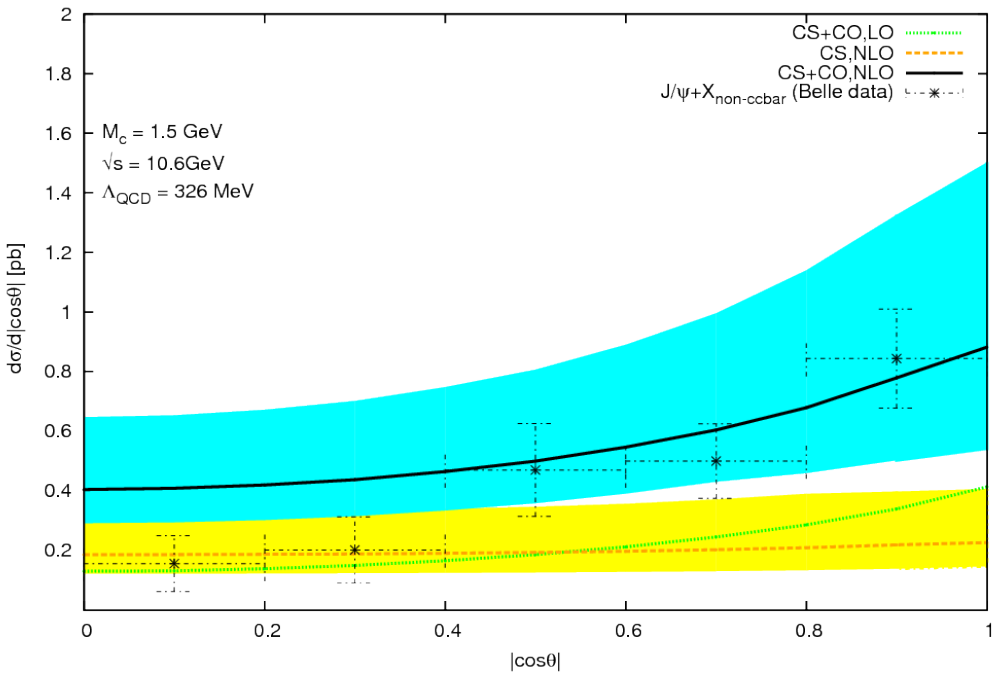

Figure 5.11: The error bands here are plotted varying the renormalization scale μ_R from $m_t/2$ to $2m_t$, and the mean value is taken at $\mu_R = m_t$.

$2 \to 3$ process. Therefore, the results for $\frac{d\sigma}{dP_{J/\psi}}$ should not be relied upon for these two states with an exploding behavior. We also could integrate the distribution with respect to the production angle of J/ψ to get the total cross section, which at LO is 0 for CS states but is 0.21pb for the contributing CO states. At NLO, we could reproduce the values of total cross-section for CS states and for the sum of all the CS and CO states pesented in fig.1p of [13]. Considering the theoretical and experimental uncertainties and the fact of non-establishment of the universality of LDMEs, these results seem to be comparable with the Belle measurements, giving a value 0.43 ± 0.13pb, for the data with $J/\psi + c\bar{c}$ subtracted. The explanations presented in [13] for the differences with the experimental data are valid here too.

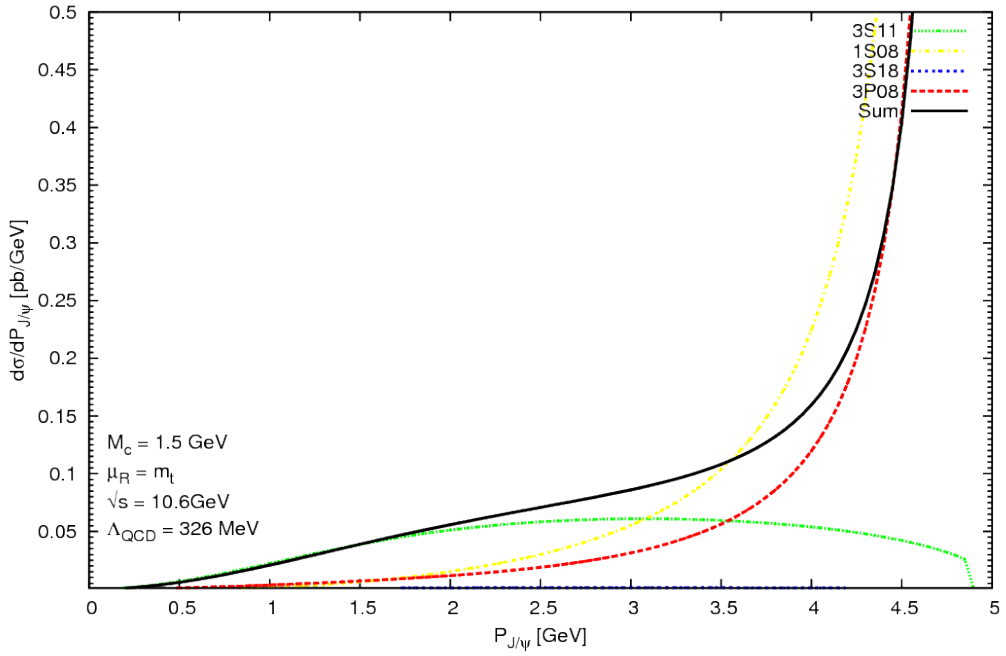

Figure 5.12: Differential cross section distribution with respect to J/ψ momentum, where the line representing ${}^3P_0^8$ intermediate state is negative.

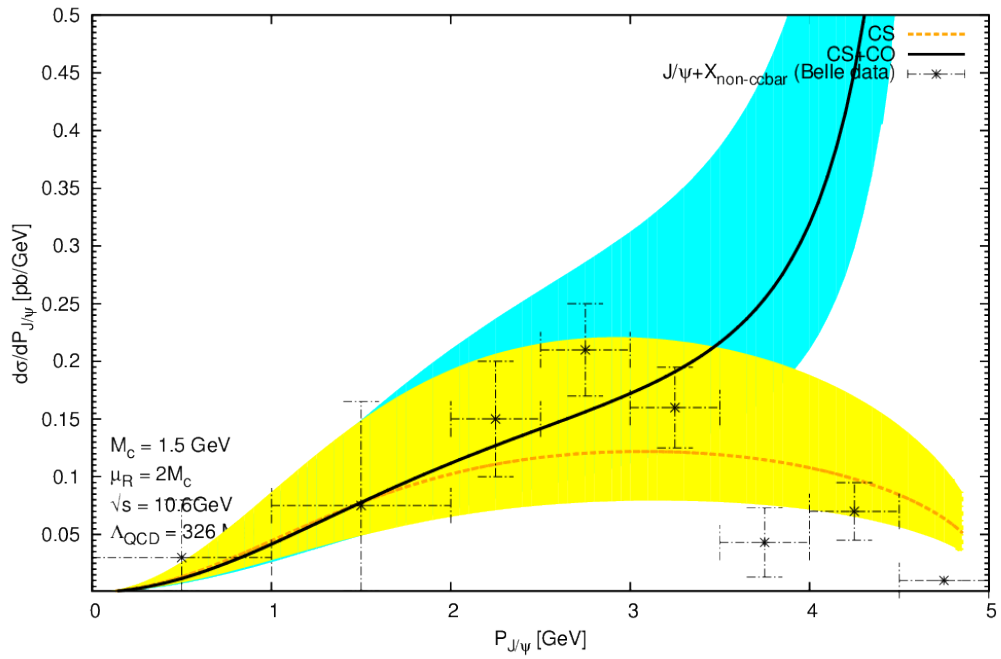

Figure 5.13: The error bands here are plotted varying the renormalization scale μ_R from $m_t/2$ to $2m_t$, and the mean value is taken at $\mu_R = m_t$. The LO $2 \to 2$ processes do not vary with $P_{J/\psi}$.

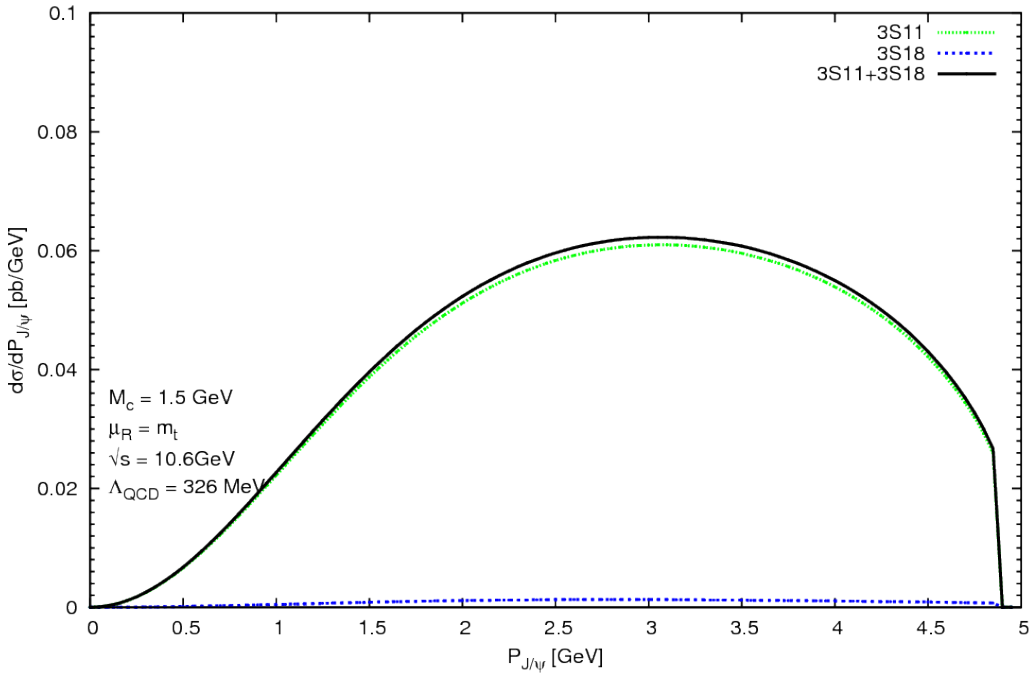

Figure 5.14: Differential cross section distribution with respect to J/ψ momentum, where the line representing ${}^3P_0^8$ intermediate state is negative.

6 Summary and Outlook

The production and decay of heavy quarkonia are well investigated using the rigorous factorization theorem provided by nonrelativistic QCD. The inclusion of both the color singlet (or color neutral) and color octet (or color charged) states is a key feature of this theory. This could resolve the issue of left over infrared divergences in the case of P-wave charmonia, and could also explain the transverse momentum, p_T, distribution of hadroproduction of J/ψ at Tevatron. Besides these undeniable successes, the significance of the color octet mechanism needs to be investigated in other high energy experiments, and the universality of the long distance matrix elements for these color octet states need to be established. This in turn will enhance the chances of nonrelativistic QCD to be considered as the correct theory for heavy quarkonia studies.

We have addressed here one of the open challenges to NRQCD posed by the recent Belle data [7], with much larger values than expected by NRQCD for $J/\psi+c\bar{c}$ associated production. We have investigated this process at other colliders, and for photo- and hadro-productions as well, like LEP, HERA, Tevatron and LHC, where it also plays an important contribution at the next-to-leading order (NLO) corrections.
Since several recent studies on the inclusive and exclusive charmonium production were able to reduce the conflict between the color singlet predictions and the experimental results, by the inclusion of color octet mechanism, we therefore found it necessary to investigate the effect of color octet states in charmonium production at B-factories, and compare our results with the recent experimental data of the Belle Collaboration [7]. For both the above studies, our calculations went through a series of validation checks, like:

- We could reproduce the already existing results in the literature, for color singlet states.
- Analytical cancellation of all the ultraviolet and infrared divergences was explicitly shown.
- We could compare our analytic expressions of the squared matrix elements with numerical results of MadOnia [38], for the real tree and born processes.
- The independence of our results on the unphysical phase space slicing parameter was analytically achieved, to test the kinematics used and verify the soft and collinear limits.

We could show that $J/\psi + c + \bar{c}$ is a very important process to be considered for J/ψ production studied at various colliders with different energy ranges. We found that for all of the colliders, this process is either of the same order of magnitude, or only an order of magnitude less than the NLO J/ψ production, when compared with the results presented in MB [13]. We could successfully reproduce the results of [11] for the CS contributions to $J/\psi + c + \bar{c}$ production at LEPII. The contributions of both the sum of color-singlet plus color-octet states and that of the CS ${}^3S_1^{[1]}$ intermediate state, was found to lie within the uncertainty bands of charm-mass and of renormalization/factorization scale at low energy scales of p_t distribution, at DELPHI for example, and $p_t/W/z$ distributions, at HERA-H1. But for high p_t values like at CDF and ATLAS, these bands are well separated, despite the cancellation of ${}^1S_0^{[8]}$ and ${}^3P_0^{[8]}$ intermediate states. This indicates the significance of ${}^3S_1^{[8]}$ intermediate state, arising from the gluon-fragmentation diagrams, for hadroproduction of $J/\psi + c + \bar{c}$ at high energies. At DELPHI and HERA, the direct photon-photon subprocess and the direct photoproduction process respectively contribute the largest part whereas the gluon-gluon process is the dominant one at hadron colliders.
We present the contributions of both the color singlet and color octet intermediate states for next to leading order J/ψ production at B-factories. The inclusion of color octet states in this process contributes well to the behavior of $\frac{d\sigma}{d(\cos\theta)}$, when compared with the recent experimental data by the Belle collaboration [7]. We are unable to draw some concrete conclusion about the color octet states' contributions in the momentum distribution, due to the exploding behavior of ${}^1S_0^8$ and ${}^3P_0^8$ states at high momentum values. This behavior is due to the integration over the whole phase space for the $2 \to 3$ process. The total cross-section was calculated to be ~ 0.7 pb. Our results are somewhat comparable with the Belle measurements [7], considering the large uncertainties in LDMEs and other dependences on input parameters, like charm mass and renormalization scale.

As an outlook for the process $J/\psi + c + \bar{c}$, we can consider where the final state open $c\bar{c}$ combines to form another charmonium state, or two other light mesons containing a charm/anti-charm quark with a light quark/anti-quark. With the set of programming scripts developed for this process, we can analogously calculate the various other charmonia/bottomonia associated production with the corresponding open heavy quark pair. Also, the techniques developed can help us to further investigate other charmonia/bottomonia production at next to leading order, not only for the direct processes at B-factories but also for resolved subprocesses at other colliders with higher energies. It will also be interesting to carry out the J/ψ polarization studies, including both the color-singlet and color-octet states for the above mentioned processes, in order to check the realization of NRQCD factorization mechanism in nature. Further investigations are emphasized to establish the universality of LDMEs by carrying out studies for quarkonia production/decay in different processes at various collider scenarios.

Appendix A: The Master Integrals

Analytical results for the scalar integrals which emerge from the Passarino-Veltman reduction of the virtual amplitude are expresses in terms of 5 master integrals listed in this Appendix. Since no imaginary part of the integrals contribute to the final results of the squared matrix elements, only the real parts are given. The four-momenta are related by $k_1 + k_2 = P + k_3$ and all particles are taken to be on-mass-shell, $k_1^2 = k_2^2 = k_3^2 = 0$ and $P^2 = 4m_c^2$.

– The scalar one-point function for tadpoles is given by

$$\begin{aligned} \mathrm{MI}_{1A} &\equiv \frac{(2\pi\mu)^{4-D}}{i\pi^2} \int \frac{\mathrm{d}^D q}{q^2 - m_c^2} \\ &= C_\epsilon \, m_c^2 \left[\frac{1}{\epsilon} + 1 + \left(1 + \frac{\pi^2}{12}\right) \epsilon \right] \end{aligned} \tag{A-1}$$

– The scalar two-point function for bubble diagrams appearing in our calculations are defined by:

$$\begin{aligned} \mathrm{MI}_{2A(-k_3)} &\equiv \frac{(2\pi\mu)^{4-D}}{i\pi^2} \int \frac{\mathrm{d}^D q}{[q^2 - m_c^2][(q + P + k_3)^2 - m_c^2]} \\ &= C_\epsilon \left[\frac{1}{\epsilon} + 2 + \beta \ln\left(\frac{1-\beta}{1+\beta}\right) \right] \end{aligned} \tag{A-2}$$

$$\begin{aligned} \mathrm{MI}_{2B(-k_3)} &\equiv \frac{(2\pi\mu)^{4-D}}{i\pi^2} \int \frac{\mathrm{d}^D q}{[q^2][(q + P/2 + k_3)^2 - m_c^2]} \\ &= C_\epsilon \, [\frac{1}{\epsilon} + 2 - \frac{s_1}{s_1 + 2m_c^2} \ln\left(\frac{s_1}{2m_c^2}\right) + \frac{\pi^2}{12}\epsilon + \frac{s_1}{s_1 + 2m_c^2}\epsilon \\ &\qquad (\ln^2\left(\frac{s_1}{2m_c^2}\right) - 2\ln\left(\frac{s_1}{2m_c^2}\right) - \ln\left(\frac{s_1}{2m_c^2}\right) \ln\left(1 + \frac{s_1}{2m_c^2}\right) \\ &\qquad\qquad -\mathrm{Li}_2\left(\frac{-s_1}{2m_c^2}\right) + \frac{8m_c^2}{s_1} - \pi^2 + \frac{\pi^2}{6} + 4)] \end{aligned} \tag{A-3}$$

– The scalar three-point function for triangle diagrams appearing in our process are:

$$\begin{aligned} \mathrm{MI}_{3D(-k_3)} &\equiv \frac{(2\pi\mu)^{4-D}}{i\pi^2} \int \frac{\mathrm{d}^D q}{[q^2]\,[(q + P/2)^2 - m_c^2]\,[(q + P/2 - k_1)^2 - m_c^2]} \\ &= C_\epsilon \, \frac{2}{t_1} \left[-\mathrm{Li}_2\left(1 + \frac{t_1}{2m_c^2}\right) + \frac{\pi^2}{6} \right] \end{aligned} \tag{A-4}$$

$$\begin{aligned}\mathrm{MI}_{3E(-k_3)} &\equiv \frac{(2\pi\mu)^{4-D}}{i\pi^2}\int \frac{\mathrm{d}^D q}{[q^2]\,[(q-P/2)^2-m_c^2]\,[(q+P/2+k_3)^2-m_c^2]} \\ &= C_\epsilon\,\frac{2}{s_1}\,[\mathrm{Li}_2\left(1-\frac{s}{2m_c^2}\right)-\mathrm{Li}_2\left(\frac{s_1+s}{s_1+\sqrt{ss_1}}\right)-\mathrm{Li}_2\left(\frac{s_1+s}{s_1-\sqrt{ss_1}}\right) \\ &\qquad +\mathrm{Li}_2\left(\frac{-4m_c^2}{s_1+\sqrt{ss_1}}\right)+\mathrm{Li}_2\left(\frac{-4m_c^2}{s_1-\sqrt{ss_1}}\right)+\frac{\pi^2}{12}]\end{aligned}$$

Appendix B: Soft Terms

Integrals: The integrals needed for our calculation of different terms in the region where outgoing gluon with momentum k_4 is soft, are:

$$\int^{soft-region} \frac{dPS_{k_4\,\text{soft}}}{(P\cdot k_4)^2} = \frac{1}{32\pi^2 m_c^2} C_\epsilon \left[-\frac{1}{\epsilon} - \frac{s+4m_c^2}{s_1}\ln(\frac{s}{4m_c^2}) + \ln(\frac{\delta_s^2 s}{m_c^2}) \right] \tag{B-1}$$

$$\int^{soft-region} \frac{dPS_{k_4\,\text{soft}}}{k_3\cdot k_4 P\cdot k_4} = \frac{1}{8\pi^2 s_1} C_\epsilon [\frac{1}{\epsilon^2} - \frac{1}{\epsilon}\ln(\frac{s^2\delta_s^2}{4m_c^4}) + \frac{1}{2}\ln^2(\frac{s^2\delta_s^2}{4m_c^4}) + 2\text{Li}_2(\frac{-s_1}{4m_c^2}) - \frac{\pi^2}{4} \tag{B-2}$$

$S^{(1)}_{k_4\,\text{soft}}(n)$**:** Using the summation over gluon polarizations as in eq.(3.25), we get the expression for $S^{(1)}_{k_4\,\text{soft}}(n)$ term as:

$$\int^{soft-region} dPS_{k_4\,\text{soft}} \sum_{col,pol} S^{(1)}_{k_4\,\text{soft}}(n) = g_s^2 \sum_{col,pol} \langle n, \text{Born}|\mathbf{T}_3\mathbf{T}_3|n,\text{Born}\rangle \times \int^{soft-region} dPS_{k_4\,\text{soft}} \left(\frac{2P\cdot k_3}{k_3\cdot k_4 P\cdot k_4} + \frac{P^2}{(P\cdot k_4)^2} \right) \tag{B-3}$$

where we calculate the value for the factor

$$\sum_{col,pol} \langle n, \text{Born}|\mathbf{T}_3\mathbf{T}_3|n,\text{Born}\rangle = C_A \sum_{col,pol} |\mathcal{M}_{\text{Born}}(n)|^2. \tag{B-4}$$

With the insertion of the results for the integrals above, we get the expression for contribution of the soft term $S^{(1)}_{k_4\,\text{soft}}(n)$ into the partonic cross section as:

$$d\hat{\sigma}^{S^{(1)}_{k_4\,\text{soft}}(n)} = \frac{g_s^2 C_A}{8\pi^2} C_\epsilon d\hat{\sigma}^{Born}(e^+e^- \to c\bar{c}[n]+g)[\frac{1}{\epsilon^2} + \frac{1}{\epsilon}\left(1 - \ln(\frac{\delta_s^2 s^2}{4m_c^4})\right) - \ln(\frac{\delta_s^2 s}{m_c^2}) + \frac{1}{2}\ln^2(\frac{\delta_s^2 s^2}{4m_c^4}) + \frac{s+4m_c^2}{s_1}\ln(\frac{s}{4m_c^2}) + 2\text{Li}_2(-\frac{s_1}{4m_c^2} - \frac{\pi^2}{4})] \tag{B-5}$$

$S^{(2)}_{k_4\,\text{soft}}(n)$**:** Again using the polarization summation for gluon in eq.(3.25) and $n = {}^3P_J^{[8]}$ for this term, the integral

$$\int^{soft-region} dPS_{k_4\,\text{soft}} \sum_{col,pol} S^{(2)}_{k_4\,\text{soft}}(n) = 4g_s^2 \int^{soft-region} dPS_{k_4\,\text{soft}} \sum_{col,pol} \frac{k_3\cdot\epsilon(k_4) k_3\epsilon^*(k_4)}{k_3\cdot k_4 P\cdot k_4} \varepsilon^{(J)}_{\alpha\beta} \times \langle {}^3P_J^{[8]}, \text{Born}\,|\mathbf{T}_3(\mathbf{T}_c - \mathbf{T}_{\bar{c}})\text{Tr}[\mathcal{C}_8\Pi_1^\alpha|\text{Born}\rangle]|_{q=0}\,,$$

$$= 4g_s^2 \int^{soft-region} dPS_{k_4\ \rm soft} \sum_{col,pol} \times((-\frac{k_3^\beta}{k_3\cdot k_4 P\cdot k_4}) + (\frac{P^\beta}{(P\cdot k_4)^2})$$
$$+\frac{(P\cdot k_3)k_4^\beta}{(k_3\cdot k_4)(P\cdot k_4)^2} - \frac{P^2 k_4^\beta}{(P\cdot k_4)^3}) \times \varepsilon^{(J)}_{\alpha\beta}\langle {}^3P_J^{[8]}, \text{Born}\,|\mathbf{T}_3(\mathbf{T}_c - \mathbf{T}_{\bar{c}})\text{Tr}[\mathcal{C}_8\Pi_1^\alpha|\text{Born}\rangle]|_{q=0}\,,$$
$$= 4g_s^2(P^\beta - \frac{P^2}{P\cdot k_3}k_3^\beta)\sum_{col,pol}\varepsilon^{(J)}_{\alpha\beta}\langle {}^3P_J^{[8]}, \text{Born}\,|\mathbf{T}_3(\mathbf{T}_c - \mathbf{T}_{\bar{c}})\text{Tr}[\mathcal{C}_8\Pi_1^\alpha|\text{Born}\rangle]|_{q=0}$$
$$\times \int^{soft-region} \frac{dPS_{k_4\ \rm soft}}{(P\cdot k_4)^2}, \tag{B-8}$$

so that we can use the integral (B-1) to get the partonic contribution of this term, as:

$$d\hat{\sigma}^{S^{(2)}_{k_4\ \rm soft}({}^3P_J^{[8]})} = \frac{1}{4}\frac{1}{2s}\frac{1}{8\pi s}\frac{g_s^2}{8\pi^2 m_c^2}C_\epsilon[-\frac{1}{\epsilon} - \frac{s+4m_c^2}{s_1}\ln(\frac{s}{4m_c^2}) + \ln(\frac{\delta_s^2 s}{m_c^2})](P^\beta - \frac{P^2}{P\cdot k_3}k_3^\beta)$$
$$\times[\sum_{col,pol}\varepsilon^{(J)}_{\alpha\beta}\langle {}^3P_J^{[8]}, \text{Born}\,|\mathbf{T}_3(\mathbf{T}_c - \mathbf{T}_{\bar{c}})\text{Tr}[\mathcal{C}_8\Pi_1^\alpha|\text{Born}\rangle]|_{q=0}]\,dt \tag{B-9}$$

which can not generally be further factorized in terms of the Born cross-section. For our process, evaluation of the above factor involving colors results into vanishing contribution of this term.

$\underline{S^{(3)}_{k_4\ \rm soft}(n)}$**:** This term also contributes only for the case when $n = {}^3P_J^{[8]}$. So the integration over phase space using the expression for summation over gluon polarization can proceed as:

$$\int^{soft-region} dPS_{k_4\ \rm soft}\sum_{col,pol} S^{(3)}_{k_4\ \rm soft}(n) = 4g_s^2\int^{soft-region} dPS_{k_4\ \rm soft}\sum_{col,pol}\frac{\epsilon^{\beta'}(k_4)\epsilon^{*\beta}(k_4)}{(P.k_4)^2}$$
$$\times\varepsilon^{(J)*}_{\alpha'\beta'}\varepsilon^{(J)}_{\alpha\beta}\text{Tr}[\langle\text{Born}|\Pi_1^{*\alpha'}\mathcal{C}_8]|_{q=0}(\mathbf{T}_c - \mathbf{T}_{\bar{c}})(\mathbf{T}_c - \mathbf{T}_{\bar{c}})\text{Tr}[\mathcal{C}_8\Pi_1^\alpha|\text{Born}\rangle]|_{q=0},$$
$$= 4g_s^2\int^{soft-region} dPS_{k_4\ \rm soft}(-\frac{g^{\beta\beta'}}{(P\cdot k_4)^2} + \frac{P^\beta k_4^{\beta'} + P^{\beta'}k_4^\beta}{(P\cdot k_4)^3} - \frac{P^2 k_4^\beta k_4^{\beta'}}{(P\cdot k_4)^4})$$
$$\times\sum_{col,pol}\varepsilon^{(J)*}_{\alpha'\beta'}\varepsilon^{(J)}_{\alpha\beta}\times\text{Tr}[\langle\text{Born}|\Pi_1^{*\alpha'}\mathcal{C}_8]|_{q=0}(\mathbf{T}_c - \mathbf{T}_{\bar{c}})(\mathbf{T}_c - \mathbf{T}_{\bar{c}})\text{Tr}[\mathcal{C}_8\Pi_1^\alpha|\text{Born}\rangle]|_{q=0},$$
$$= 4g_s^2\frac{D-2}{D-1}(-g^{\beta\beta'} + \frac{P^\beta P^{\beta'}}{P^2})\int^{soft-region}\frac{dPS_{k_4\ \rm soft}}{(P\cdot k_4)^2}\sum_{col,pol}\varepsilon^{(J)*}_{\alpha'\beta'}\varepsilon^{(J)}_{\alpha\beta}$$
$$\times\text{Tr}[\langle\text{Born}|\Pi_1^{*\alpha'}\mathcal{C}_8]|_{q=0}(\mathbf{T}_c - \mathbf{T}_{\bar{c}})(\mathbf{T}_c - \mathbf{T}_{\bar{c}})\text{Tr}[\mathcal{C}_8\Pi_1^\alpha|\text{Born}\rangle]|_{q=0},$$
$$= 4g_s^2\frac{D-2}{(D-1)^2}N_{pol}({}^3P_J^{[8]})(-g_{\alpha\alpha'} + \frac{P_\alpha P_{\alpha'}}{P^2})\int^{soft-region}\frac{dPS_{k_4\ \rm soft}}{(P\cdot k_4)^2}$$
$$\times\sum_{col,pol}\text{Tr}[\langle\text{Born}|\Pi_1^{*\alpha'}\mathcal{C}_8]|_{q=0}(\mathbf{T}_c - \mathbf{T}_{\bar{c}})(\mathbf{T}_c - \mathbf{T}_{\bar{c}})\text{Tr}[\mathcal{C}_8\Pi_1^\alpha|\text{Born}\rangle]|_{q=0},$$

(B-10)

where alongwith the simple tensor reduction, we made use of the equations (3.16-3.21) for the above transformation. Again making use of the equations 3.14 and 3.16, we may simplify the above expressions as:

$$\int^{soft-region} dPS_{k_4\ \mathrm{soft}} \sum_{col,pol} S^{(3)}_{k_4\ \mathrm{soft}}(n) = 4g_s^2 \frac{D-2}{(D-1)^2} N_{pol}({}^3P_J^{[8]}) \int^{soft-region} \frac{dPS_{k_4\ \mathrm{soft}}}{(P\cdot k_4)^2}$$
$$\times \sum_{col,pol} \langle {}^3S_1^{[8]}, \mathrm{Born}|(\mathbf{T}c - \mathbf{T}\bar{c})(\mathbf{T}c - \mathbf{T}\bar{c})|{}^3S_1^{[8]}, \mathrm{Born}\rangle. \quad \text{(B-11)}$$

For our process, we could explicitly express the factor containing amplitudes and colors as:

$$\sum_{col,pol} \langle {}^3S_1^{[8]}, \mathrm{Born}|(\mathbf{T}c - \mathbf{T}\bar{c})(\mathbf{T}c - \mathbf{T}\bar{c})|{}^3S_1^{[8]}, \mathrm{Born}\rangle = \sum_{col,pol} (\frac{C_A^2-4}{C_A}|\mathcal{M}_{\mathrm{Born}}({}^3S_1^{[8]})|^2$$
$$+8C_AC_F|\mathcal{M}_{\mathrm{Born}}({}^3S_1^{[1]})|^2) \quad \text{(B-12)}$$

so that with the insertion of integral (B-1) we could finally express the contribution of this term to the partonic cross-section as:

$$d\hat{\sigma}^{S^{(3)}_{k_4\ \mathrm{soft}}({}^3P_J^{[8]})} = \frac{g_s^2}{36\pi^2 m_c^2} N_{pol}({}^3P_J^{[8]}) C_\epsilon [-\frac{1}{\epsilon} - \frac{s+4m_c^2}{s_1}\ln(\frac{s}{4m_c^2}) + \ln(\frac{\delta_s^2 s}{m_c^2}) - \frac{1}{3}]$$
$$\times (\frac{C_A^2-4}{C_A} d\hat{\sigma}\mathrm{Born}(e^+e^- \to c\bar{c}[{}^3S_1^{[8]}] + g) + 8C_AC_F d\hat{\sigma}_{\mathrm{Born}}(e^+e^- \to c\bar{c}[{}^3S_1^{[1]}] + g). \quad \text{(B-13)}$$

In our process, the both of $|\mathcal{M}_{\mathrm{Born}}({}^3S_1^{[1]})|^2$ and $|\mathcal{M}_{\mathrm{Born}}({}^3S_1^{[8]})|^2$ are zero, so we do not get any contribution from this term. It is important to note that the IR term appearing in the above expression gets canceled by those appearing in the loop corrections of the corresponding operators $\langle \mathcal{O}^{J/\psi}[n]\rangle$ for the states, ${}^3S_1^{[1]}$ and ${}^3S_1^{[8]}$. Furthermore, an equal contribution of all these soft terms must be considered for the case when the gluon with momentum k_3 is soft. However, an additional factor $\frac{1}{2}$ comes in for two identical particles (gluons) in the finals state, balancing the mentioned factor 2 emerging from the addition of two soft contributions.

Bibliography

[1] J. Beringer *et al.* [Particle Data Group], Phys. Rev. D **86**, 010001 (2012).

[2] Final Activity Report - NREFT (Non-Relativistic Effective Filed Theories of QCD), 23.11.2011 at http://cordis.europa.eu/search

[3] A. Mosher, sLAC **0245**.

[4] E. Braaten, hep-ph/9702225.

[5] M. B. Voloshin Prog. Part. Nucl. Phys. **61**,455-511 (2008).

[6] A. A. Affolder *et al.* [CDF Collaboration], Phys. Rev. Lett. **85**, 2886 (2000).

[7] P. Pakhlov *et al.* [Belle Collaboration], Phys. Rev. D **79**, 071101(R) (2009).

[8] B. Aubert *et al.* [BABAR Collaboration], Phys. Rev. D **72**, 031101 (2005).

[9] C. Adolff *et al.* [H1 Collaboration] Eur. Phys. J. C **25**, 25 (2002);
F. D. Aaron *et al.* [H1 Collaboration] Eur. Phys. J. C **68**, 401 (2010).

[10] P. L. Cho and A. K. Leibovich, Phys. Rev. D **54**, 6690 (1996);
F. Yuan, C. F. Qiao and K. T. Chao, Phys. Rev. D **56**, 321 (1997);
S . Baek, P. Ko, J. Lee and H. S. Song, J. Korean Phys. Soc. **33**, 97 (1998);
K. Y. Liu, Z. G. He and K. T. Chao, Phys. Rev. D **68**, 031501 (2003);
K. Y. Liu, Z. G. He and K. T. Chao, Phys. Rev. D **69**, 094027 (2004);
Z. G. He, Y. Fan and K. T. Chao, Phys. Rev. D **75**, 074011 (2007);
Y. J. Zhang and K. T. Chao, Phys. Rev. Lett. **98**, 092003 (2007);
B. Gong and J. X. Wang, Phys. Rev. D **80**, 054015 (2009).

[11] C. F. Qiao and J. X. Wang, Phys. Rev. D **69**, 014015 (2004);
R. Li and K. T. Chao, Phys. Rev. D **79**, 114020 (2009).

[12] P. Artoisenet, J. P. Lansberg and F. Maltoni, Phys. Lett. B **653**, 60 (2007);
K. Hagiwara, W. Qi, C. F. Qiao and J. X. Wang, arXiv:0705.0803v3;
P. Artoisenet, ECONF C0706044: 21,(2007);
M. Klasen and J. P. Lansberg, Nucl. Phys. Proc. Suppl. 179-180, 226 (2008);
Z.G. He, R. Li and J.X. Wang, Phys. Rev. D **79**, 094003 (2009);
J. P. Lansberg, Eur. Phys. J. C **61**, 693 (2009).

[13] M. Butenschoen and B. A. Kniehl, Nucl. Phys. B Proceedings Supplement XX (2012) 1-11.

[14] S. P. Baranov, Phys. Rev. D **73**, 074021 (2006).

[15] Y. -J. Zhang, Y. -Q. Ma, K. Wang and K. -T. Chao, Phys. Rev. D **81**, 034015 (2010) [DOI:10.1103/PhysRevD.81.034015]

[16] N. Brambilla, S. Eidelman, B. K. Heltsley, R. Vogt and G. T. Bodwin, *et al.*, Eur. Phys. J. C **71**, 1534 (2011).

[17] H. Fritzsch, Phys. Lett. B **67**, 217 (1977).

[18] G. T. Bodwin, E. Braaten and J. Lee, Phys. Rev. D **72**, 014004 (2005).

[19] R. Gavai *et al.*, Int. J. Mod. Phys. A **10**, 3043 (1995), hep-ph/9502270.

[20] E. L. Berger and D. L. Jones, Phys. Rev. D **23**, 1521 (1981).

[21] E. Braaten, arXiv: hep-ph/9509210v1.

[22] G. A. Schuler, arXiv: hep-ph/9403387v1.

[23] A. Sansoni *et al.* [CDF Collaboration], Nuovo Cim. 109A, 827 (1996).

[24] G. P. Lepage, L. Magnea, C. Nakhleh, U. Magnea and K. Hornbostel, Phys. Rev. D **46**, 4052 (1992).

[25] W. E. Caswell and G. P. Lepage, Phys. Lett. B **167**, 437 (1986).

[26] G. T. Bodwin, E. Braaten and G. P. Lepage, Phys. Rev. D **51**, 1125 (1995) [Erratum-ibid. D **55**, 5853 (1997)].

[27] G. T. Bodwin, E. Braaten and G. P. Lepage, Phys. Rev. D **46**, 1914 (1992);
B. Grinstein, Int. J. Mod. Phys. A **15**, 461 (2000).

[28] E. Braaten and S. Fleming, Phys. Rev. Lett. **74**, 3327 (1995).

[29] P. L. Cho and A. K. Leibovich, Phys. Rev. D **53**, 150 (1996);
P. L. Cho and A. K. Leibovich, Phys. Rev. D **53**, 6203 (1996).

[30] E. J. Williams, Phys. Rev. **45**, 729 (1934); C. F. von Weizsacker, Z. Phys. **88**, 612 (1934); S. Frixione, M. L. Mangano, P. Nason and G. Ridolfi, Phys. Lett. B **319**, 339 (1993) [arXiv:hep-ph/9310350].

[31] A. Petrelli, M. Cacciari, M. Greco, F. Maltoni and M. L. Mangano, Nucl. Phys. B **514**, 245-309 (1998) [arXiv:hep-ph/9707223v2].

[32] J. H. Kühn, J. Kaplan and E. G. O. Safiani, Nucl. Phys. B **157**, 125 (1979);
B. Guberina, J. H. Kühn, R. D. Peccei and R. Rückl, Nucl. Phys. B **174**, 317 (1980);
E. L. Berger and D. Jones, Phys. Rev. D **23**, 1521 (1981).

[33] R. Baier and R. Rückl, Z. Phys. B **19**, 251(1983);
B. Humpert, Phys. Lett. **184**,105 (1987);
R. Gastmans, W. Troost and T. T. Wu, Nucl. Phys. B **291**, 731 (1987).

[34] M. Butenschön DESY report: DESY-THESIS-2009-021, (2009)

[35] T. Hahn, Comput. Phys. Commun. **140**, 418 (2001).

[36] R. Mertig, M. Bohm and A. Denner, Comput. Phys. Commun. **64**, 345 (1991).

[37] J. A. Vermaseren, Report No. NIKHEF-00-032, arXiv:math-phys/0010025 (2000).

[38] P. Artoisenet, F. Maltoni and T. Stelzer JHEP 0802:102 (2008), DOI: 10.1088/1126-6708/2008/02/102.

[39] M. E. Peskin and D. V. Schroeder, "An Introduction to Quantum Field Theory", Addison-Wesley Publishing Company, 1995.

[40] E. Byckling and K. kajantie, "Particle Kinematics", Wiley London, New York, 1973.

[41] G. P. Lepage, J. Comput. Phys. **27**, 192 (1978).

[42] P. Aurenche, M. Fontannaz and J. Ph. Guillet DOI:10.1140/epjc/s2005-02355-1, arXiv:hep-ph/0503259v2 (2005).

[43] J. Pumplin, D. R. Stump, J. Huston, H. L. Lai, P. Nadolsky and W. K. Tung, DOI:10.1088/1126-6708/2002/07/012, arXiv:hep-ph/0201195v3 (2002).

[44] M. Klasen, B. A. .Kniehl, L. N. Mihaila and M. Steinhauser, Nucl. Phys. B **713**, 487 (2005).

[45] B. W. Harris and J. F. Owens, Phys. Rev. D **65**, 094032 (2001).

[46] H. Anlauf, "Radiative Corrections in Gauge Theories" (lectures given at the Adriatic School on Particle Physiocs, Split, Sept. 11-21 2001)(unpublished).

[47] G. Altarelli and G. Parisi, Nucl. Phys. B **126**, 298 (1977).

[48] B. Gong and J. X. Wang Phys. Rev. Lett. **102**, 162003 (2009)

[49] B. Gong and J. X. Wang Phys. Rev. D **80**, 054015 (2009)

Acknowledgments

I would like to thank my PhD supervisor, Prof. Bernd Kniehl, for assigning me this project. I would also like to thank Prof. Moch and Prof. Kramer for being the second referees of my dissertation and disputation, respectively. I can not thank enough Mathias Butenschön for teaching, inspiring and guiding me throughout this project, for bearing with my silly questions, and for helping me get motivated and keep going, when times were tough. Thanks are due also to my office room-mates, Frank Fugel, Torben Kneech, Carlos Sandoval and Elena Scherbakova for useful discussions. Many thanks to the post-doctoral members of the group, for occasional thoughtful advices. No words can ever explain how much indebted I am to my family and friends, for their unconditional love and support. And most importantly, the maximum share of credit goes to my best friend and beloved husband, Dr. Fahad Saeed, for always having faith in me and my abilities, even when I felt like losing, myself. Thanks for being part of my life. And thank you little Isa Fahad, for filling our lives with wonders and joys.

I dedicate this thesis to my beloved teacher Prof. Riazuddin (Nov. 1930 - Sept. 2013)